To
U.S. Army Mobility
Equipment Research and Development Center
Fort Belvoir, Virginia

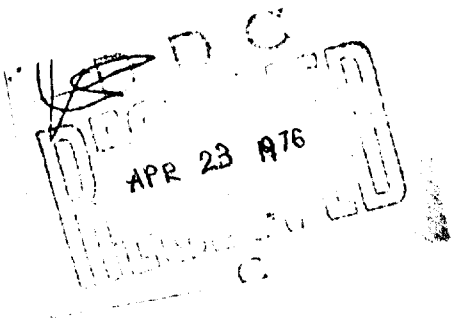

NOTICES

DISTRIBUTION STATEMENT

THIS DOCUMENT HAS BEEN APPROVED FOR PUBLIC RELEASE AND SALE.
ITS DISTRIBUTION IS UNLIMITED.

DISCLAIMERS

THE FINDINGS IN THIS REPORT ARE NOT TO BE CONSTRUED AS AN OFFICIAL DEPARTMENT OF THE ARMY POSITION, UNLESS SO DESIGNATED BY OTHER AUTHORIZED DOCUMENTS.

THE CITATION OF TRADE NAMES AND NAMES OF MANUFACTURERS IN THIS REPORT IS NOT TO BE CONSTRUED AS OFFICIAL GOVERNMENT ENDORSEMENT OR APPROVAL OF COMMERCIAL PRODUCTS OR SERVICES REFERENCED HEREIN.

DISPOSITION

DESTROY THIS REPORT WHEN IT IS NO LONGER NEEDED.
DO NOT RETURN IT TO THE ORIGINATOR.

UNCLASSIFIED

SECURITY CLASSIFICATION OF THIS PAGE (When Data Entered)

REPORT DOCUMENTATION PAGE

READ INSTRUCTIONS BEFORE COMPLETING FORM

1. REPORT NUMBER

2. GOVT ACCESSION NO.

(9) Technical Rept. No.

4. TITLE (and Subtitle)

(6) Research on Electrochemical Energy Conversion Systems

(Final) Report Oct 71-Jun 75

6. PERFORMING ORG. REPORT NUMBER

7. AUTHOR(s)

(10) Adams, Alayne A. [redacted] Adams, Robert T. Foley

8. CONTRACT OR GRANT NUMBER(s)

(15) DAAK02-72-C-0084

9. PERFORMING ORGANIZATION NAME AND ADDRESS

The American University
Washington, D. C. 20016

10. PROGRAM ELEMENT, PROJECT, TASK AREA & WORK UNIT NUMBERS

(16) DA-1T161102A34A 03 100 EF

11. CONTROLLING OFFICE NAME AND ADDRESS

U. S. Army Mobility Equipment Research and Development Center, Fort Belvoir, Virginia

(11) 12. REPORT DATE

December 1975 (12) 120p.

13. NUMBER OF PAGES

106 + viii

14. MONITORING AGENCY NAME & ADDRESS (if different from Controlling Office)

(17) 1-T-161102-H-34-A-03

15. SECURITY CLASS. (of this report)

Unclassified

15a. DECLASSIFICATION/DOWNGRADING SCHEDULE

16. DISTRIBUTION STATEMENT (of this Report)

Approved for public release and sale; distribution unlimited.

17. DISTRIBUTION STATEMENT (of the abstract entered in Block 20, if different from Report)

18. SUPPLEMENTARY NOTES

19. KEY WORDS (Continue on reverse side if necessary and identify by block number)

Electrochemistry, Fuel Cells, Electrolytes, Trifluoromethanesulfonic acid monohydrate, Phosphoric acid, Corrosion.

20. ABSTRACT (Continue on reverse side if necessary and identify by block number)

The research on electrochemical energy conversion systems has involved work on two tasks: a search for electrolytes alternative to phosphoric acid for direct and indirect hydrocarbon-air fuel cells, and a study of the corrosion characteristics of electrolytes for intermediate-temperature hydrocarbon-air fuel cells.

A tabulation of the characteristics of an "ideal" fuel cell electrolyte established that there were five classes of chemical compounds that could

DD FORM 1 JAN 73 1473 EDITION OF 1 NOV 65 IS OBSOLETE S/N 0102-014-6601

027650

UNCLASSIFIED

SECURITY CLASSIFICATION OF THIS PAGE (When Data Entered)

No. 20 (Continued)

be the sources of new, improved electrolytes. One class, the fluorinated sulfonic acids, through one member of the class, trifluoromethanesulfonic acid monohydrate, was investigated in some depth. This compound, when used as an electrolyte in hydrocarbon-air half cells, exhibits exceptional properties in comparison to conventional electrolytes such as phosphoric acid. The electrooxidation of propane and hydrogen is increased by an order of magnitude. The limiting current for the electroreduction of oxygen is increased somewhat but the open circuit potential for the air electrode is increased from 0.98 v (in phosphoric acid) to 1.13 v.

Other fuels were investigated. The CO in H_2-CO mixtures appears to produce a dilution effect rather than a poisoning effect. Methanol, as a fuel, gave low activity in this electrolyte, presumably because of vaporization at elevated temperatures.

An apparatus was built to measure solubilities of gases in electrolytes and several measurements were made on the solubility of propane in $CF_3SO_3H \cdot H_2O$.

The corrosion rates of a number of alloys were measured in phosphoric acid and in $CF_3SO_3H \cdot H_2O$. Generally, the rates were lower in the latter electrolyte and the possibility exists of using a low alloy steel as a construction material for fuel cells using this electrolyte.

Unclassified

Report No. 7

Research on Electrochemical Energy Conversion Systems

Final Technical Report

by

A. A. Adams and R. T. Foley

December 1975

to

U. S. Army Mobility Equipment Research
and Development Center

Fort Belvoir, Virginia

Prepared by

The American University

Washington, D. C.

Contract No. DAAK02-72-C-0084

DA Project/Task Area/Work Unit No. 1T161102A34A 03 100 EF

Approved for public release and sale

distribution unlimited

Unclassified

TABLE OF CONTENTS

SUMMARY

The research on electrochemical energy conversion systems has involved work on two tasks: a search for electrolytes alternative to phosphoric acid for direct and indirect hydrocarbon-air fuel cells, and a study of the corrosion characteristics of electrolytes for intermediate-temperature hydrocarbon-air fuel cells.

A tabulation of the characteristics of an "ideal" fuel cell electrolyte established that there were five classes of chemical compounds that could be the sources of new, improved electrolytes. One class, the fluorinated sulfonic acids, through one member of the class, trifluoromethanesulfonic acid monohydrate, was investigated in some depth. This compound, when used as an electrolyte in hydrocarbon-air half cells, exhibits exceptional properties in comparison to conventional electrolytes such as phosphoric acid. The electrooxidation of propane and hydrogen is increased by an order of magnitude. The limiting current for the electroreduction of oxygen is increased somewhat but the open circuit potential for the air electrode is increased from 0.98 v (in phosphoric acid) to 1.13 v.

Other fuels were investigated. The CO in H_2-CO mixtures appears to produce a dilution effect rather than a poisoning effect. Methanol, as a fuel, gave low activity in this electrolyte, presumably because of vaporization at elevated temperatures.

An apparatus was built to measure solubilities of gases in electrolytes and several measurements were made on the solubility of propane in $CF_3SO_3H \cdot H_2O$.

The corrosion rates of a number of alloys were measured in phosphoric acid and in $CF_3SO_3H \cdot H_2O$. Generally, the rates were lower in the latter electrolyte and the possibility exists of using a low alloy steel as a construction material for fuel cells using this electrolyte.

FOREWORD

This research on electrochemical energy conversion systems has been sponsored by the U. S. Army Mobility Equipment Research and Development Center at Fort Belvoir, Virginia, under Contract No. DAAK02-72-C-0084 with The American University. The work was authorized under DA Project/Task area/Work Unit No. 1T161102A34A 03 100 EF.

List of Figures

Page

Page

Page

List of Tables

1.0 Introduction

This is the final semi-annual report on Contract No. DAAK02-72-C-0084 sponsored by the U. S. Army Mobility Equipment Research and Development Center at Fort Belvoir, Virginia. The project, entitled "Research on Electrochemical Energy Conversion Systems," consists of two technical tasks, both of which are directed toward the improvement of the hydrocarbon-air fuel cell for ground power systems and vehicular propulsion.

Task I A search for alternative electrolytes to phosphoric acid for direct and indirect hydrocarbon-air fuel cells.

Task II A study of the corrosion characteristics of electrolytes for intermediate-temperature hydrocarbon-air fuel cells.

2.0 Task I A Search for Alternative Electrolytes to Phosphoric Acid for Direct and Indirect Hydrocarbon-Air Fuel Cells

2.1 Introductory

2.1.1 Characteristics of a Fuel Cell Electrolyte

There is general agreement that the "ideal" electrolyte in the hydrocarbon-air fuel cell should possess the following properties or characteristics:

a. the electrolyte should be a good medium for the efficient oxidation of the hydrocarbon,

b. the electrolyte should be a good medium for ionic charge transport,

c. the electrolyte should be a good solvent for active materials, e.g., propane, oxygen, water,

d. the electrolyte should be a good medium for material transport, e.g., removal of CO_2,

e. the electrolyte should be chemically and electrochemically stable over the temperature and voltage operating range of the fuel cell,

f. the electrolyte should possess suitable physical properties e.g., viscosity and vapor pressure,

g. the electrolyte should not interfere with catalytic reactions,

h. the electrolyte should be a good medium for the air electrode, and finally,

i. the electrolyte should not be strongly reactive to construction materials or the fuel cell matrix.

Phosphoric acid is considered to be the most suitable electrolyte at this time. While phosphoric acid possesses some of the desirable characteristics tabulated above, it also has certain detrimental characteristics. Specific deficiencies include undesirable corrosivity toward structural materials at 125-150°C, low solubility with respect to propane and oxygen, undesirable adsorption of anions competitive with propane adsorption, and a tendency for potential cycling at an electrode during operation with hydrocarbons. These adverse characteristics are sufficiently pronounced to make the replacement of phosphoric acid electrolyte in the hydrocarbon-air fuel cell very desirable.

2.1.2 Classes of Electrolytes

A previous survey (1) has identified certain classes of compounds that deserve consideration in the selection or the development of an alternative electrolyte:

a. sulfonic acids, e.g., CF_3SO_3H,

b. alpha-halo disubstituted carboxylic acids, e.g., $CHCl_2COOH$,

c. perfluorocarboxylic acids, e.g., C_2F_5COOH,

d. dialkyl phosphate esters, e.g., $(C_2H_5O)_2P(O)OH$,

e. polyphosphates, e.g., Graham's salt,

2.1.3 Literature Background on Electrolytes

A promising system of compounds is the perfluoroalkanesulfonic acids. These acids have high acid strengths and are excellent ionic conductors (2). The simplest acid, trifluoromethanesulfonic acid, forms a stable monohydrate which melts at 33.8°C (3) and boils at 217-218°C at 756.9 mm (4). Literature values for the vapor pressure

of trifluoromethanesulfonic acid monohydrate are 1 mm at 96°C (5) and 15 mm at 120°C (6).

Several perfluorocarboxylic acids, representative of the third class above, are available from the 3M Co. The physical properties of four of these are listed in Table I (7). From the work of Hollahan and Cady (8) there is definite indication of formation of a 1:1 molar monohydrate species, $C_3F_7COOH \cdot H_2O$, freezing at -11.0°C. No literature reference on the stability of this monohydrate in the liquid state, or whether the monohydrate would boil congruently, was found.

Dichloroacetic acid is one of the strongest organic acids with a pK = 1.48 (9). It is extremely stable, boiling congruently at 193°C (10). It is non-hygroscopic, but soluble in all proportions with H_2O forming no eutectics of hydrates.

In this report, reference to organic electrolytes means such solutions as lithium perchlorate in gamma-butyrolactone or propylene carbonate, as contrasted to strong organic acids mentioned above as alternate electrolytes. Such systems were considered as they offer the possibility of providing solutions to some of the problems encountered in aqueous systems. It would be expected that fuel solubility would be greater in organic electrolytes with an accompanying increase in anode limiting current density. It would be expected that the rate of adsorption of the hydrocarbon would be altered and consequently the efficiency of electrocatalysis. The degree of side reactions and polymerization would also be affected, whether favorably or unfavorably, would be difficult to predict.

The work done with organic electrolytes in fuel cells has been

TABLE I

PHYSICAL PROPERTIES OF PERFLUOROCARBOXYLIC ACIDS (From Reference 7)

Compounds	Formula	Freezing Point	Boiling Point	Vapor Pressure
Trifluoroacetic Acid	CF_3COOH	-15.6°	71.1° at 734 mm	191 mm at 37° 625 mm at 66.7°
Perfluoropropionic Acid	C_2F_5COOH		96° at 740 mm	
Perfluorobutyric Acid	$CF_3CF_2CF_2COOH$	-17.50°	120.0°at 735 mm	44 mm at 56° 455 mm at 107.4°
Perfluorooctanoic Acid	$C_7F_{15}COOH$	53°	187-189°	

limited, excluding, of course, work done with the ion-exchange membrane type which might be thought of as an organic electrolyte. A study was performed by Smith (11) using hydrazine and N_2O_4 as fuels. N_2O_4 reacted with some of the organic solvents and in solvents such as propylene carbonate, acetonitrile, and dimethyl formamide, the cell voltages were low suggesting slow diffusion processes, slow adsorption, or other slow reactions.

Polyphosphates, e.g., Graham's salt, would be used in a fuel cell along with electrolyte at such concentration as to obtain the proper specific conductivity. The degree of polymerization would be such that the solution would be stable but not of such high viscosity as to render transport difficult. It would appear reasonable to incorporate the electrolyte in a stable matrix. Whereas the polyelectrolyte is more stable at a neutral pH, it would appear feasible to work at a pH such as 5 - 6, accepting a steady-state degradation in the degree of polymerization to achieve an acid rejecting composition.

The properties of polyelectrolytes have been studied by Strauss and his coworkers. For example, in a study of binding of univalent cations by polyphosphates, Strauss and Bluestone (12) constructed the following table of electrical transport data of polyphosphates (Graham's salt preparations) in 0.2 M electrolyte solution.

Electrolyte	M_s	Δ_p	u x 10_4 cm^2/volt-sec	Δ_s	t_c	λ_c
LiBr	0.203	6.51	1.23	51.1	0.313	16.0
NaBr	0.199	7.35	1.14	57.2	0.384	22.0
KBr	0.216	12.8	1.41	70.8	0.488	34.6
tetramethyl-ammonium bromide	0.209	14.7	2.07	48.3	0.362	17.5

where M_s is the actual stoichiometric molarity of the simple electrolyte

Δ_p is the equivalent conductance of the polyphosphate salt

u is the electrophoretic mobility of the polyphosphate salt

Δ_s is the equivalent conductance of the simple electrolyte

t_c is the transference number of the cation

λ_c is the equivalent conductance of the counterion in the solution of simple electrolyte as a solvent.

2.2 Experimental

2.2.1 Electrochemical Apparatus and Techniques

The cells used for the experiments were standard three-compartment cells. The cell used for the experiments on trifluoromethanesulfonic acid monohydrate shown in Figure 1 was of approximately 30 ml capacity. The working electrode in the central compartment of the cell consisted of a platinum wire of approximately 0.4 cm^2 geometric area sealed in a Pyrex tube which was graded into the quartz cell body. A platinum wire mesh electrode spot-welded to a platinum wire lead of approximately 8.0 cm^2 was substituted for the wire during experiments in which potential-current curves were measured. The counter electrode compartment was separated from the working compartment by a fritted glass disc. The counter electrode used in the original cells was a fuel cell electrode connected to a platinum wire lead. The counter electrode (left compartment, Figure 1) in the smaller cell, was a platinized platinum mesh connected to a platinum wire lead.

The reference electrode system was separated from the working electrode compartment by inserting a fritted glass disc behind the Luggin capillary. The reference electrode is of the dynamic reference electrode design of Giner (13). This reference electrode system consists of two platinized platinum electrodes [A] and [B]. When a current density of 1 ma/cm^2 is impressed between electrode [A] and [B], H_2 is evolved from the cathode, [A], and O_2 is evolved from the anode, [B]. The cathode is kept 1 - 2 cm lower than the anode to prevent diffusion of O_2 from the anode to the cathode. Temperature control was achieved by maintaining the cell in an oil bath or an air oven.

The technique used to study the rate of propane adsorption was a

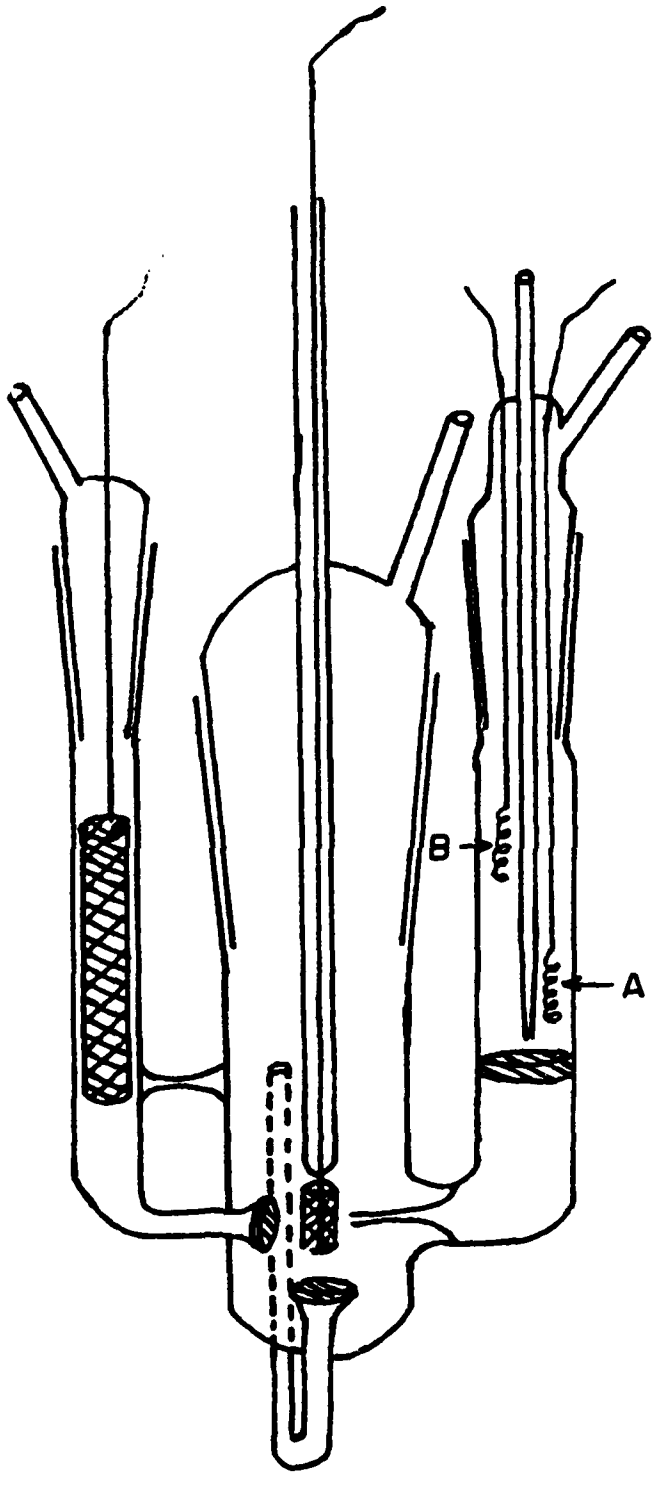

Figure 1. Electrochemical cell used for experiments with trifluoromethanesulfonic acid

modified multipulse potentiostatic (MSP) technique. The technique uses programmed sequences of potentials to provide a clean reproducible electrode surface for the adsorption process. After adsorption takes place at a potential of interest an anodic or cathodic galvanostatic pulse is imposed and a chronopotentiogram recorded on a Tektronix Type 564B oscilloscope using a Type 3 AB vertical amplifier. The potential-time sequences were generated by switching potentiometers into the imput circuit of a Wenking potentiostat. Mercury-wetted relays were fired at prescribed times in the range of 1 msec to 10 seconds with electronic pulse generators (Tektronix, Type 162). The circuit for activating the relays with pulse generators was of the Tyco design (14). For times longer than 10 seconds, the relay was fired manually. Switching from potentiostatic control to the galvanostatic circuit was was done by switching the counter electrode of the cell from the potentiostat to the battery circuit. The electrical block diagram is shown in Figure 2. Several of the potential step sequences used are shown in Figure 3. All of the potentials given are with reference to the dynamic hydrogen electrode. "Sequence 1" was used to determine the "real" surface area of the electrode. The pretreatment steps are used to prepare a reproducible electrode surface for each measurement. During step B the electrode is brought to +1.35 volts which oxidizes oxidizable impurities on the electrode surface and forms a passive oxide layer on the platinum surface. The potential is stepped down to +0.05 volts, step C, where the oxide layer is reduced. The potential is then raised to 0.95 volt, step D, to desorb H atoms adsorbed at 0.05 volt. Step D was set at 0.95 volt after variations in measured surface areas were observed when potentials below 0.75 volt were used.

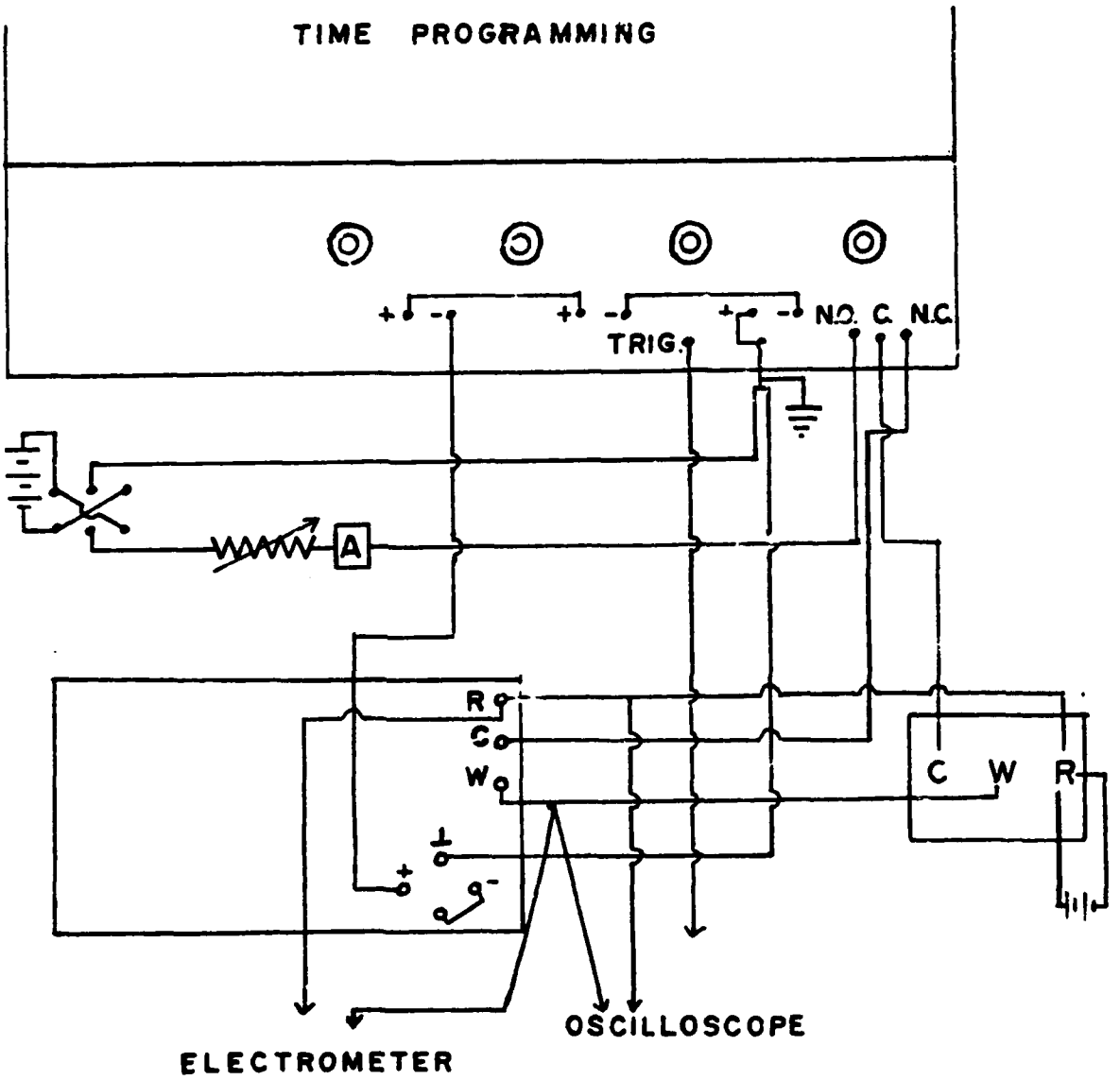

Figure 2 Block diagram of the electrical set-up used for the pre-treatment and galvanostatic pulse sequences.

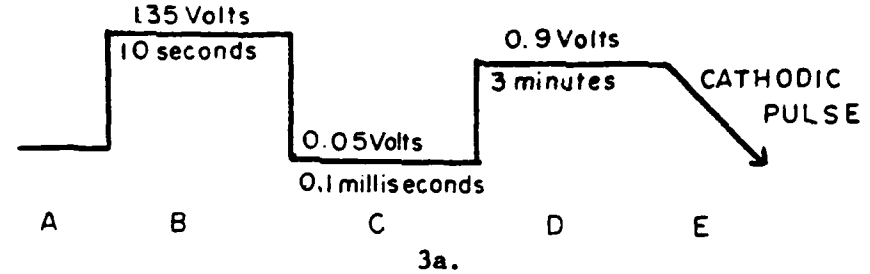

3a.

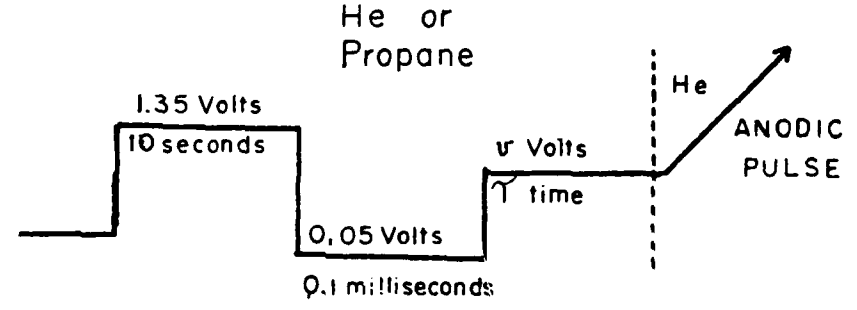

3b.

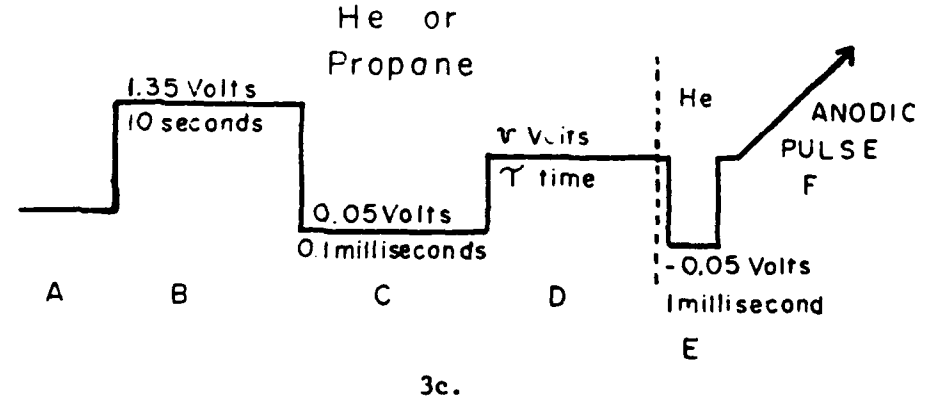

3c.

Figure 3 Potential step sequences used for adsorption studies.
a. The sequence used for surface area measurements.
b. The sequence used to determine the surface concentration of adsorbed material.
c. The sequence used to determine the amount of material cathodically desorbable.

Potentials above 0.75 volt gave reproducible values for the surface area. A cathodic galvanostatic pulse of 25 to 75 milliamps/cm^2 was applied, (step E), to measure the charge associated with the coverage of hydrogen. The maximum cathodic galvanostatic charge for depositing H atoms on a clean electrode prior to H_2 evolution, after correction for double layer effects, is 210 μcoulombs/cm^2. It is known that this value changes with temperature and electrolyte composition to some degree, however, within experimental limitations used here, the value of 210 μcoulombs/cm^2 may be used (15).

The platinum electrode tends to roughen in hot H_3PO_4 even after the electrode is flamed. In some cases, particularly after the passage of propane, a deposit was noted on the electrode causing the electrode area to increase in an erratic manner. The deposit could be flamed off but frequent monitoring of the electrode surface area was essential.

The second pulse sequence intended to determine the surface concentration of some adsorbed compound such as propane is shown in Figure 3b. Steps A through C are identical to sequence 1. During step D adsorption of the compound, e.g., propane, occurs. Its duration is from 15 to 360 seconds and the potential at step D varies from 0.15 to 0.6 volt. During step E an anodic galvanostatic pulse is imposed and the voltage-time curves are used to determine the surface concentration of the adsorbed material.

The pulse sequence, 3c, measures the amount of material cathodically desorbed. Steps A through D are the same as the second pulse sequence. Step E is a cathodic galvanostatic pulse held for a millisecond while the cathodically desorbable species is removed from the electrode. The potential is allowed to return to the adsorption potential under

helium and an anodic galvanostatic pulse, step F, imposed. Sequence 3 and sequence 2 may be compared to determine the amounts of cathodically desorbable and nondesorbable species.

A comparison of the background curve obtained by running sequence 2 under helium with the same sequence run with propane followed by helium, as shown in Figure 3b, gives the amount of charge obtained from the oxidation of all the surface species on the electrode. In a similar manner the anodic charging curve, compared to the background using sequence 3, gives the amount of charge needed to oxidize the species not cathodically desorbed.

In the study of the propane adsorption process in $CF_3SO_3H \cdot H_2O$ two multipulse potentiodynamic methods were used. In the first instance, a potential ramp was imposed on the electrode following a series of pretreatment steps. In the second instance, a potential triangle was imposed following the pretreatment steps. In these techniques, the electrode was pretreated to develop a reproducible surface, an adsorption step was conducted at the potential of interest, and finally a potential wave form (ramp or triangle) was imposed on the electrode.

In order to better understand the adsorption process in the trifluoromethanesulfonic acid monohydrate electrolyte, experiments were initiated using a multipulse potentiodynamic method (16). The apparatus shown in the electrical block diagram of Figure 4 was assembled. This technique involves the imposition of a series of potential ramps on the electrode following pretreatment steps. Thus, the electrode would be pretreated to develop a reproducible surface, an adsorption step conducted according to the Figure 3b sequence, and

a potential ramp imposed on the electrode. In the electrical circuit as assembled and shown in Figure 4, the lowest (most cathodic) value of the potential ramp from the function generator (Exact Model 7060) was always in the system. The applied potentials were then algebraically added to this value at the input of the potentiostat (Wenking Model 66 T S3). Following adsorption at a predetermined potential of interest, the anodic potential ramp is imposed and the current-time curves displayed on an oscilloscope (Tektronix Type 555) with a differential vertical amplifier (Tektronix Type 2'7). The potential ramp was displayed simultaneously using a vertical amplifier (Tektronix Type CA). The potential-time sequences for the pretreatment and adsorption steps were generated by switching potentiometers into the input circuit of the Wenking potentiostat as described above. Switching from potentiostatic control to the potential ramp and triggering the oscilloscope was done by firing the function generator and oscilloscope by a six volt power supply shown in Figure 4.

In performing the current versus potential runs, a potential value was set and the system allowed to equilibrate for 5 minutes before the current value was recorded for any of the gases used. The potential was moved in both the cathodic and the anodic directions to obtain an indication of the electrolyte behavior and an accurate determination of the open-circuit potential.

Current vs. potential diagrams were constructed with measurements for helium and hydrogen. Propane was run at 55°, 95°, 115° and 135°C. A digital panel meter (Electronic Research Co., Model 4000) was wired to read voltage and cell current values (Figure 5). The digital panel meter was used for most of the current-potential diagrams reported below.

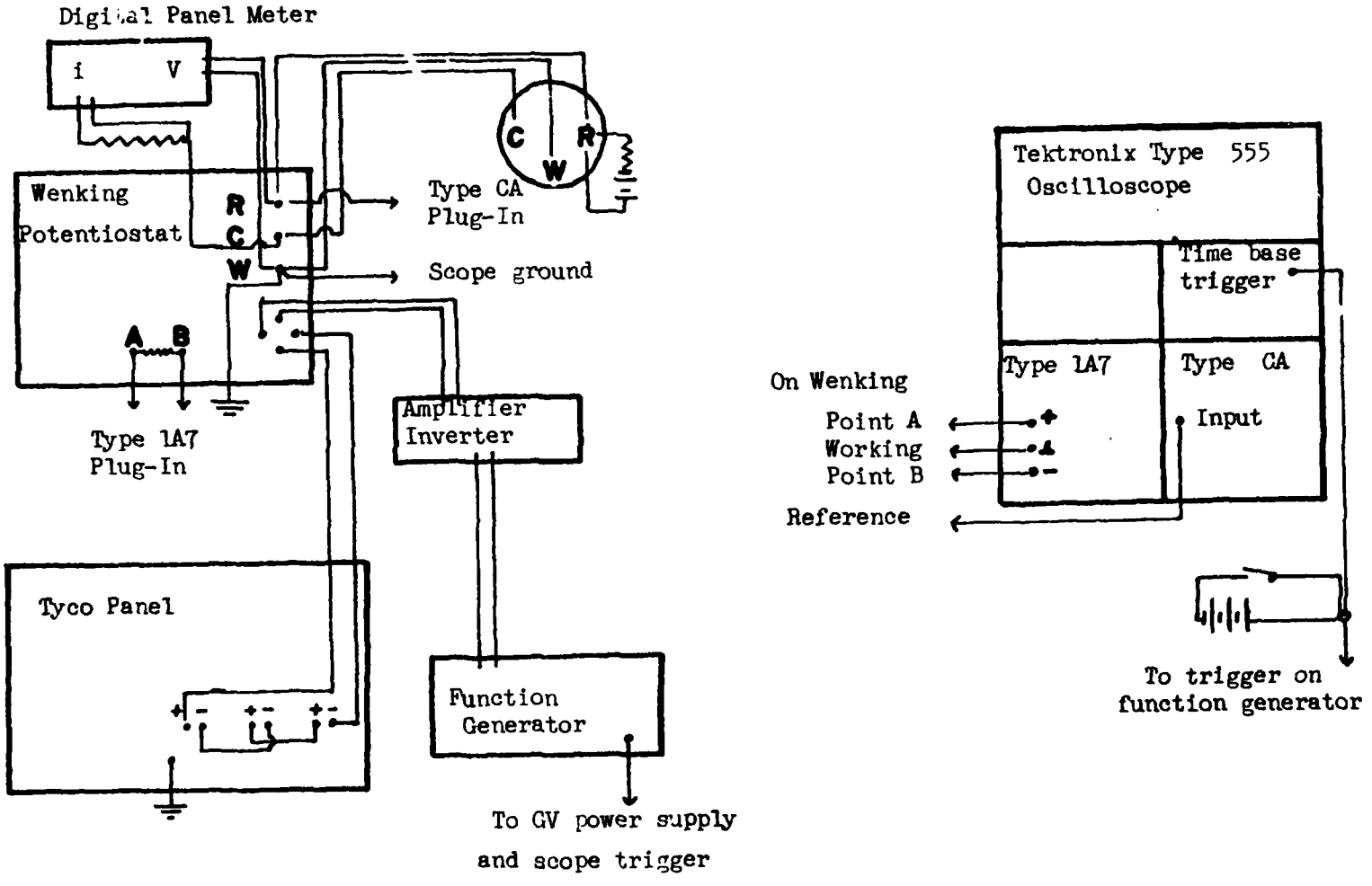

Figure 4. Electrical Block Diagram of apparatus for potential ramp techniques

In the last phase of the project an automated electrochemical station was designed which will be capable of handling most electrochemical experiments. The schematic of the system is shown in Figure 6. The system consists of A, the programmable timing controller, B, the potential step device, C, the basic electrochemical system, D, the data acquisition system, and E, the computer to process data.

The programmable timing controller, an AutoMate 32 (Reliance Electric Company, Cleveland, Ohio 44177), is a solid-state device having a stored program which controls outputs in a predetermined way in response to the action of the inputs. The major elements of the AutoMate 32 are shown in Figure 7. In addition to those shown, there is a manual programmer with its internal memory and processor which is used to program the Erasable Programmable Read Only Memory (EPROM). The major elements of the AutoMate 32 are A, the controller chassis, containing the power supply, processor and controller monitor; B, input cards; C, output cards; D, timer counter latch (TCL) cards; E, program memory module; F, communication interface and G, input and output blocks which connect with the input or output cards in the controller chassis. The analog timer elements (Model 325), mounted in the TCL card, are adjustable from 0.5 to 127.5 seconds per timer element. Times longer than 127.5 seconds are controlled by counter elements. Programming* is done via a ladder diagram which symbolically represents the elements of the control circuit. The input devices and interlocking contacts are placed in the desired parallel or series combinations across the rung of the ladder with

*The program is obtainable from the Authors.

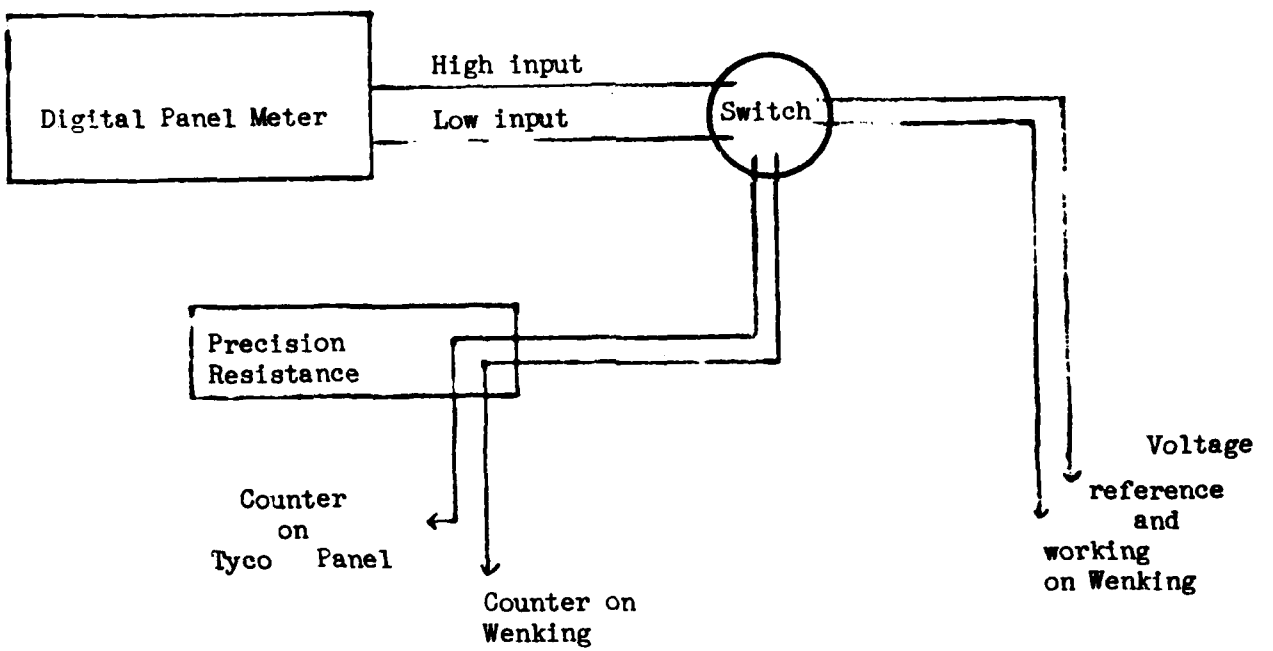

Figure 5. Electrical arrangement for digital panel meter

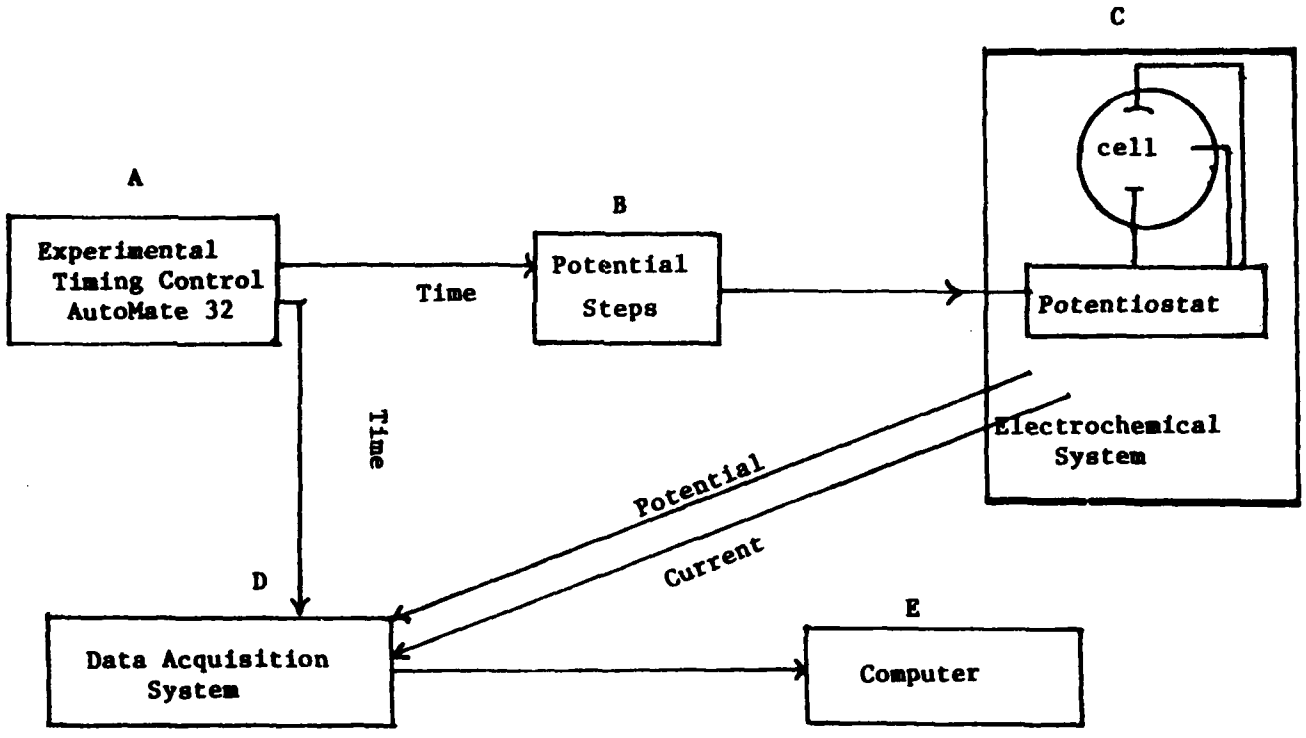

Figure 6. Schematic diagram of automated electrochemical station

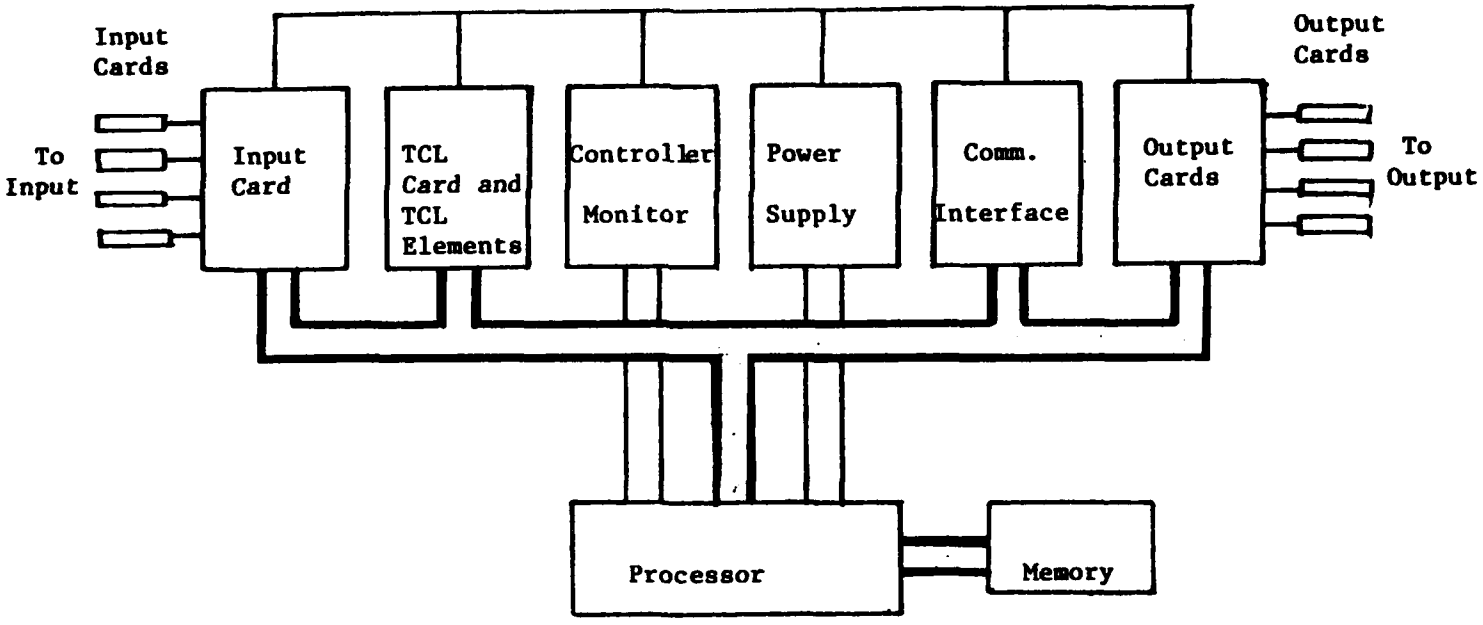

Figure 7. Major elements of Automate 32

the last element on the rung being the output associated with the sequence.

The potential step device shown in Figure 6 has a variable base potential step and 2 times, 4 times, and 8 times this base step. These steps can be used individually, or in any combination, allowing 15 possible potential steps. These steps are programmed in any sequence from the controller. If the base potential step is 10 mv a total of 150 mv may be algebraically added in 10 mv steps to the potential set in the potentiostat. If 50 mv is the base potential step, 750 mv may be added to the set potential. Initially the device will be used for development of current potential diagrams where time at each potential step is equal. However, it is possible to vary the time at any step or steps allowing great flexibility of the system.

The basic electrochemical unit is the potentiostat with function generator or galvanostat plugin and the electrochemical cell. This portion of the overall system can be used manually in the traditional manner or be tied to the controller for automated control.

The data acquisition system (Dymec DY-7061) consists of a 25 channel input scanner (Model No. 2901B, Dymec Division, Hewlett Packard, Palo Alto, California), a digital clock (Model No. 3440A), a digital recorder (Model No. N39562A) and a paper tape punch (Model No. 5655). The data acquisition system scans up to 25 input signals, measures the dc voltage of each signal, and records the voltage measurements. This data system is quite old but is still adequate to record data for current-potential diagrams. In the future, to cope with faster reactions, this portion of the electrochemical station will have to be updated. At this time, data are taken in eight channels, 2 for potential and 6 for

current for a set period of time after equilibration time at a set potential (e.g., 30 seconds data recording after 5 minutes equilibration time.)

The Computer (Xerox Sigma 2) processes the data, at present stored on punch paper tape, to read potential and current density values. The current values over all channels scanned are averaged and divided by the real surface area of the electrode. The potential values and current density values are printed on the print-out for future graphing of data. The graphing could be done via the computer by an addition to the computer program.

The entire system allows for automated control of the basic electrochemical system with data recorded and stored for future processing. This capability allows the basic system to be run overnight when no operator is available, or, particularly for current-potential diagrams, relieve the operator from the tedious task of taking data at prescribed intervals. Also, a greater number of current readings can be taken, allowing for greater precision in the current readings than is possible with a single reading by the operator.

2.2.2 Solubility Measurements

One of the important properties of the fuel cell electrolyte is the solubility of propane, hydrogen, and oxygen in the electrolyte. To measure these solubilities in trifluoromethanesulfonic acid monohydrate, an apparatus which represents a modification of that described by Loprest (17) was constructed. This apparatus is shown in schematic diagram in Figure 8. The relatively simple procedure involves introducing a measured quantity of gas into a system containing a known volume of solvent (electrolyte) and measuring the

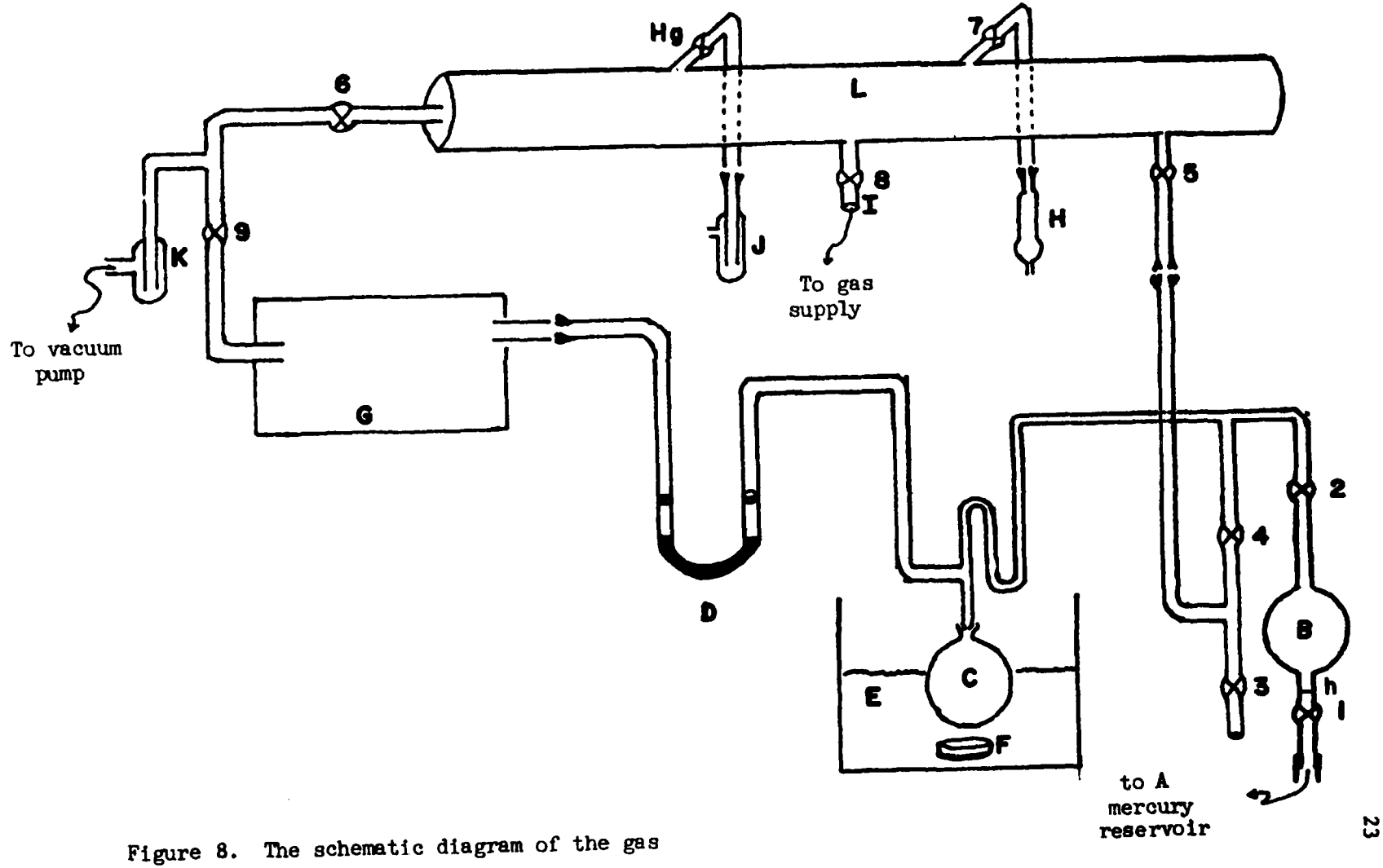

Figure 8. The schematic diagram of the gas solubility apparatus

equilibrium pressure of the system.

The individual parts of the system may be located by reference to the figure:

A. a mercury leveling bulb connected to the system with tubing,

B. a glass flask gas reservoir (volume calibrated from mark h up to and including the bore of stopcock 2, about 100 ml),

C. a glass flask of known weight that serves as a solvent reservoir,

D. a mercury-filled U-tube with medium porosity fritted glass discs which do not permit the passage of mercury,

E. the oil bath,

F. a magnetic stirrer,

G. a precision pressure gauge (Texas Instruments, Model No. 145-02,

H. a drying tube,

I. the gas supply,

J. a mercury bubbler,

K. a trap containing molecular sieves,

L. the manifold.

The volume of flask B, the gas reservoir, and adjacent portions of the system was carefully calibrated before attachment to the manifold. This was accomplished by standard procedures, by filling with water and mercury and weighing. The solvent reservoir, flask C, was accurately weighed.

The solubility measurement, e.g., the solubility of propane in trifluoromethanesulfonic acid monohydrate, was conducted with a procedure

that involved the following consecutive steps:

1. With the solvent flask (flask C) empty, stopcock 1 is opened and the mercury level in the gas flask (flask B) is adjusted to the level, h, which is just above stopcock 1, with the mercury leveling bulb.

2. With stopcock 1 closed, stopcock 2 and 4 and valves 5, 6, and 9 are opened with the system evacuated. Valves 5 and 6 are closed and the solute gas is introduced with valves 8 and Hg open. Valve 5 is opened slowly maintaining bubbling through the mercury trap. The gas tank valve and valve 8 are closed. (At this point, the gas pressure in the system will be quite close to atmospheric pressure. Valve 6 may be opened slightly to reduce the pressure below atmospheric if desired.)

3. After thermal equilibrium has been established, the pressure and the temperature of the gas is recorded. Stopcock 2 is closed. The volume of gas (number of moles) in gas flask B is calculated.

4. The system, exclusive of the gas flask (B) is brought to atmospheric pressure with air or N_2 by opening valves 5 and 7. The solvent flask (C) is removed, an appropriate amount of solvent is added to it and it is replaced in the system. Valve 7 is closed.

5. The solvent is degassed. Stopcock 5 and valves 5 and 6 are opened and the system is evacuated. Valve 5 is closed for 15 minutes then opened to re-evacuate the system. (If necessary the solvent can be frozen and a series of freeze-evacuate-thaw cycles can be used to degas.)

6. The solvent flask (C) is brought to the desired temperature with the oil bath and the differential pressure is measured. (The

differential pressure is the pressure difference between atmospheric pressure and the pressure in the system.) Degassing of the solvent is continued until a constant pressure value is obtained. The pressure measurement is made with stopcock 4 and valves 5, 6 and 9 closed and valve 7 open. The levels of mercury in D should be the same. The differential pressure is read on the precision pressure gauge (G). After the differential pressure measurement is taken, valves 6 and 9 are opened.

7. With stopcock 4 closed and stopcocks 1 and 2 opened, mercury flows into the gas flask (b).

8. The solvent is stirred and the system is allowed to come to equilibrium. The pressure of the system is measured with valve 9 and stopcocks 1 and 2 open.

9. The temperature of the bath is raised or lowered and the system is again equilibrated to obtain solubility data over a temperature range. (This may be done with a single charging of the solvent flask and the weight of the solvent is determined at the conclusion of the experiment.)

In the calculation of the solubility the following assumptions are made:

a) the ideal gas laws are obeyed,

b) the vapor pressure of the saturated solvent is the same as the vapor pressure of the gas-free solvent,

c) Henry's law is in force up to a pressure of one atmosphere.

These assumptions do produce deviations but these deviations are considered to be less than experimental error.

2.2.3 Preparation of Electrolytes

The phosphoric acid used was Fisher's 85% A.C.S. Grade. Commercial phosphoric acid has been found to be impure with the impurities yielding a large background current on electrolysis (18). In order to remove these impurities commercial H_3PO_4 was refluxed with 30% H_2O_2(A.C.S. Grade stabilized with $Na_4P_2O_7$) in a 2:1 mixture until bubbling ceased (approximately 24 hours). The H_3PO_4solution was then evaporated slowly to a concentration of greater than 85% and then diluted back to 85% with triply distilled water. The resultant acid solution was pre-electrolyzed at 0.30 volt using a pair of large fuel cell electrodes. This refluxed pre-electrolyzed acid was used as the electrolyte in the electrochemical cell.

The electrolyte was cleaned further in the cell with a cleaning electrode maintained at 0.30 volt overnight with a Wenking Potentiostat. The cleaning electrode was a fuel cell electrode replacing the working electrode assembly in the cell. The cleaning electrode was subjected to alternate oxidations and reductions of 3 volts for 45 minutes duration in H_3PO_4, ending on an oxidation. This procedure served to keep the electrolyte clean on a day-to-day basis.

Trifluoromethanesulfonic acid monohydrate was prepared from trifluoromethanesulfonic acid (3M Corp., Lot 7 "Fluorochemical Acid FC-24") and water by the method of Gramstad and Haszeldine (5). Equimolar quantities of trifluoromethanesulfonic acid and water were added to a distillation flask. Fractional distillation was carried out with the fraction below 110°C collected and removed. The fraction above 110°C was collected as a white crystalline product with some viscous clear liquid. This fraction was distilled a second time with

all material distilled below 150°C rejected and the fraction above 150°C retained for a third distillation. In the third distillation only the fraction between 217-218°C (756.9 mm Hg) was retained as a white needle-like crystalline product, trifluoromethanesulfonic acid monohydrate. The $CF_3SO_3H \cdot H_2O$ was found to have a melting point of 33.8°C which agrees well with the value of 34°C given by Gramstad and Haszeldine (5). No further purification was done before the trifluoromethanesulfonic acid monohydrate was added to the electrochemical cell.

Graham's salt $(NaPO_3)_x$ may be prepared by the quenching of any melt having a $NaO:P_4O_{10}$ ratio between 2:1 and 10:3 (19). The degree of polymerization appears to depend on the heating temperature with the maximum polymerization at 1100°C. A quantity of $NaH_2PO_4 \cdot 2H_2O$ is placed in a platinum dish and dehydrated for 2 hours above 200°C. The material is placed in an electric furnace for 4 hours at the desired temperature and the melt quenched as quickly as possible by pouring into an iron dish containing dry ice and CCl_4. The vitreous product can be filtered off and the glassy material should be stored immediately in an air-tight container. Graham's salt is extremely hygroscopic, becoming moist and sticky with short exposure to air. The salt dissolves slowly in cold water and is quite soluble in water over 30°C (solubility at 20°C, 973.2 g/liter; at 80°C, 1744 g/liter). Graham's salt is a glassy chain polymer containing a small percentage of cyclic rings; the glass is considered to be of a metaphosphate composition, $Na_2O \cdot P_2O_5$ (20).

Perfluorobutyric acid was obtained from Mathieson, Coleman and Bell. The acid was purified by vacuum distillation, and from the

distillation range no significant impurities were indicated. The distilled acid was kept in tightly stoppered Pyrex flasks and was only handled once after collection from the distillation; this when the acid was pipetted into the quartz cell. The perfluorobutyric acid is a water-white, nonviscous liquid that has only a mildly offensive odor at room temperature. Although the acid has an odor reminiscent of butyric acid it is not persistent or pungent and does not appear to present any problem due to its odor.

Dichloroacetic acid is readily and cheaply available in relatively pure form and it is easily vacuum distilled to high purity (typically 80-81°C at 6 mm). Since in pure form $CHCl_2COOH$ has extremely poor conductivity, the acid must be either diluted with water or a supporting electrolyte must be introduced. The acid, obtained directly from the middle fraction of the vacuum distillation, was added to distilled water in the test cell until the desired 80% acid solution was obtained. In all cases, the electrolyte was homogeneous, of crystal-clear color, and convenient conductivity (0.083 ohm^{-1}).

2.2.4 Preparation and Treatment of Reactants

Helium, hydrogen, hydrogen-3% CO, CO_2, propane, air, and methyl alcohol were used in different experiments. Helium (AIRCO) was passed over hot copper turnings to remove traces of oxygen before being passed into the cell. Hydrogen (AIRCO) and hydrogen-3% CO (AIRCO) were passed through a commercial catalytic purifier for electrolytic hydrogen (DEOXO, Engelhard Gas Equipment Division) before entrance to the cell. Propane (Matheson, high purity) was used without pretreatment. The methyl alcohol used was Allied Chemical, General

Chemical Division, reagent grade. The methyl alcohol solutions were prepared to 1 molar methyl alcohol in $CF_3SO_3H \cdot H_2O$. Before passage through the cell with 85% H_3PO_4 helium was passed through a pre-saturator. The pre-saturator served to saturate the helium with water at approximately the same vapor pressure as the cell. The gas lines were heated so the gas entering the cell was close to the temperature of the electrolyte in the cell.

2.3 Results and Discussion

2.3.1 Results with Trifluoromethanesulfonic Acid Monohydrate

An investigation of the behavior of $CF_3SO_3H \cdot H_2O$ with helium, hydrogen, hydrogen-3% CO, propane, "reduced" carbon dioxide, and methanol at various temperatures was conducted during this contract period. Data on helium provide background information on the electrolyte. The investigation of the behavior of hydrogen is of interest due to the renewed interest in H_2-air fuel cells. Hydrogen-carbon monoxide mixtures, the products of reforming procedures, are of use for "indirect" hydrocarbon-air fuel cells. Propane and methanol are used in direct oxidation fuel cells.

The results, using helium in $CF_3SO_3H \cdot H_2O$ on platinum mesh at 55°, 95°, and 115° C, are summarized in Figure 9. The results have been normalized for surface area and adjusted to one open circuit potential. The results at 55° C show somewhat higher current density values than those at 95° and 115° C. Other anomalies occurred at 55° C which will be discussed later. The current density values at a set potential are slightly lower at 95° than at 115° C. These results would appear to be as normally expected. There is nothing in the polarization curves with helium to suggest that the $CF_3SO_3H \cdot H_2O$ electrolyte undergoes any detrimental reaction through the potential range tested. The current carrying capacity goes up with temperature. From the fact that there was no breakdown with temperature and considering the greater current carrying capacity, it was concluded that the compound showed promise as an electrolyte for the direct hydrocarbon fuel cell.

Separate experiments involved anodic pulsing of the electrode from approximately 0.3 volts to 1.8 volts. After repeated pulses, the

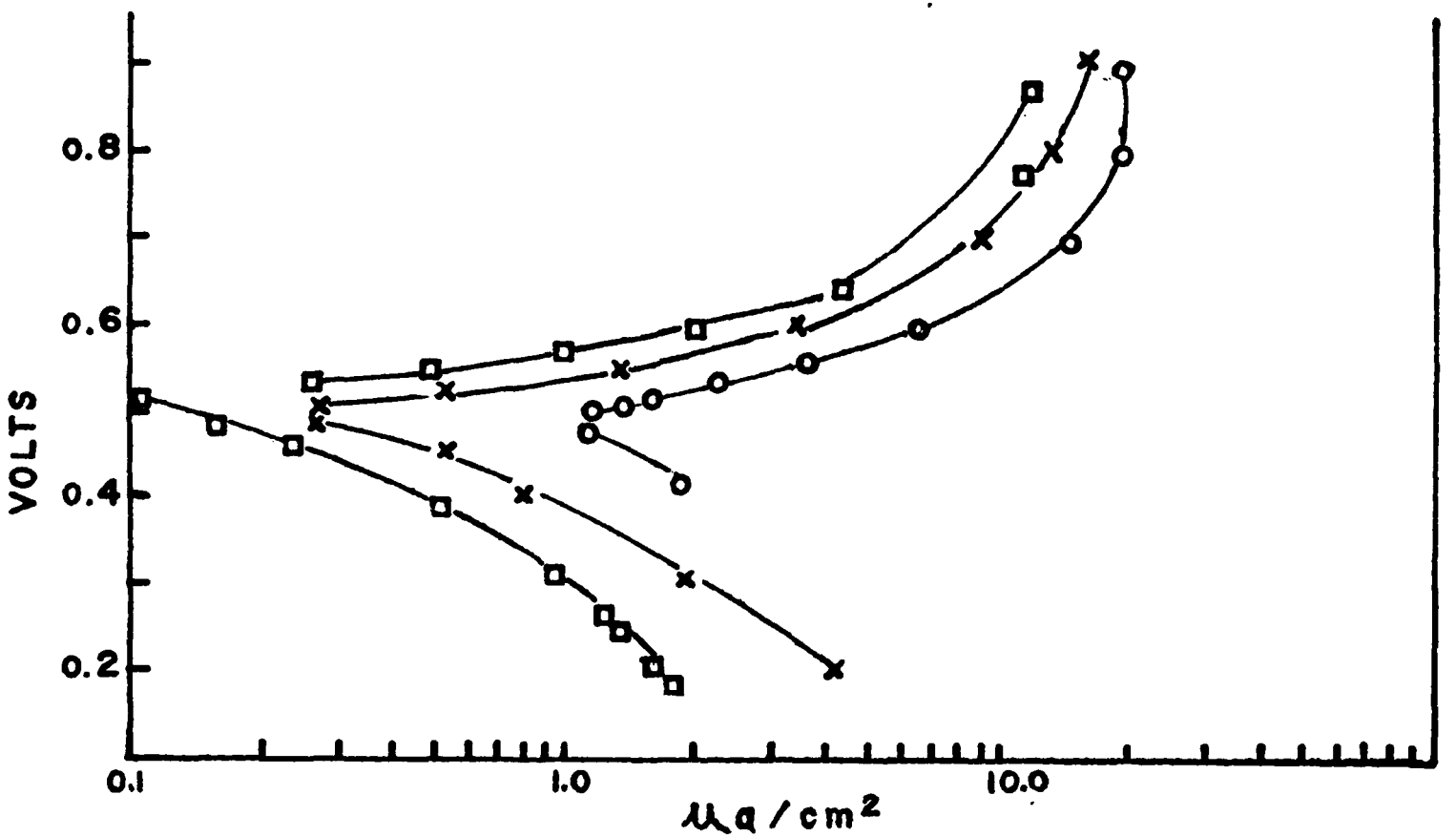

○ - 55°C
□ - 95°C
× - 115°C

Figure 9. Polarization curves for He in $CF_3SO_3H \cdot H_2O$ at 55, 95, and 115°C

anodic charging curves were identical with the initial anodic charging curve. There was no indication of breakdown of the electrolyte over the potential range of the pulse.

2.3.1.1 Electrochemical behavior of H_2 in $CF_3SO_3H \cdot H_2O$

The open circuit potential of H_2 on a platinum electrode in $CF_3SO_3H \cdot H_2O$ gives a measure of the reliability of the dynamic hydrogen electrode reference system in $CF_3SO_3H \cdot H_2O$. This potential ideally should be zero. The open circuit potential of H_2 was measured at various temperatures for several separate runs prior to measurement of the polarization curves.

The average open circuit potential at 55° C was 26.4 mv ±7.8 mv, at 95° C was -8.4 mv ±12.4 mv, at 115° C was 17.5 mv ±10.8 mv. As is evident, the open circuit potentials produced by H_2 bubbled over a platinum mesh electrode vs. the dynamic hydrogen electrode in $CF_3SO_3H \cdot H_2O$, at all temperatures are well within the limits of accuracy (13). From the data it was concluded that the dynamic hydrogen electrode system is an acceptable reference system for half cell research work on $CF_3SO_3H \cdot H_2O$.

The polarization curves for H_2 at 55°, 95° and 115° C in $CF_3SO_3H \cdot H_2O$ are shown in Figure (10). The anodic hydrogen reaction is the oxidation of molecular hydrogen according to the reaction:

$$H_2 \rightarrow 2H^+ + 2e^-$$

The limiting current values are typical for the anodic hydrogen reaction. The diffusion rate of molecular hydrogen establishes a limiting diffusion current density, i_d, and the rate of dissociation or adsorption establishes the total limiting reaction current density, i_r.

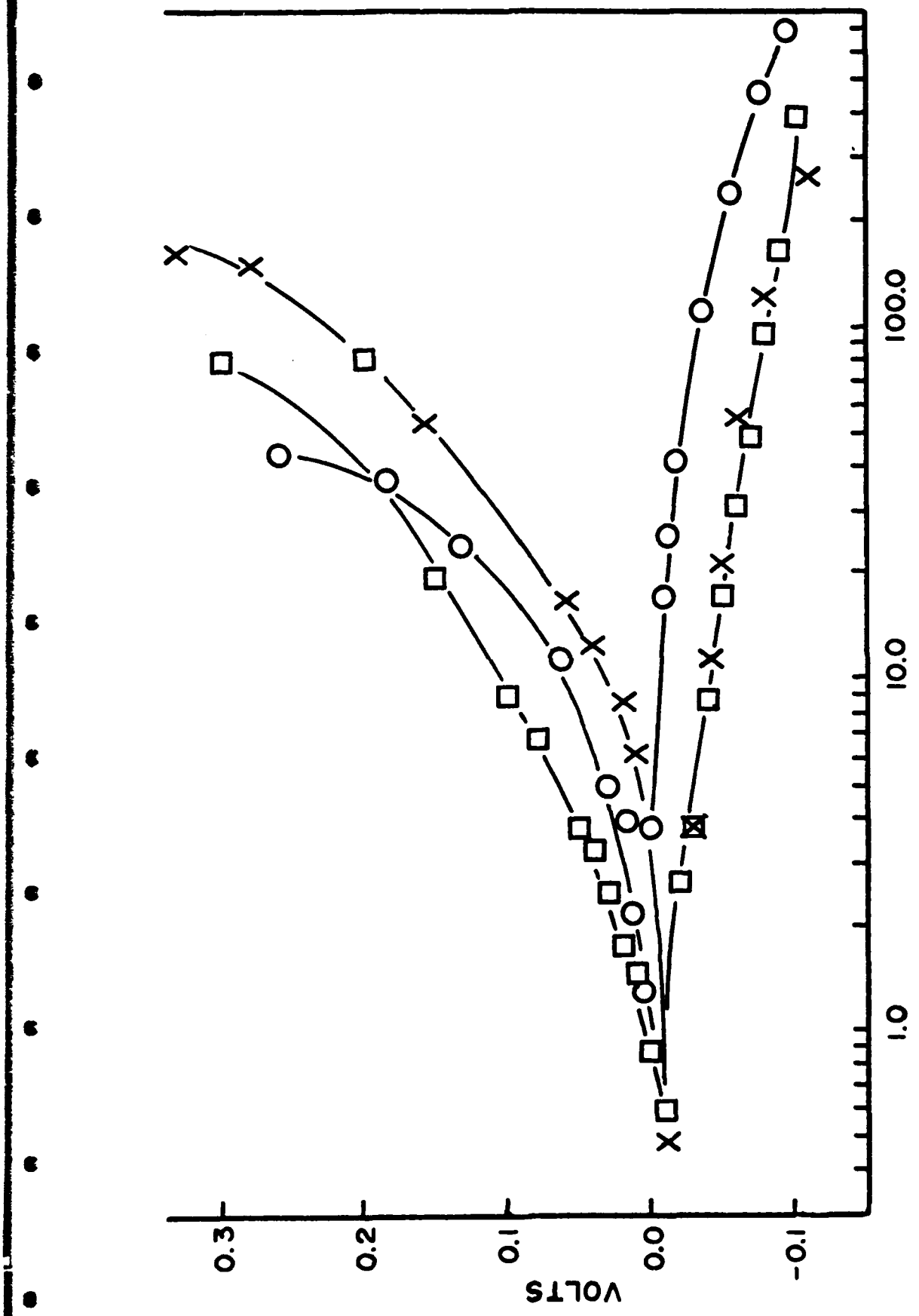

Figure 10. Polarization curves for H_2 in $CF_3SO_3H \cdot H_2O$ at 55°, 95°, and 115°C.

O-55°C; □-95°C; X-115°C

For the anodic reaction at 115° and 95°C, respectively, Tafel slopes of 0.16 and 0.14 were calculated from the slope of voltage versus log current density. Corrected to 25°C the Tafel slopes are 0.114 and 0.113. The Tafel slope, b, is equal to $\frac{2.3\ RT}{\alpha nF}$, where n is the number of charges transferred, R is the gas constant, T is the absolute temperature, F the faraday, and α the transfer coefficient dependent on the electrode material. The transfer coefficients at 115°C and 95°C are 0.48 and 0.52 for smooth platinum which appears to be reasonable.

On the cathodic side a cathodic limiting current density is not observed, which is consistent with previous experimental work (21). The cathodic reaction is the evolution of hydrogen from hydrogen ions. It is unnecessary to review the mechanisms for hydrogen evolution here. The Tafel slope, b, for the evolution of hydrogen at 95°C is 0.039. The current density values at various potentials for the reaction are quite high for both the anodic and cathodic reactions.

Comparison of the electrooxidation of hydrogen in phosphoric acid and in trifluoromethanesulfonic acid monohydrate

Figure 11 shows current density-potential plots for the oxidation of hydrogen in $CF_3SO_3H \cdot H_2O$ and in 85% H_3PO_4 at room temperature. The limiting current density value is produced in H_3PO_4 at a lower potential than in $CF_3SO_3H \cdot H_2O$. The limiting current value is reached after approximately 60 mv in 85% H_3PO_4 but not for approximately 120 mv in $CF_3SO_3H \cdot H_2O$. The limiting current density is somewhat higher for the reaction in $CF_3SO_3H \cdot H_2O$ than for the reaction in 85% H_3PO_4 -- approximately

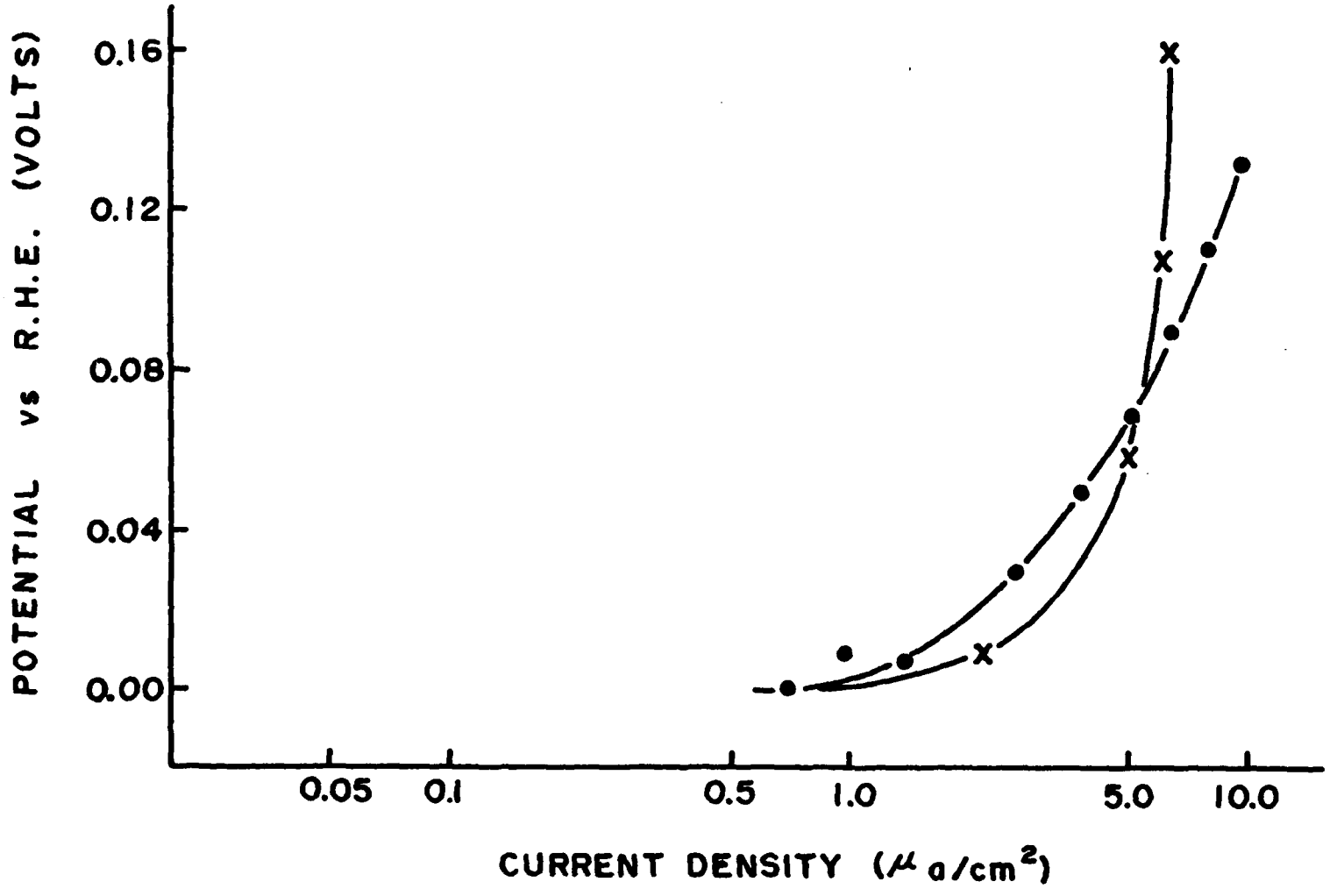

Figure 11. Current-potential diagrams for the hydrogen electrode at 23°C. X, 85% H_3PO_4; ●, $CF_3SO_3H.H_2O$

10 μamp cm^{-2}.

The current-potential behavior of hydrogen in phosphoric acid at 135°C was determined to make possible a comparison with the reaction in $CF_3SO_3H \cdot H_2O$. This comparison is shown graphically in Figure 12. The current density-potential curve for hydrogen at a platinum electrode in 85% H_3PO_4 electrolyte at 135°C is compared with curves in $CF_3SO_3H \cdot H_2O$ at 95°C and 115°C. The data are taken from previous progress reports (1) (4). The limiting current density for the hydrogen oxidation reaction in 85% H_3PO_4 at 135°C is approximately 20 μamp cm^{-2}. The limiting current densities for the reaction in $CF_3SO_3H \cdot H_2O$ at 95°C and 115°C are approximately 75 and 118 μamp cm^{-2}, respectively. Thus, at a temperature 20° lower, the oxidation rate in the new electrolyte is almost six times as rapid as in phosphoric acid.

2.3.1.2 The electrooxidation of hydrogen-3% CO

The electrooxidation of hydrogen-3% CO on smooth platinum was undertaken to support findings for the oxidation of hydrogen-3% CO on platinized platinum by G. W. Walker at MERDC, Ft. Belvoir. As is observed in Figure 13 there is a very short Tafel region observed for the electrooxidation of hydrogen-3% CO on smooth platinum in $CF_3SO_3H \cdot H_2O$. The current levels at any potential indicated that the current density levels on platinized platinum and smooth platinum are virtually identical. The current density levels at a potential are a factor of ten higher in $CF_3SO_3H \cdot H_2O$ than in 85% H_3PO_4.

In inorganic acids CO has been found to act as a poison to the electrode reaction for hydrogen. This is evidenced by an increase in

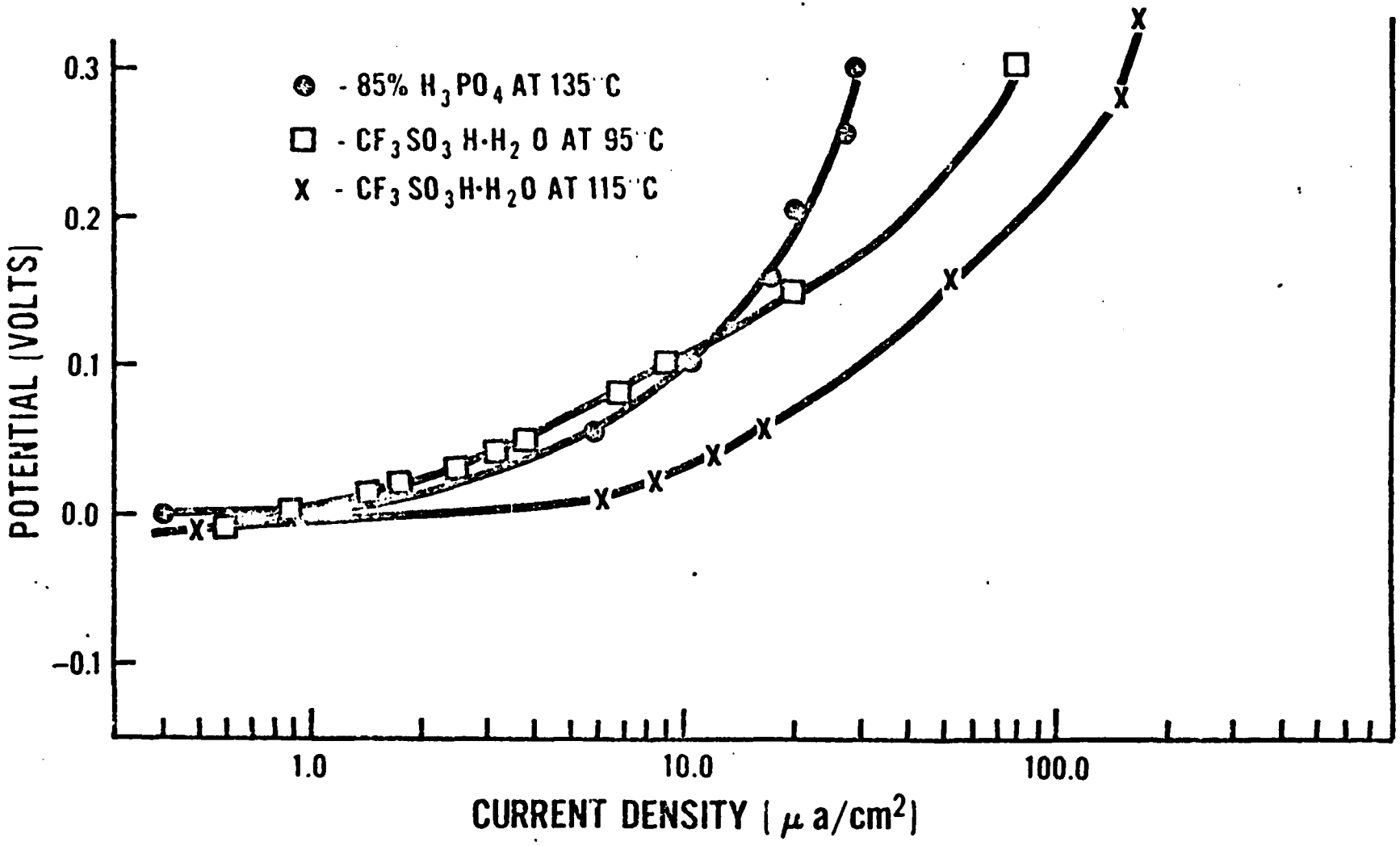

Figure 12. The current density-potential curve for hydrogen at a platinum electrode in 85% H_3PO_4 electrolyte at 135°C compared with H_2 in $CF_3SO_3H \cdot H_2O$ electrolyte at 95°C and 115°C.

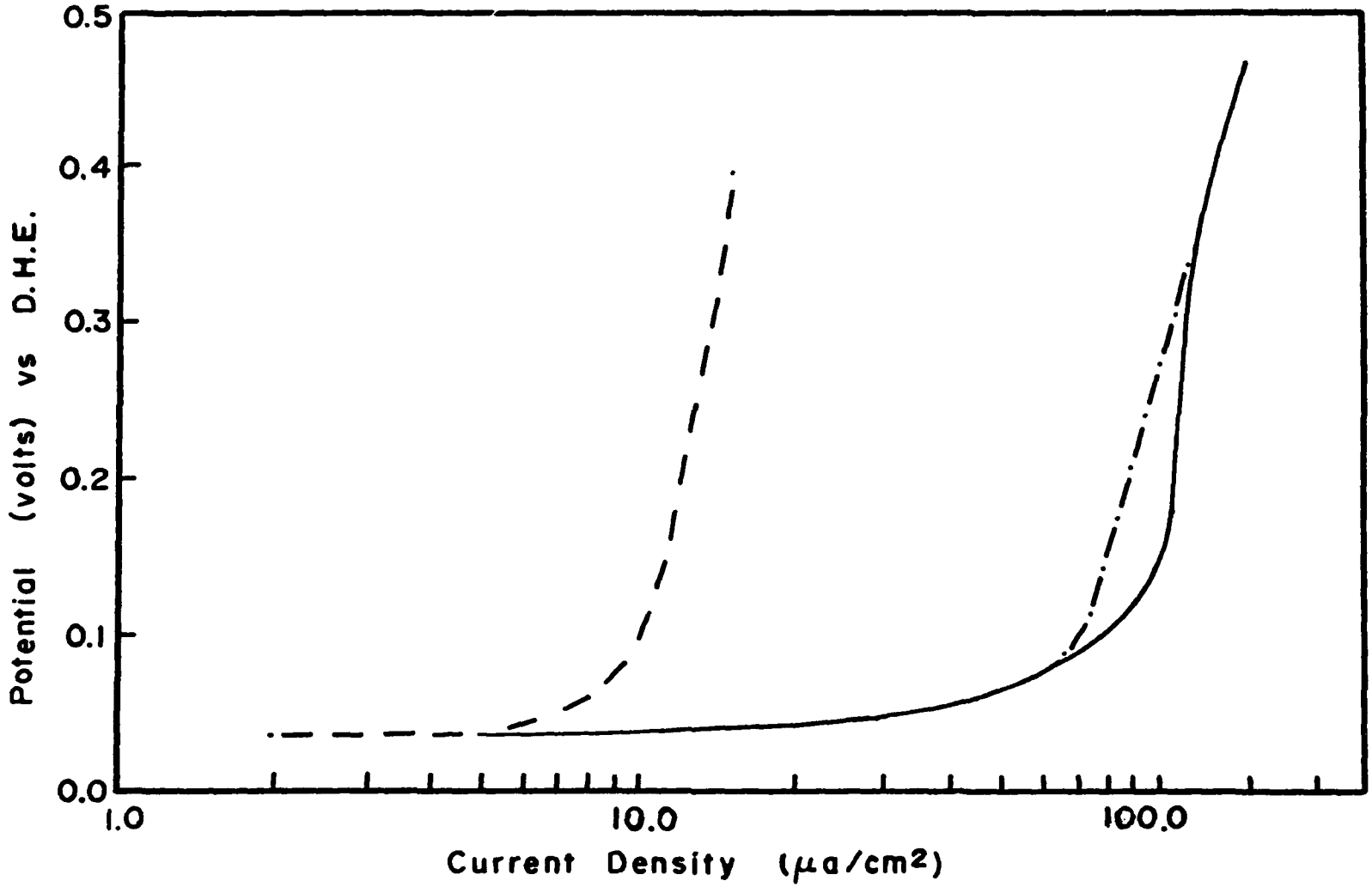

Figure 13. Electrooxidation of 3% CO-H_2-mixture in $CF_3SO_3H \cdot H_2O$ at 115°C

– – – – – 85% H_3PO_4; – · – · – · – Platinized Pt; ———— Smooth Pt.

open circuit potential and a decrease in current density levels at a set potential on potential cycling. In this case, CO appears to act more as a diluent to H_2 than as an electrode poison.

In Figure 14 the temperature dependence of the oxidation of hydrogen-3% CO from 25° to 115° C is shown. The behavior of the reaction is what would be expected; increased activity is observed with increased temperature.

2.3.1.3 Electrochemical behavior of propane in $CF_3SO_3H \cdot H_2O$.

The current-potential behavior for propane at 95°, 115°, and 135° C is summarized in Figure 15. It is assumed that the overall anodic reaction is the oxidation of propane to carbon dioxide. However, from the current-voltage curves alone it is not possible to establish the mechanism for the oxidation process.

At 95° C the limiting current value is approximately 24 μamp cm^{-2}. At 115° C the limiting current value is approximately 17 μamp cm^{-2}. The two curves are quite close to one another. The limiting current value at 135° C is approximately 82 μamp cm^{-2}. The results at 135° C in $CF_3SO_3H \cdot H_2O$ will be compared with the results in 85% H_3PO_4 and discussed later. On examination of Figure 15, it is visible that as the temperature increases the current density values at each potential are higher, as expected. At 95° and 115° C the current density values did not show a decline at more anodic potentials or were not run far enough to show the characteristic hydrocarbon anodic curve clearly visible at 135° C.

Figure 16 shows the current density-potential plot for the oxidation of propane in $CF_3SO_3H \cdot H_2O$ at ambient temperature. These results can be compared in a general way to the oxidation of propane in 85% H_3PO_4.

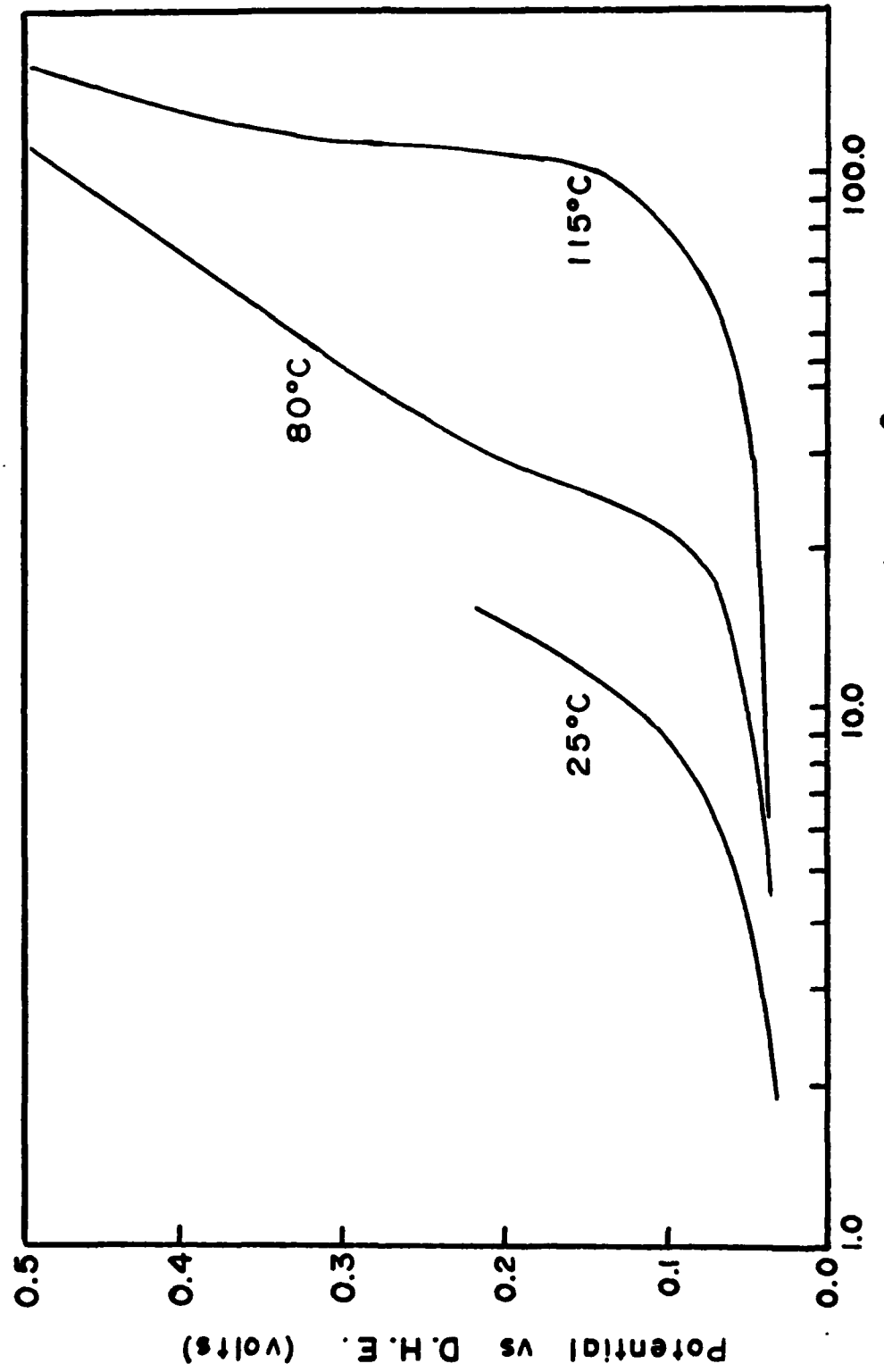

Figure 14. The temperature dependence of the oxidation of 3% $CO-H_2$ mixture

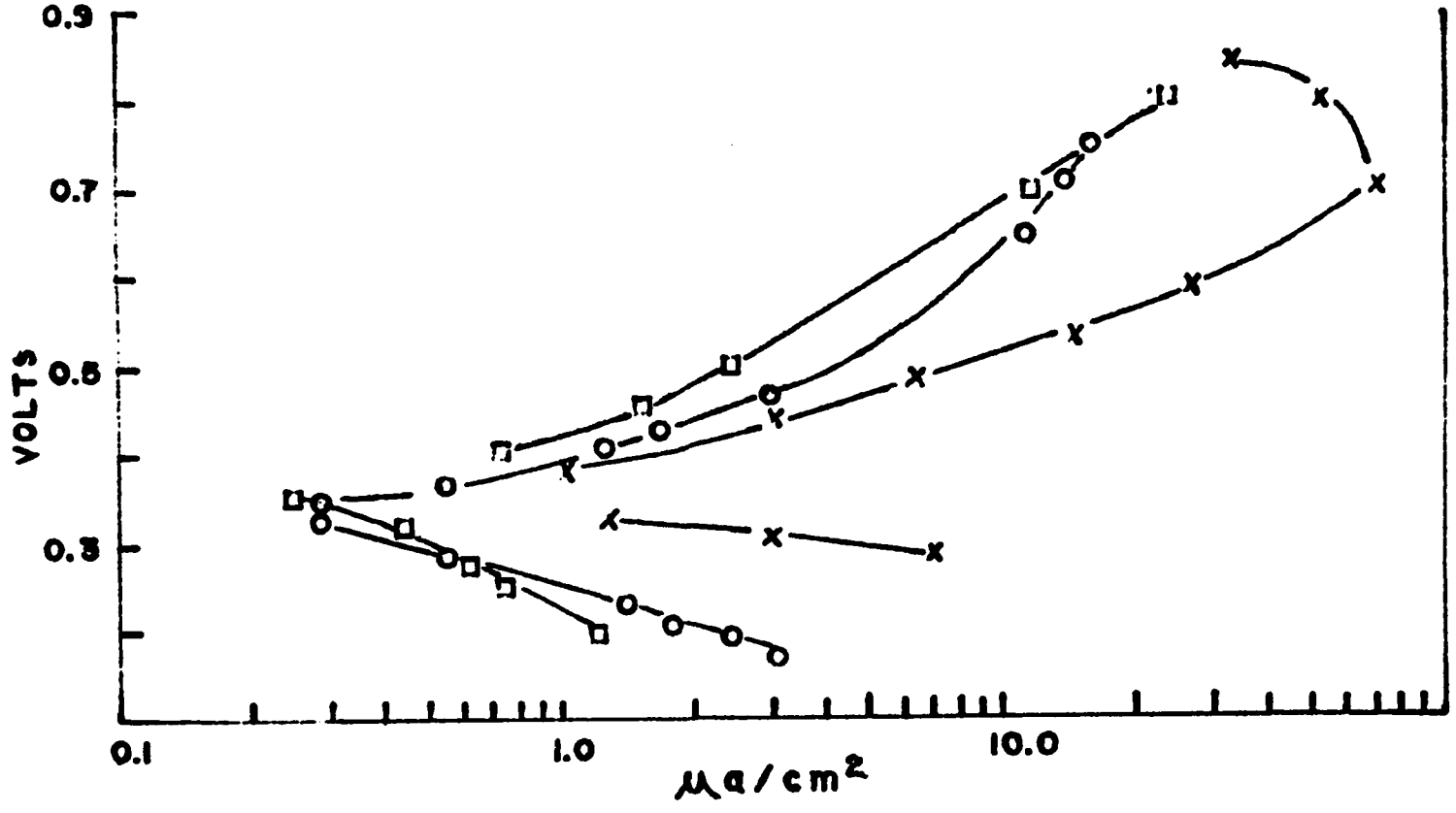

□ - 95°C
○ - 115°C
× - 135°C

Figure 15. Polarization curves for propane in $CF_3SO_3H \cdot H_2O$ at 95, 115, and 135°C

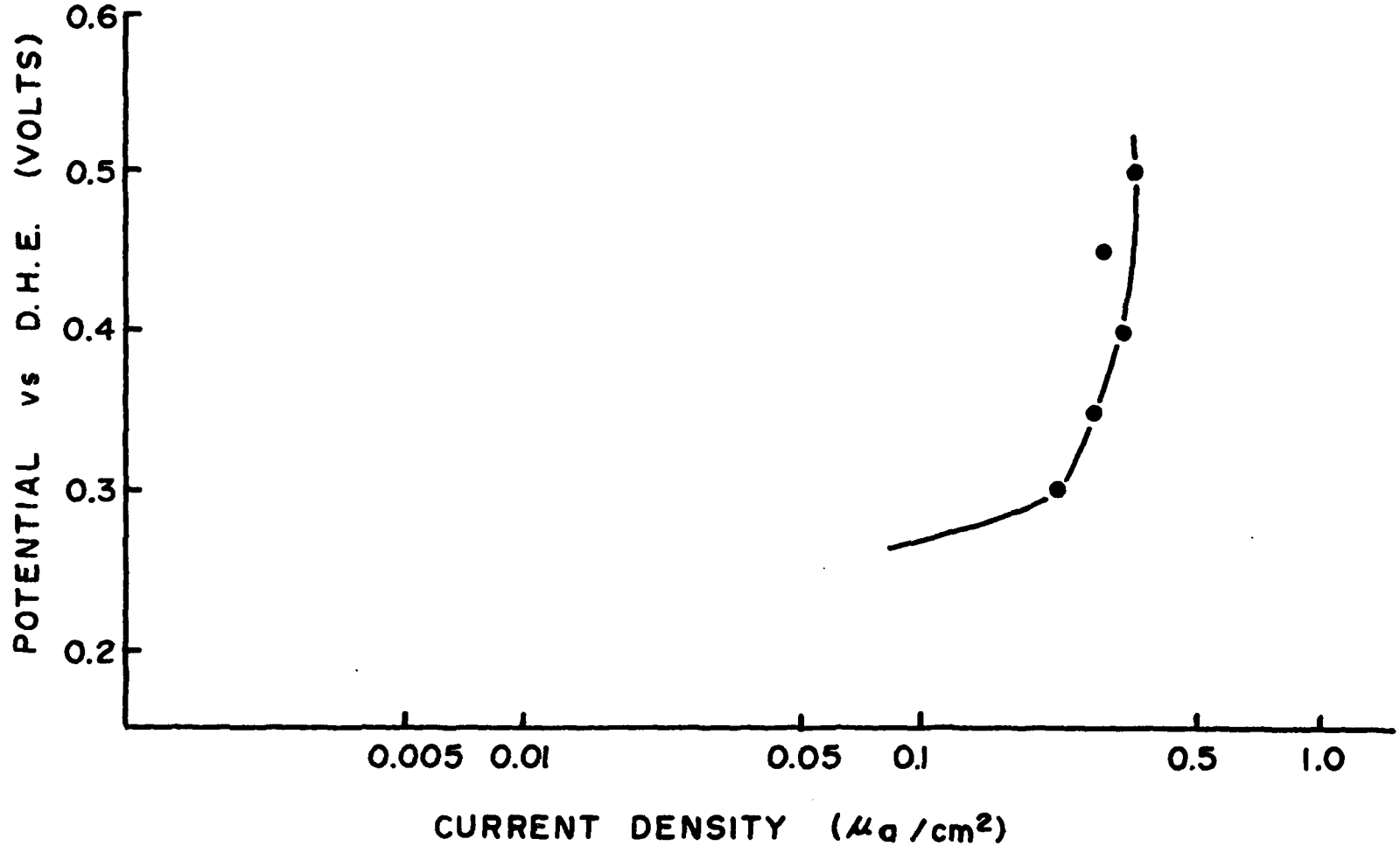

Figure 16. Current-potential diagrams for the electrooxidation of propane in $CF_3SO_3H.H_2O$ at 23°C.

The conductivity of phosphoric acid at room temperature is quite low and the current values were low and erratic. The open circuit potential is approximately 0.28 volts and the limiting current density is approximately 0.37 $\mu amp\ cm^{-2}$ for the oxidation of propane in $CF_3SO_3H \cdot H_2O$.

The temperature dependence of the current density is shown in the Arrhenius-type plot of Figure 17. In this plot the logarithm of the current density at 0.5 volts is plotted versus the reciprocal of the absolute temperature. The overall activation energy is composed of the activation enthalpy, $\Delta H^{\ddagger}$, and the term $\alpha nF\eta$, where α is the transfer coefficient, n is the number of charges transferred, F is the Faraday, and η is the overpotential. The relationship is given as:

$$\frac{d \ln i}{d t} = \frac{\Delta E_A}{RT^2} = \frac{\Delta H^{\ddagger} + \alpha nF\eta}{RT^2}$$

The energy of activation for the oxidation of propane in various electrolytes has been given as 16 kcal/mole, where $\Delta H^{\ddagger}$ and $\alpha nF\eta$ are considered equal (22).

The value for the activation energy for the oxidation of propane in $CF_3SO_3H \cdot H_2O$ can be calculated from Figure 17 to be 13 kcal/mole. This value is lower than the activation energies reported for other electrolytes (22), which would indicate that the oxidation process of propane has less "barrier" energy to overcome in $CF_3SO_3H \cdot H_2O$, a very desirable feature. The reason for the decrease in the activation energy is not apparent from these data, however, the implications of this lower activation energy may be cited. To achieve a reaction rate equivalent to that observed in $CF_3SO_3H \cdot H_2O$ at 135° C, it would be necessary to operate the electrode in 85% H_3PO_4 at 262° C.

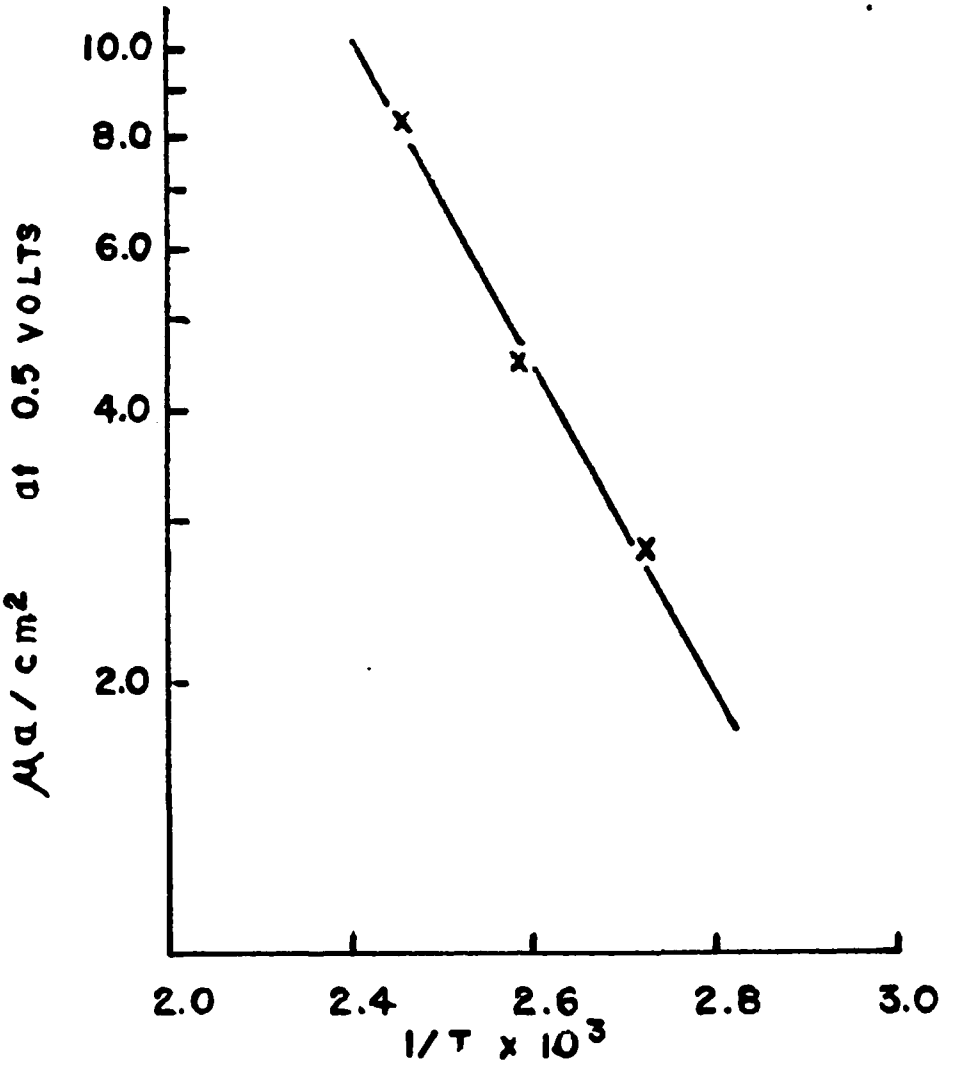

Figure 17. Temperature dependence of current density for anodic oxidation of propane in $CF_3SO_3H \cdot H_2O$

The results of experiments performed to this point suggest that the mechanism by which the electrooxidation of propane proceeds in $CF_3SO_3H \cdot H_2O$ is quite different from that in H_3PO_4. The elucidation of this mechanism would be important in the intelligent utilization of this electrolyte in fuel cells.

The shape of the galvanostatic anodic charging curve for propane in phosphoric acid exhibits a characteristic double wave profile. On the other hand, the galvanostatic anodic charging curve for propane in $CF_3SO_3H \cdot H_2O$ shows a single wave profile (compare upper and lower curves in Figure 18). The latter observation might imply the absence of an intermediate in the oxidation process or a different reaction mechanism in the two electrolytes.

The determination of the charge due to propane adsorption in phosphoric acid was made by the well-accepted treatment of anodic charging curves. In this technique the total anodic charge under helium is subtracted from the total charge under propane. The assumption is made that the charge corresponding to the oxidation of the electrode surface, the charging of the double layer, and the evolution of oxygen would be common for both helium and propane in $CF_3SO_3H \cdot H_2O$ and the technique could be employed to establish the adsorption characteristics of propane in this electrolyte.

Anodic charging experiments indicate that the difference between the total charge under helium and the total charge under propane in $CF_3SO_3H \cdot H_2O$ was very low, i.e., 50 μcoulomb cm^{-2} or less, at all adsorption potentials. Adsorption potentials from 0.20 to 0.6 volt were covered at 0.05 volt increments. Adsorption times from two

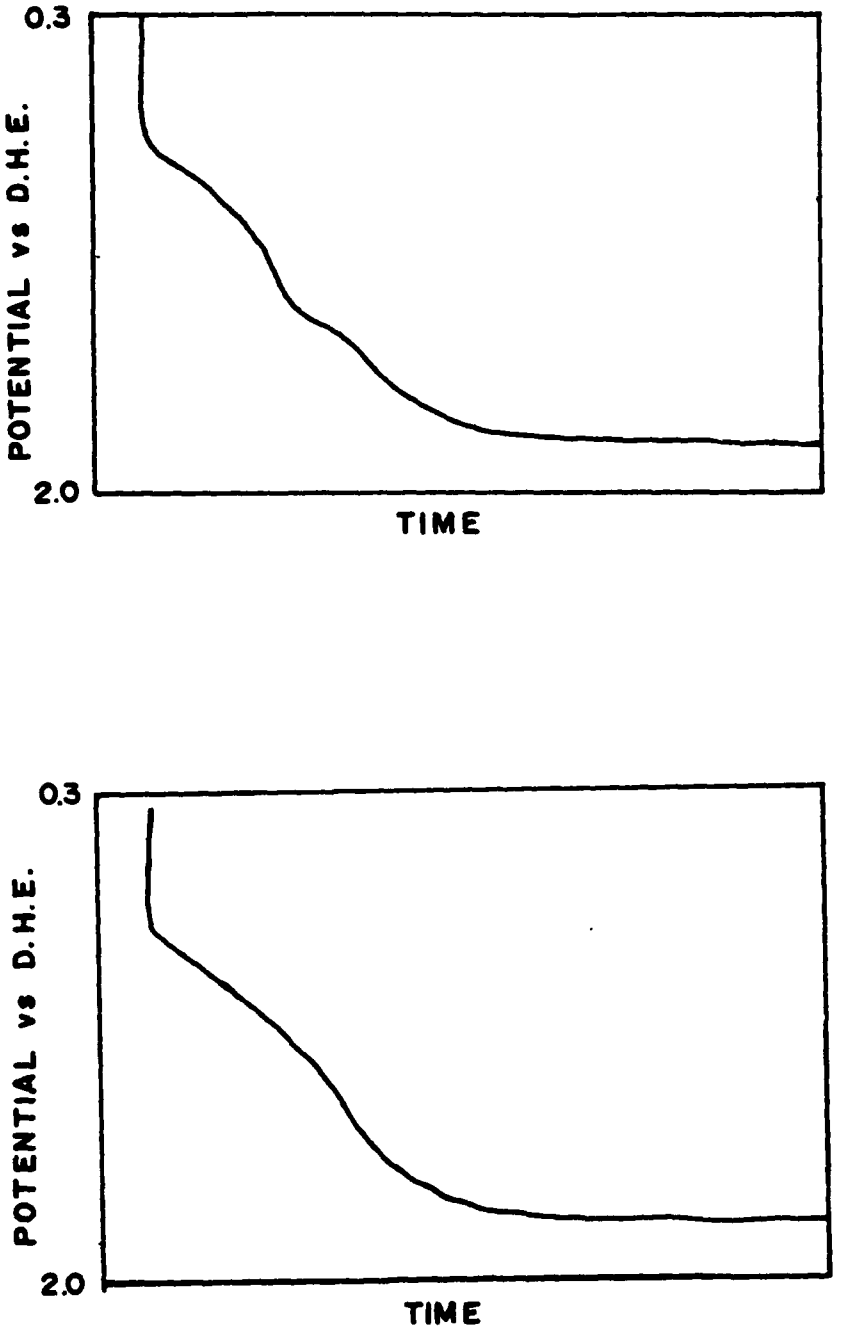

Figure 18. Galvanostatic charging curves
Upper; anodic charging curve (potential versus time) for the oxidation of propane in H_3PO_4; lower: anodic charging curve (potential versus time) for the oxidation of propane in $CF_3SO_3H.H_2O$.

minutes to ten minutes were used. These durations should be more than adequate to achieve optimum adsorption if experience with phosphoric acid is applicable. A charge of the order of magnitude 50 μcoulomb cm^{-2} must be considered as too low for accurate determination and in certain cases the measurements were within the limits of experimental error.

Since these measurements were difficult to interpret, an effort was made to expand our knowledge of propane adsorption using the potential ramp technique described in the Experimental Section 2.2.1, above.

The measurements included an adsorption range of 0.20 to 0.60 volts and adsorption times varying from 2 to 10 minutes. Typical curves for propane oxidation in the two comparison electrolytes are given in Figure 19. At all adsorption potentials and at all adsorption times a single oxidation peak was observed for the oxidation of propane in $CF_3SO_3H \cdot H_2O$. In 75% H_3PO_4 two oxidation peaks are clearly distinguishable (23). These results corroborate the results observed using the galvanostatic pulse technique (24).

A limited number of cyclic voltammograms were run to support the observations made with other techniques regarding the anodic oxidation of propane. A typical cyclic voltammogram is shown in Figure 20. This voltammogram was run after a 5 minute adsorption of propane at an adsorption potential of 0.30 volt. The single oxidation peak is observed at approximately 0.8 volt.

The three techniques, galvanostatic pulse, potential ramp, and cyclic voltammetry support the conclusion of the existence of a different reaction mechanism for the anodic oxidation of propane in $CF_3SO_3H \cdot H_2O$ as contrasted to that in H_3PO_4.

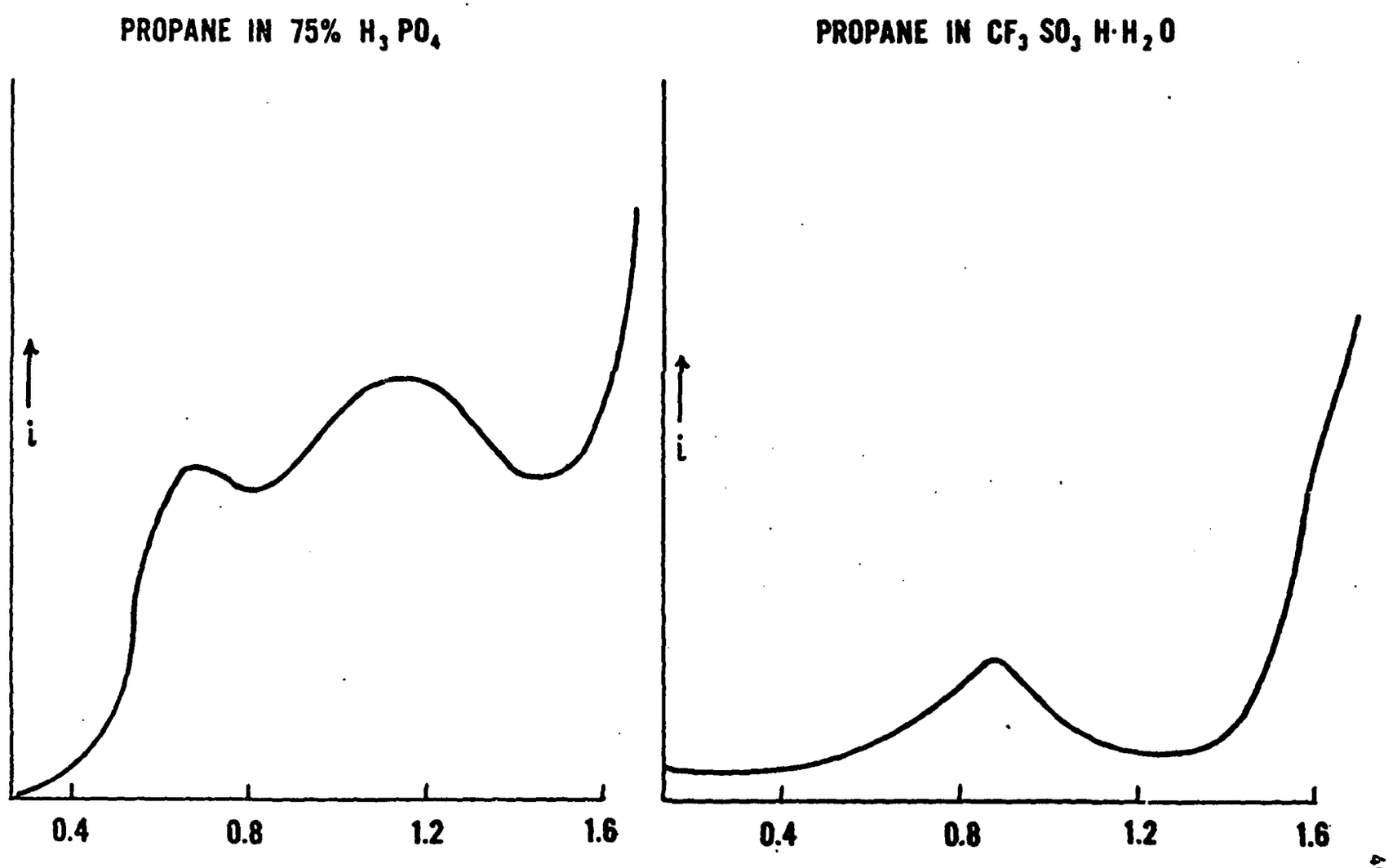

Figure 19. Anodic oxidation of propane in 75% H_3PO_4 and in $CF_3SO_3H.H_2O$ - Potential Ramp Technique

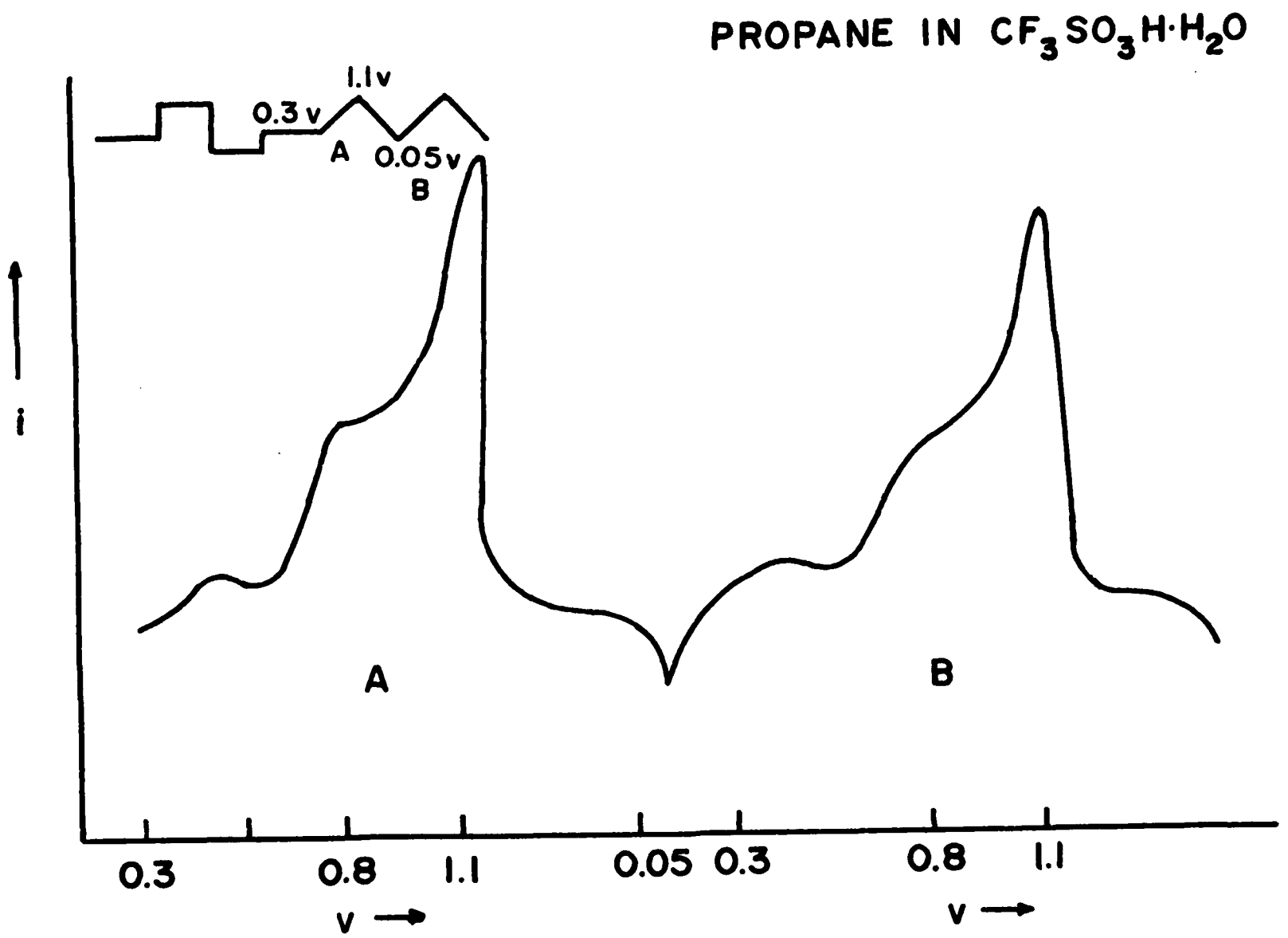

Figure 20. Anodic oxidation of propane in $CF_3SO_3H \cdot H_2O$ - Cyclic Voltammogram.

Experiments were run to study the decay of current density, at set potentials, with time. Three potentials were taken, 0.60, 0.65, and 0.75 volts, where current density values were found to be quite high. After one hour at a set potential the current densities declined to approximately 80-85% of the current density values after 5 minutes when the polarization data were taken. After one hour, the current values remained essentially constant over the length of the experiment, approximately 2.5 hours.

Trifluoromethanesulfonic acid monohydrate has been used in cells for as long as two months with no loss of performance noted. Current density levels at a set potential remain as high for electrolyte which has undergone numerous potential cyclings as a freshly prepared electrolyte sample. In many instances the electrolyte has also undergone temperature cycling as well as potential cycling.

2.3.1.4 Electrochemical behavior of "reduced" CO_2 in $CF_3SO_3H \cdot H_2O$

In the literature dealing with the electrooxidation of hydrocarbons on platinum electrodes, two types of intermediates have been identified by other investigators (15,25). One type is desorbed by a cathodic pulse while the second is not. The cathodically desorbable type is postulated to consist of hydrocarbon radicals or fragments of the larger molecule. The nondesorbable type of intermediate is postulated to consist of oxidized carbon and a polymeric compound.

Experiments were conducted with carbon dioxide as a reactant to establish whether or not the highly oxidized species observed in phosphoric, sulfuric, and perchloric acid were present on the electrode in $CF_3SO_3H \cdot H_2O$. Following the potential pretreatment steps outlined

in Figure 3b, CO_2 was adsorbed at a potential of 0.15 volt. Presumably, the adsorbed film at this potential would be similar to the highly oxidized intermediate observed in the anodic oxidation of hydrocarbons in inorganic acids (23). The subsequent anodic charging curve for "reduced" CO_2 in $CF_3SO_3H \cdot H_2O$ was similar to curves obtained with propane and helium. Also, all the anodic charging curves obtained for He, propane, and "reduced" CO_2 in $CF_3SO_3H \cdot H_2O$ were analogous to the "reduced" CO_2 anodic charging curve in H_3PO_4(26). These results would argue that species akin to the adsorbed polymeric species observed during the anodic oxidation of propane in phosphoric acid are not produced during the oxidation of propane in trifluoromethanesulfonic acid monohydrate.

2.3.1.5 Electrooxidation of methanol

The use of methanol as a fuel in a fuel cell system is attractive due to its low cost, ease of purification, and "clean" oxidation. Methanol was run as the fuel over a temperature range of 23° to 135° C. The air reaction was also run in the presence of methanol from 23° to 115° C.

Figure 21 shows the potential-current density plots for the electrooxidation of methanol (concentration one molar) at 23°, 80°, 115° and 135° C in $CF_3SO_3H \cdot H_2O$. Also shown in this figure are the results reported by Bagotzky and Vassiliev (27) for one molar CH_3OH in 1N H_2SO_4 at 80° C. At 23° C the open circuit potential is 0.4 volt and the limiting current density is 0.29 $\mu amp\ cm^{-2}$. Obviously the electrochemical activity of the system is quite low at ambient temperatures. At 80° C the open circuit potential is 0.375 volt and the limiting current density is about 4.0 $\mu amp\ cm^{-2}$. At 80° C the system was quite stable over a

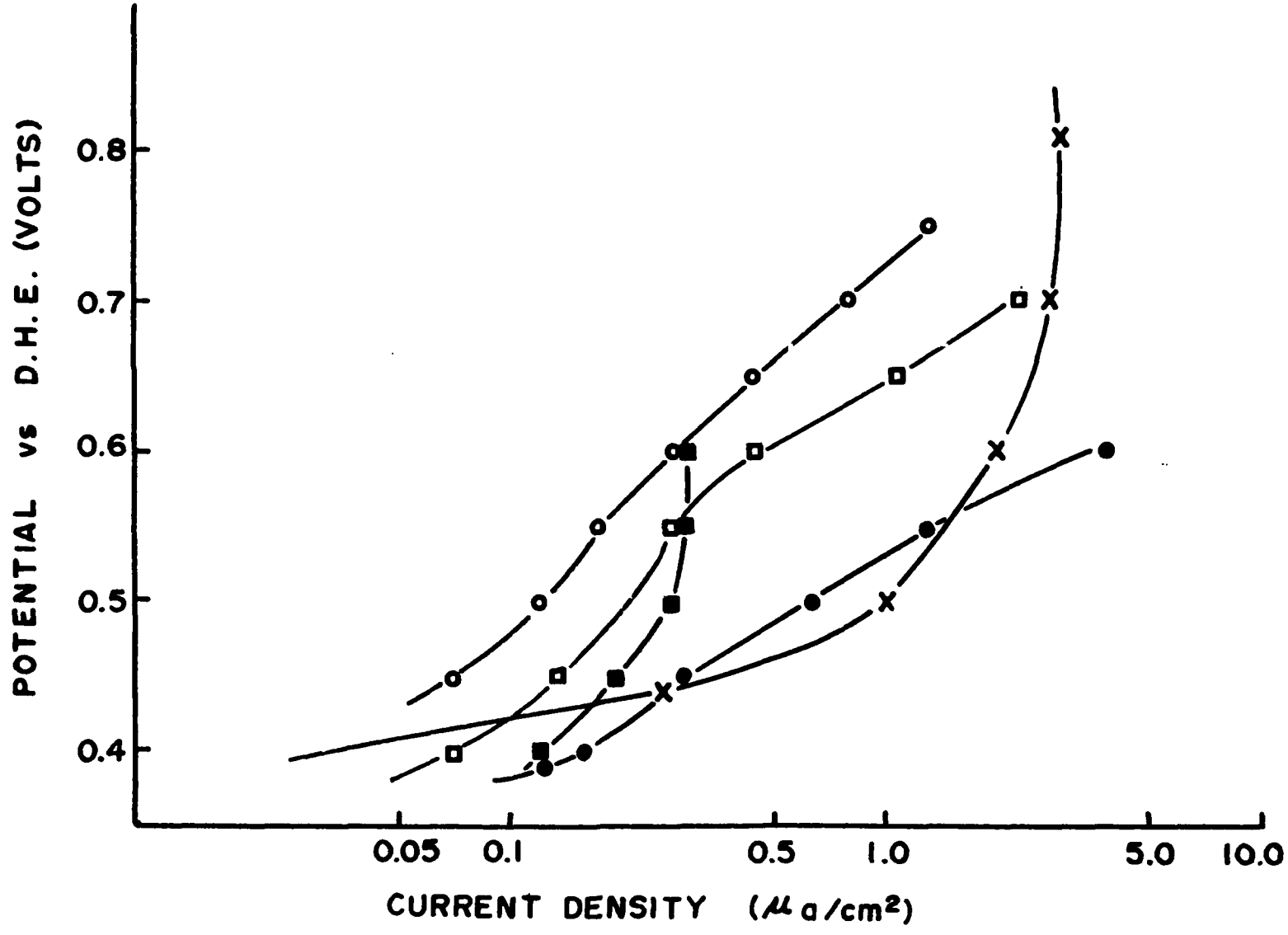

Figure 21. Current-potential diagrams for the electrooxidation of methanol. ■ , 23°C; ● , 80°C; □ , 115°C; ○ , 135°C; ✕ data from reference 27.

number of days indicating little loss of methanol due to vaporization from the cell containing a solution that was originally one molar in methanol. At 115° C the open circuit potential was 0.364 volt and the limiting current density about 2.2 μamp cm^{-2}. Some deterioration of current at a set potential over time was observed. At 135° C the open circuit potential was 0.365 volt and the limiting current density was 1.33 μamp cm^{-3} for freshly prepared solutions. The current density values were not reproducible from run to run, decreasing with time. After two days no electrochemical activity was evidenced by the solution. A second methanol-electrolyte solution of the same methanol concentration was prepared and similar results were observed at 135° C. From these experiments it was concluded that the vaporization of methanol became excessive at temperatures above 100° C. The nmr examination of solutions from cells held at 115° to 135° C showed a decline in height of the CH_3 peak from that measured in the initial one molar solution. This was indicative of a lowering of concentration of available CH_3 group in the electrolyte.

The methanol-air fuel cell has been treated thermodynamically (28). Calculations based on heats of reaction indicate that a cell will be maintained at 60° C by the exothermic heat produced in the cell. Thus the collection of data under 60° C is not encouraged. On the other hand the excess vaporization of methanol above 100° C would argue against going to a higher temperature to get enhanced oxidation.

Methanol has been shown to interfere with the electroreduction of air or oxygen in H_2SO_4 (29). The air reduction in a 1M MeOH - $CF_3SO_3H \cdot H_2O$ solution was run at temperatures from 23° to 115° C.

Figure 22 shows the electroreduction of air in $CF_3SO_3H \cdot H_2O$ and in 1M methanol-$CF_3SO_3H \cdot H_2O$ at 23° C. Figure 22 also shows the electroreduction of air in 1M MeOH - $CF_3SO_3H \cdot H_2O$ at 95° and at 115° C compared to the electroreduction of air in $CF_3SO_3H \cdot H_2O$ in the absence of methanol at 115° C. The addition of 1M MeOH to $CF_3SO_3H \cdot H_2O$ lowers the open circuit potential from 1.13 volts to approximately 0.78 volt. At any potential the current density for the air reduction is lowered by the addition of MeOH to the system. At 115° C there is less interference by the addition of 1M MeOH but it is still quite severe. These results correlate with those obtained in the experiments related to the anodic oxidation of MeOH. In those experiments, at higher temperatures , the rate of the electrooxidation of methanol was reduced.

Both results can be explained on the basis of the undesirable, excessive, vaporization of methanol at elevated temperatures.

Methanol was run as a vapor by passing helium through a methanol bath using the gaseous mixture as a fuel. It was desirable to use a porous electrode for this experiment, however, an appropriate porous electrode was not obtained. In a limited number of experiments methanol was run as a vapor on the wire electrode in the standard three-compartment cell. As would be expected, the current density levels were dependent on the flow rate of helium and the temperature of the methanol bath. The maximum current levels obtained, at the same temperature, were approximately the same as those obtained using 1M dissolved methanol. Further electrochemical work on methanol as a gaseous fuel was discontinued until a suitable porous electrode was developed.

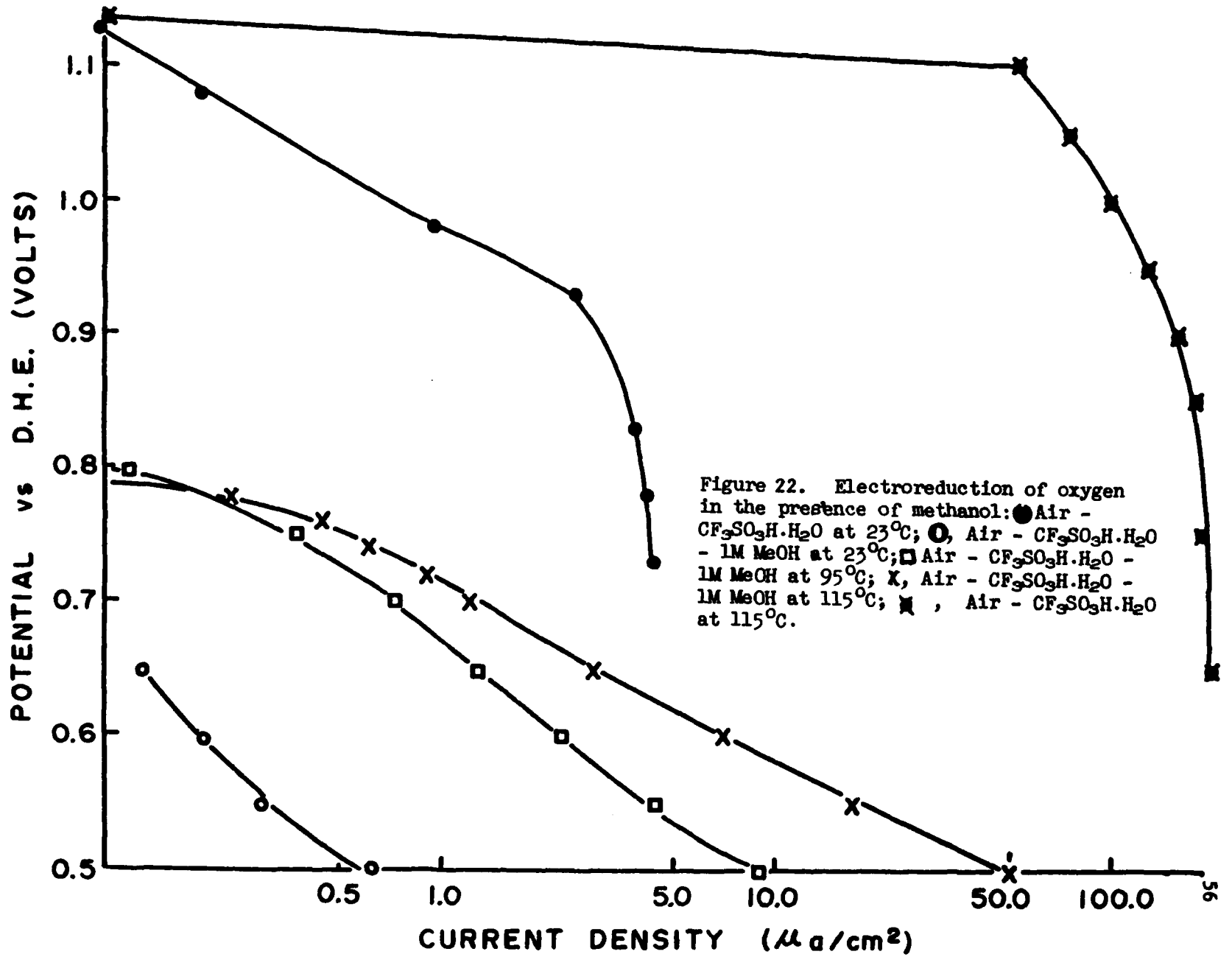

Figure 22. Electroreduction of oxygen in the presence of methanol: ● Air - $CF_3SO_3H.H_2O$ at 23°C; ○, Air - $CF_3SO_3H.H_2O$ - 1M MeOH at 23°C; □ Air - $CF_3SO_3H.H_2O$ - 1M MeOH at 95°C; X, Air - $CF_3SO_3H.H_2O$ - 1M MeOH at 115°C; ✖ , Air - $CF_3SO_3H.H_2O$ at 115°C.

2.3.1.6 Nuclear magnetic resonance measurements

The formation of esters by the reaction of CF_3SO_3H and several alcohols has been reported in the literature (2, 30). The reaction for CF_3SO_3H and C_2H_5OH is considered to be reversible at 150°C (5). No information was found for the reaction of $CF_3SO_3H \cdot H_2O$ and alcohols. Before electrochemical work was performed on the system, mixtures of methanol and $CF_3SO_3H \cdot H_2O$ were examined at room temperature with nmr. The nmr results showed the acidic H peak and peaks that would suggest the formation of the methyl ester.

A comparison of the nmr results corresponding to a known methyl peak from methyl alcohol and the unknown methyl peak from the methyl alcohol - $CF_3SO_3H \cdot H_2O$ mixture was made. The peak for the methyl group from CH_3OH occurs at 3.47 ppm. There is a shift of 0.644 ppm to 4.114 ppm for the CH_3 peak in the CH_3OH-$CF_3SO_3H \cdot H_2O$ mixture. This peak shift is convincing evidence for the formation of the methyl ester. There was no evidence of free methanol in methanol-$CF_3SO_3H \cdot H_2O$ mixtures containing up to 20 molar methanol. The formation of the ester appeared to proceed completely at room temperatures and there was a rapid exchange of all methyl groups making them equivalent.

The correlation between peak height and the concentration of methanol added to the acid monohydrate could be established. From these data it is possible to determine the concentration of MeOH added to the system, or remaining after electrochemical oxidation in the half cell.

2.3.1.7 Electrochemical reduction of air in $CF_3SO_3H \cdot H_2O$-current-density-potential diagrams

In the development of the hydrocarbon-air fuel cell the performance

of the air electrode is obviously as important as the hydrocarbon side. For that reason an investigation of the current-potential behavior of the air electrode in $CF_3SO_3H \cdot H_2O$ was conducted. These data were compared with data obtained for the reduction of air in 85% H_3PO_4. At room temperature the open circuit potential for air in $CF_3SO_3H \cdot H_2O$ is approximately 1.13 volts as compared to an open circuit potential of approximately 0.98 volt for air in H_3PO_4. This is comparable to results obtained at higher temperatures. The limiting current density is slightly higher for air in $CF_3SO_3H \cdot H_2O$ than for air in 85% H_3PO_4, i.e., 4.4 μamp cm^{-2} as compared to 2.8 μamp cm^{-2}. The significant feature seen in the comparison of the two electrolytes at 23° C is the higher open circuit potential. The limiting current density was much higher at higher temperatures, as would be expected.

The results on the electroreduction of air in $CF_3SO_3H \cdot H_2O$ on platinum mesh at 95°, 115° and 135° C are summarized in Figure 23. The results have been "normalized" for surface area and adjusted to the "average" open circuit potential. The "average" of the open circuit potentials was the average of the open circuit potentials observed for several current-potential runs at each temperature. The deviation from this average for each run was approximately 20 mv.

The current density values at a set potential increase with temperature as would be expected. The observed limiting current densities were:

135 μa/cm^2	at	95° C
170 μa/cm^2	at	115° C
190 μa/cm^2	at	135° C

It was observed during the course of running the current-potential

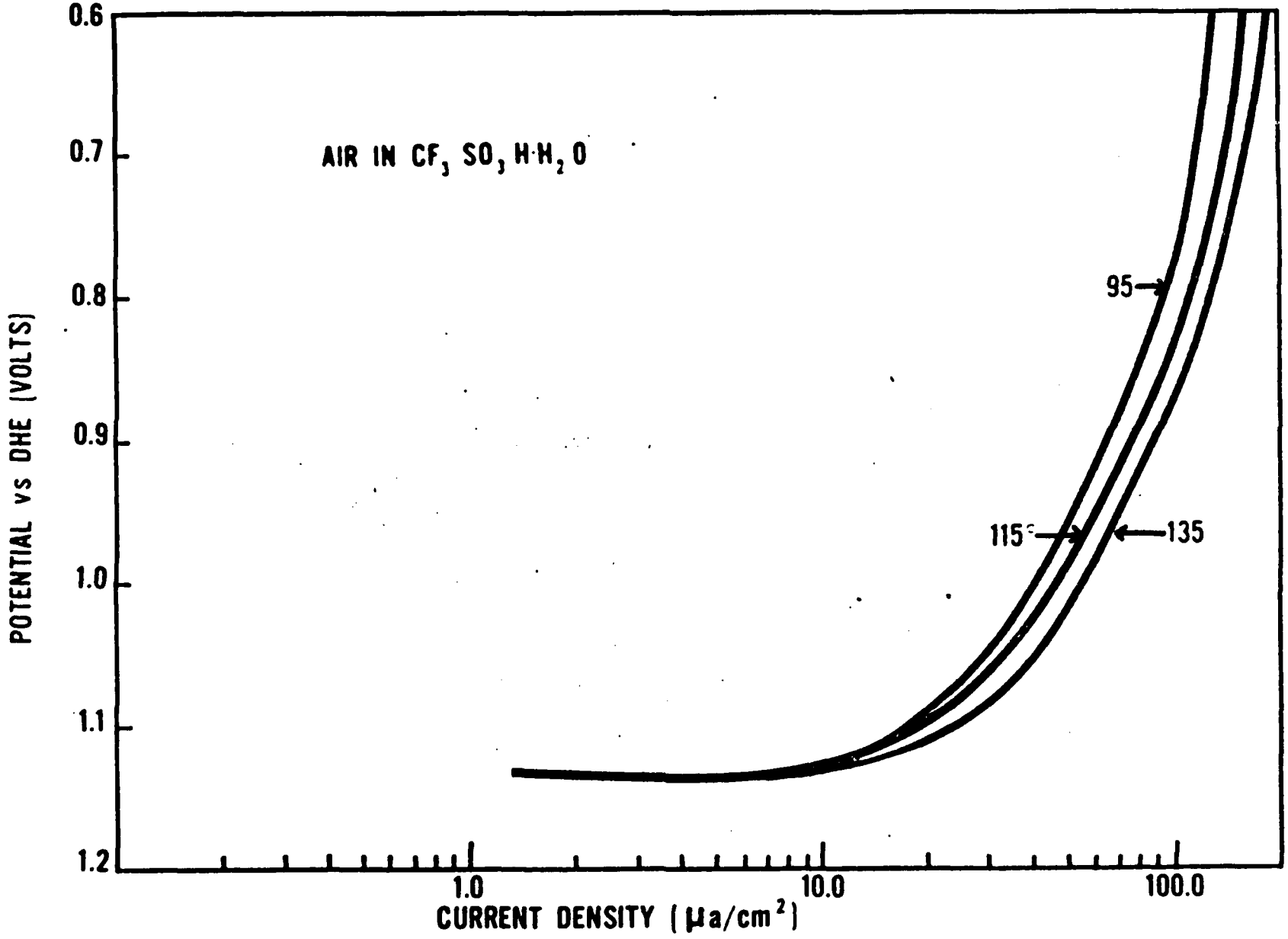

Figure 23. Electroreduction of air in $CF_3SO_3H \cdot H_2O$ at 95°, 115°, and 135°C.

curves that the open circuit potential increased during the first few runs toward the reversible thermodynamic oxygen potential. Following the first few runs the open circuit potential became stable during the remainder of the experiments. This effect is observed in the runs reported in Figure 24.

Figures 25, 26, and 27 compare the results for the reduction of air in $CF_3SO_3H \cdot H_2O$ with those for 85% H_3PO_4 at 95°, 115° and 135° C. At all temperatures the current carrying ability at any given potential is higher in $CF_3SO_3H \cdot H_2O$. The limiting current density is also higher in this electrolyte than in 85% H_3PO_4 although the dramatic enhancement observed for the propane reaction is not evident in the air reaction. The most significant feature of these plots is the higher open circuit potential (approximately 150 mv higher) for the air electrode in $CF_3SO_3H \cdot H_2O$ as compared with the open circuit potential in 85% H_3PO_4.

The open circuit potential for air in 85% H_3PO_4 reported here is approximately the same as that reported in the literature (31). The open circuit potential in inorganic acids, which is considerably lower than the thermodynamically calculated value, is usually regarded as a mixed potential.

Several models have been put forth to explain the difference between the thermodynamically calculated value and the observed mixed potential. These include the formation of peroxides during the oxygen reaction in acidic solution (32), the existence of Pt/PtO and PtO/PtO_2 couples (33), and a potential established by impurities, particularly organic impurities (34).

At the present time it would be a matter of speculation in attempting

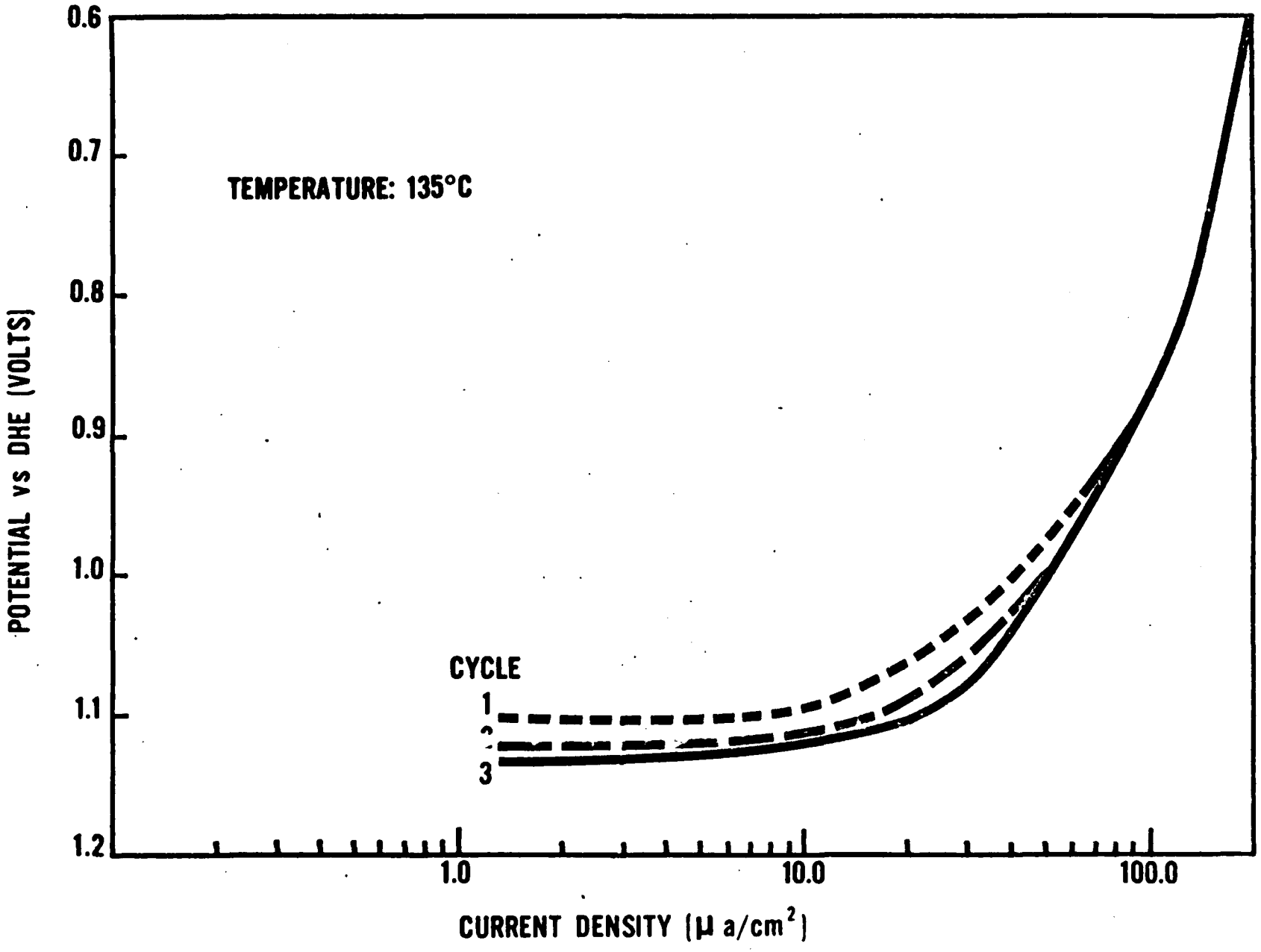

Figure 24. Electroreduction of air in $CF_3SO_3H.H_2O$. Change in open-circuit potential after first three runs.

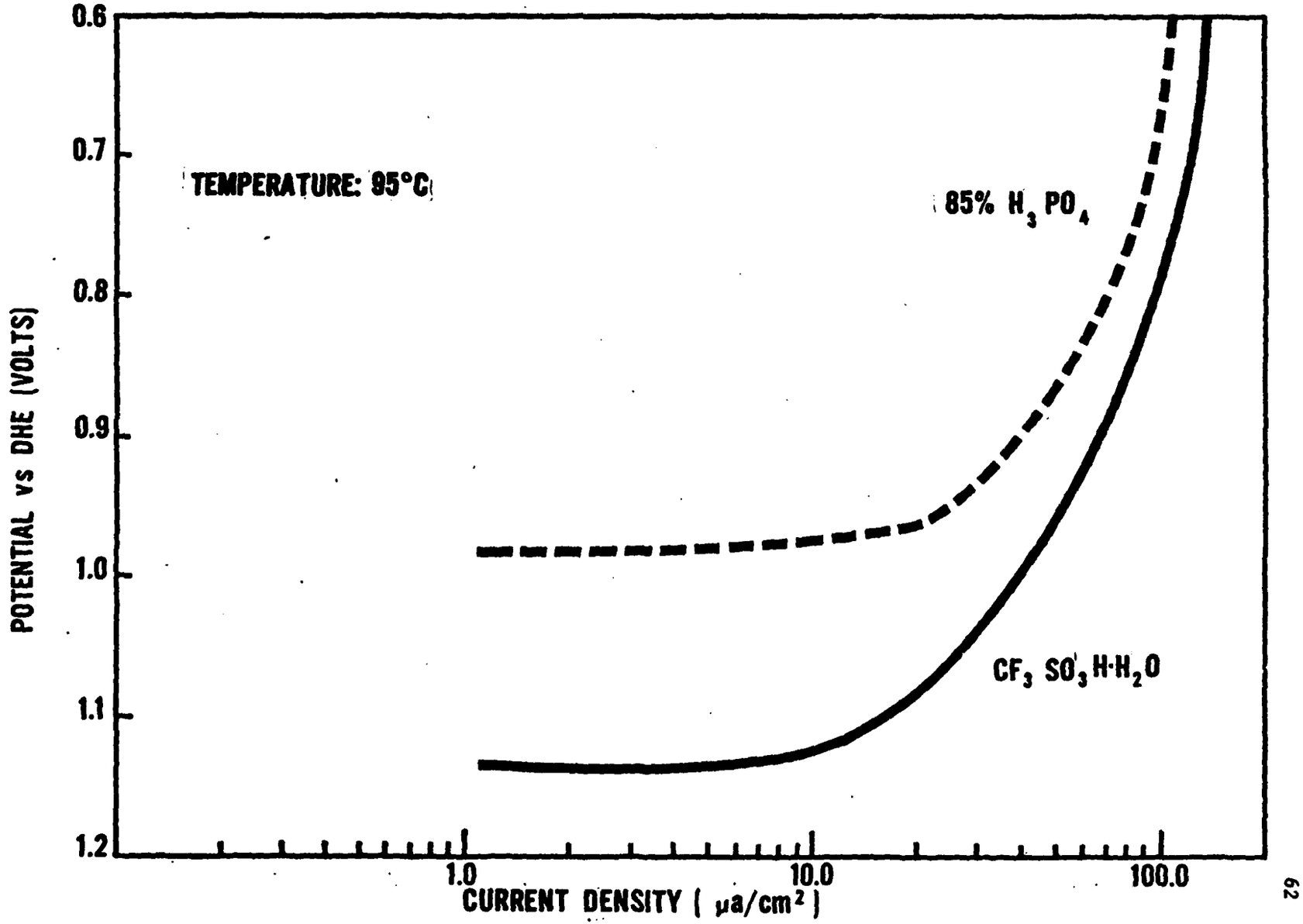

Figure 25. Electroreduction of air in $CF_3SO_3H.H_2O$ compared with reaction in H_3PO_4. Temperature 95°C.

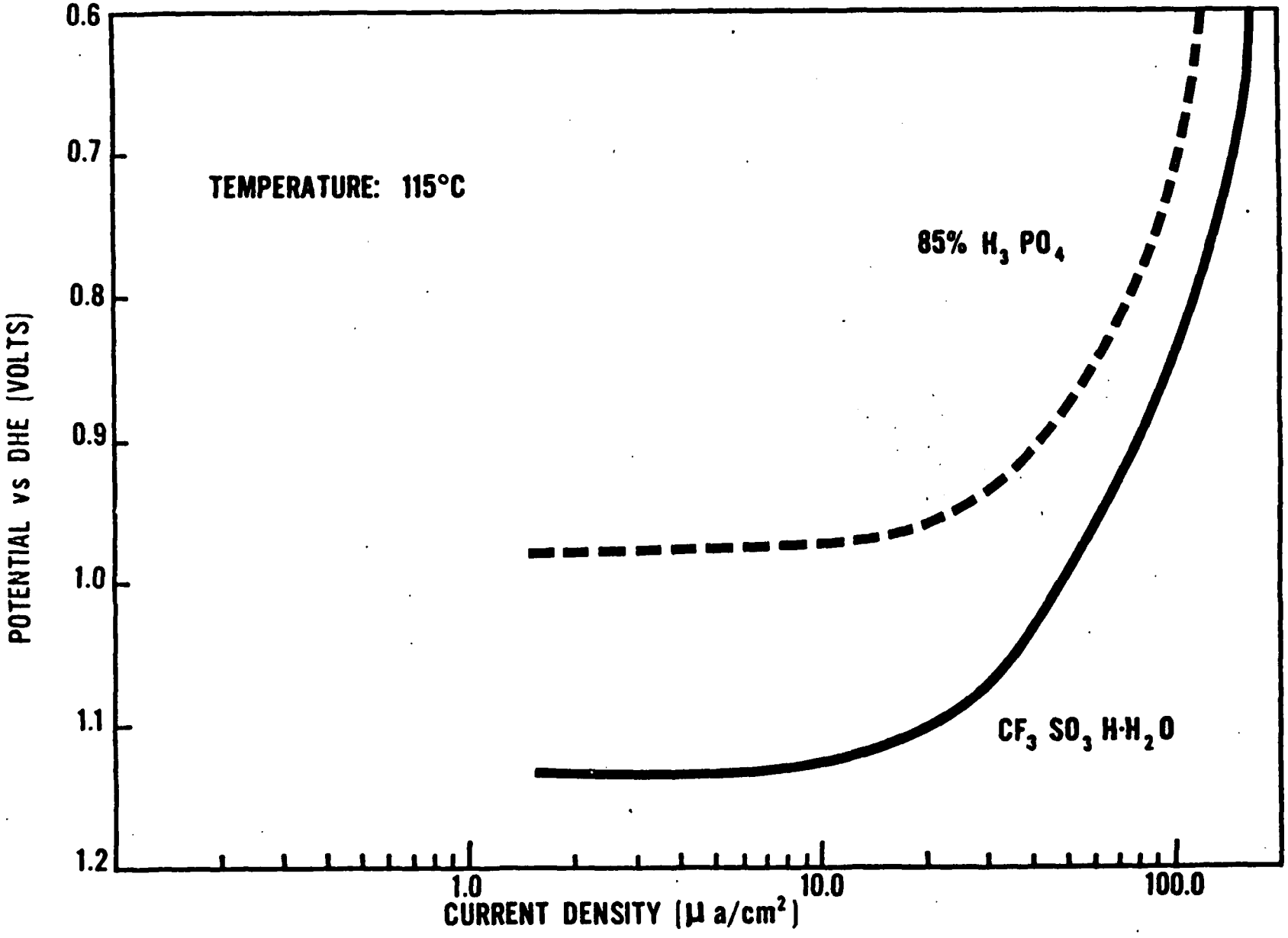

Figure 26. Electroreduction of air in $CF_3SO_3H.H_2O$ compared with reaction in H_3PO_4. Temperature 115°C.

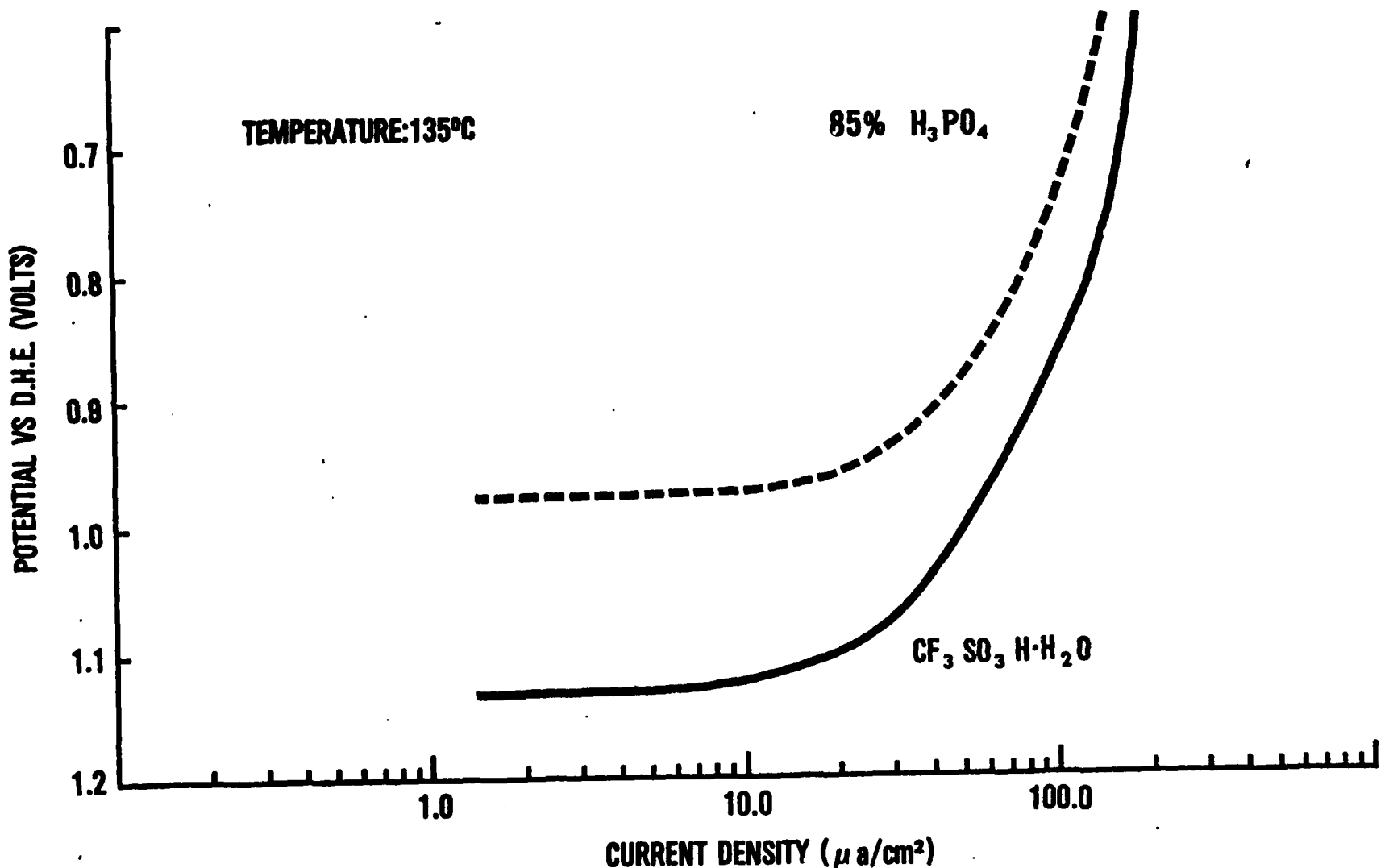

Figure 27. Electroreduction of air in $CF_3SO_3H.H_2O$ compared with reaction in H_3PO_4. Temperature 135°C.

to explain the higher potential for the air electrode in $CF_3SO_3H \cdot H_2O$.

The exchange current density calculated for the air electrode in $CF_3SO_3H \cdot H_2O$ is approximately 10^{-8} amp/cm^2. Literature values for the air electrode in 85% H_3PO_4 fall in the range of 10^{-10} to 10^{-7} amp/cm^2, the reported values depending considerably on impurities in solution and other factors. The Tafel slope calculated from the polarization curves in $CF_3SO_3H \cdot H_2O$ was 0.62 which is close to the value obtained from similar experiments in phosphoric acid.

The investigation of the air electrode in $CF_3SO_3H \cdot H_2O$ was extended to ascertain the effect of the flow rate of air on the open circuit potential and the limiting current of the electrode. The relationship between the open circuit potential and the flow rate at 135° C is shown in Figure 28. Above a flow rate of 20 ml/minute the open circuit potential is essentially independent of flow rate attaining a value of 1.13 volts. Below 20 ml/ minute the potential drops off and is erratic.

The relationship between limiting current density and the flow rate of air at 135° C is shown in Figure 29. The limiting current density was not greatly affected by the flow rate. The value for the limiting current density varied by only 6 μamp/cm^2 from a flow rate of 3 ml/minute to a flow rate of 40 ml/minute. From 20 ml/minute to 70 ml/minute, the limiting current density varied only by 3 μamp/cm^2 which is within the range of experimental error.

In Figure 30 the experimental observations on the air electrode and the propane electrode, in the two electrolytes, H_3PO_4 and $CF_3SO_3H \cdot H_2O$, both at 135° C, are brought together. It is clear that a higher potential difference is developed in the $CF_3SO_3H \cdot H_2O$ electrolyte. For example, at

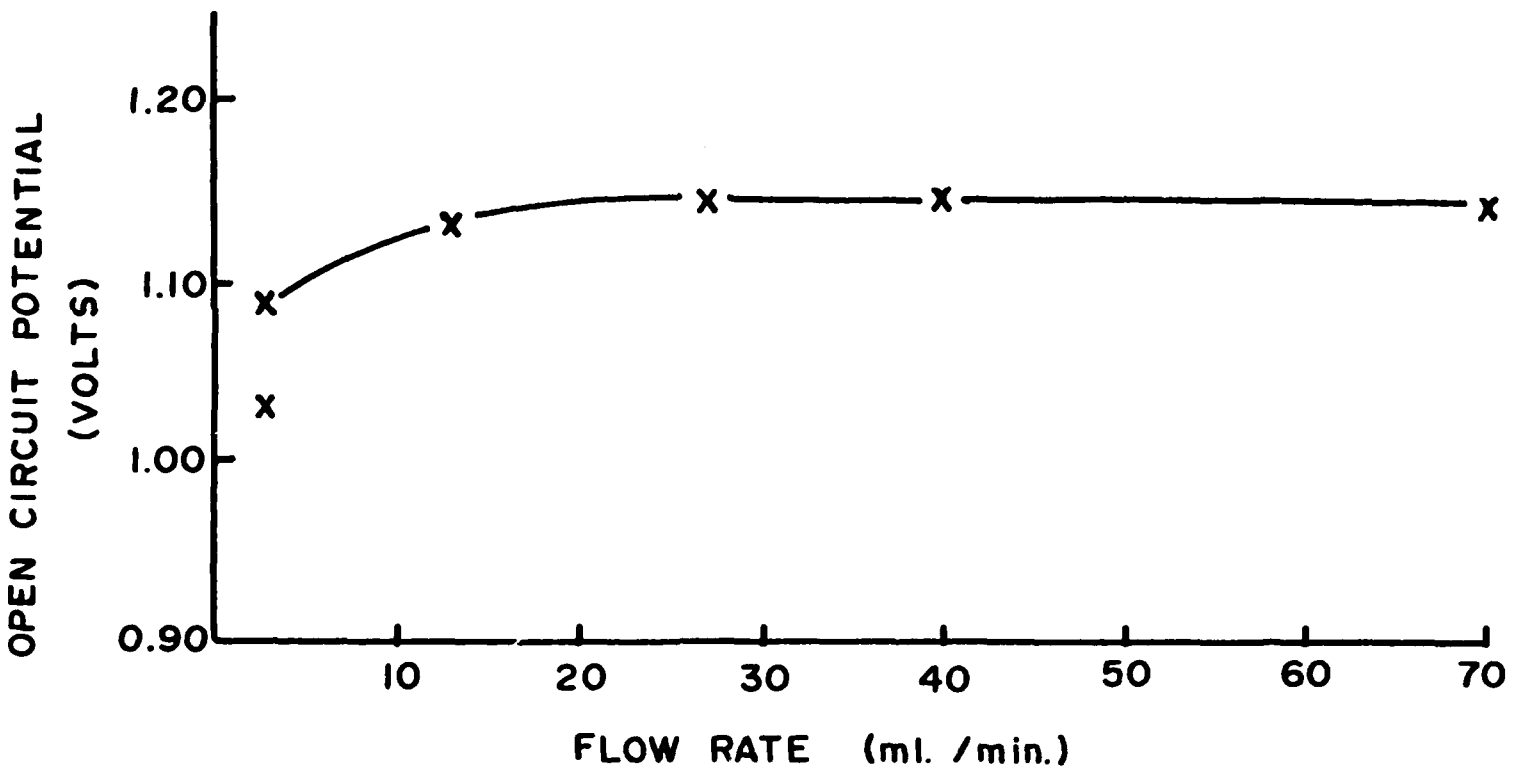

Figure 28. Relationship between open-circuit potential and flow rate of air. (Electrolyte $CF_3SO_3H.H_2O$, temperature 135°C.)

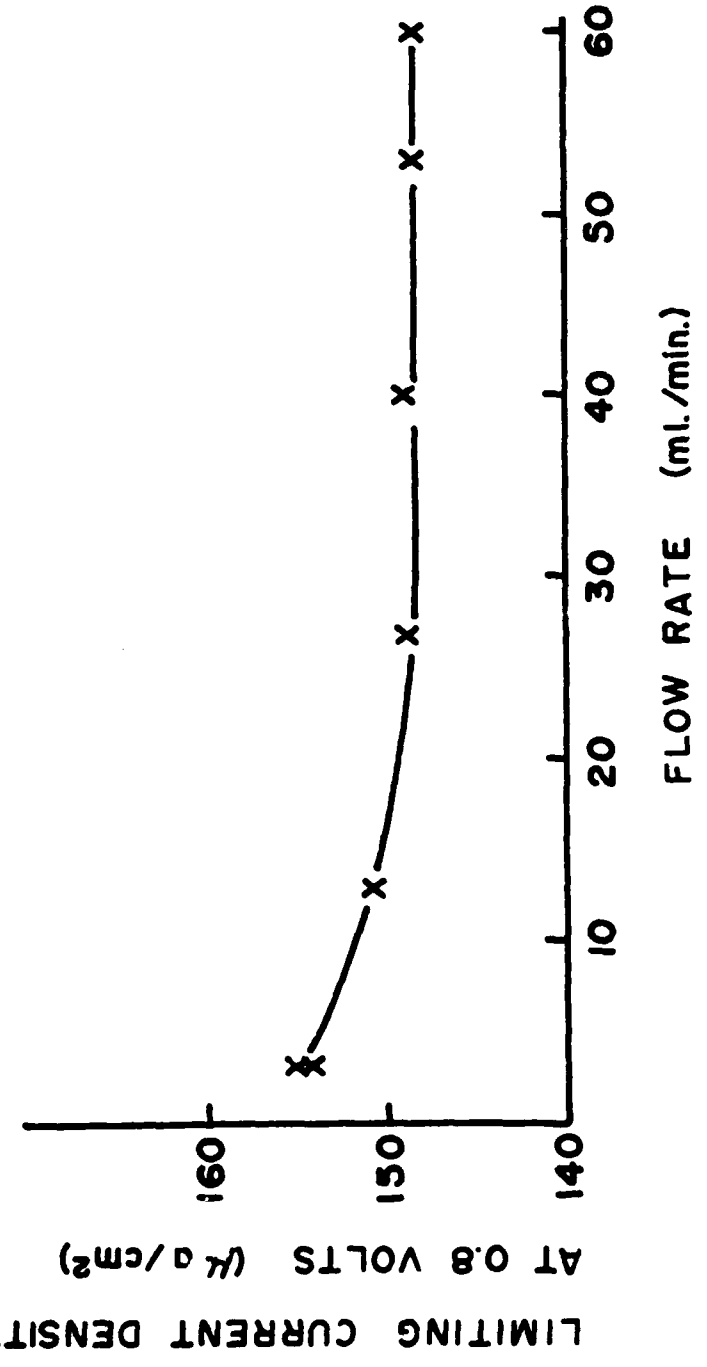

Figure 29. Relationship between limiting current density and flow rate of air (Electrolyte $CF_3SO_3H.H_2O$, temperature 135°C., potential 0.8 v.)

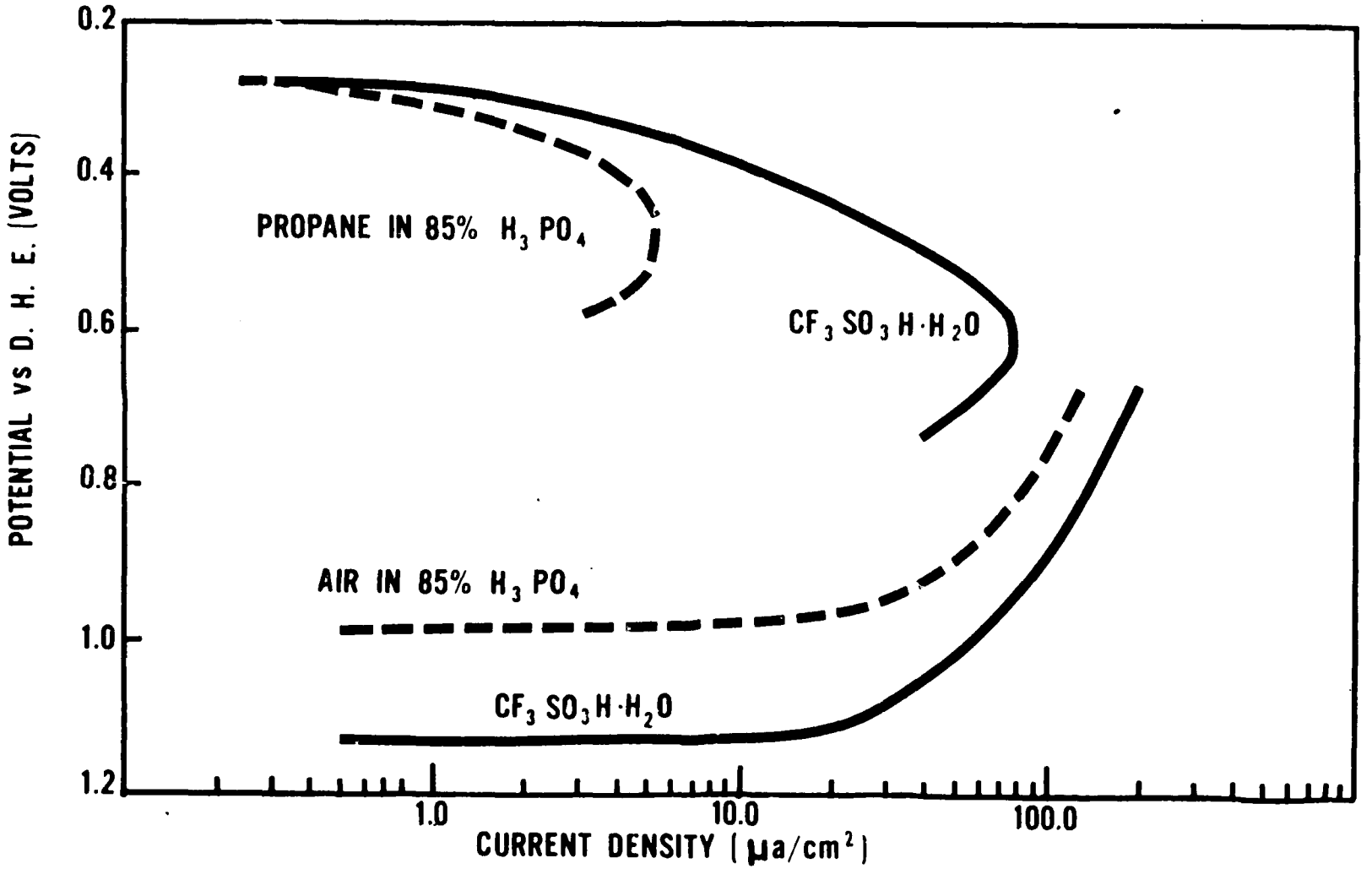

Figure 30. Current potential diagrams for propane and air compared for the two electrolytes, $CF_3SO_3H \cdot H_2O$ and H_3PO_4.

a current density of 1.0 μamp/cm^2 potential differences exist of

0.84 volt in $CF_3SO_3H \cdot H_2O$

0.76 volt in 85% H_3PO_4

or a difference of 170 mv. Correspondingly, at 4.0 μamp/cm^2, a 210 mv. potential difference exists.

2.3.2 Results with 85% H_3PO_4

Propane oxidation in H_3PO_4 was used to evaluate the experimental arrangement and the cell before a new electrolyte was introduced into the system. The data obtained with this system were used to evaluate the oxidation of propane in other electrolyte systems. It would be desirable that this reaction be at least as efficient in any new electrolyte tested.

The general shape of the galvanostatic anodic charging curves, Figure 31, agrees well with data previously reported (15, 35). In these galvanostatic anodic charging experiments the current density values used for the galvanostatic pulse was varied from 10 to 65 ma/cm^2, with most values used being above 25 ma/cm^2.

The anodic charging curve under propane does not differ significantly from the shape of the curve under helium but the charge passed is larger. Three main regions can be identified in the curve: (1) the region of rapidly rising potential from the adsorption potential to approximately 1.0 volt, the range being from 0.8 to 1.1 volt, which is dependent on the current density employed during the galvanostatic pulse; (2) the region from approximately 1.0 volt to approximately 1.8 volt (again varying with current density between 1.7 to 2.0 volts) where the potential changes less sharply and considerable charge is passed; (3) the region

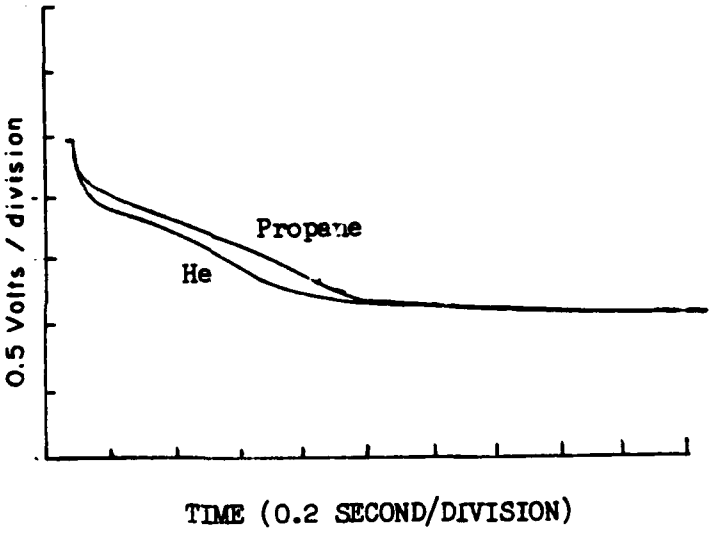

Figure 31. A typical anodic charging curve showing the curve with He only and the curve with propane adsorption.

where the potential reaches a plateau which corresponds to oxygen evolution. The middle region is the area of interest to determine the amount of charge necessary to oxidize the propane adsorbed at the adsorption potential. The total charge in this region may correspond to several processes occurring; a) the oxidation of adsorbed propane, b) the oxidation of the electrode surface and the evolution of oxygen contributing to the charge of the electrode, c) the oxidation of any propane which diffuses to the surface during the galvanostatic pulse, and d) the charging of the double layer.

It has been previously shown that the contribution of charge from the diffusion of propane during the pulse, i.e., process c), is negligible (15). The solubility of propane in phosphoric acid is quite low, less than 0.1 millimoles/liter at 130° C in 85% H_3PO_4 (36).

It would appear to be a reasonable assumption that the charge corresponding to b), the oxidation of the electrode surface and the evolution of oxygen, and d), the charging of the double layer, would be the same for the propane case and the helium case. Therefore, the subtraction of the total charge determined under helium from the total charge determined under propane should yield the quantity of propane previously adsorbed at the lower potential.

The variation of the charge/cm^2 to oxidize adsorbed propane versus $(time)^{1/2}$, is shown for 135° C in Figure 32 for an adsorption potential of 0.35 volt. Figure 32 indicates the value for the leveling off of total charge, i.e ~450 μcoulomb/cm^2. The shape of the curve and the values reported are in close agreement with the results reported by Brummer and Turner (37). In the present results the region of linearity

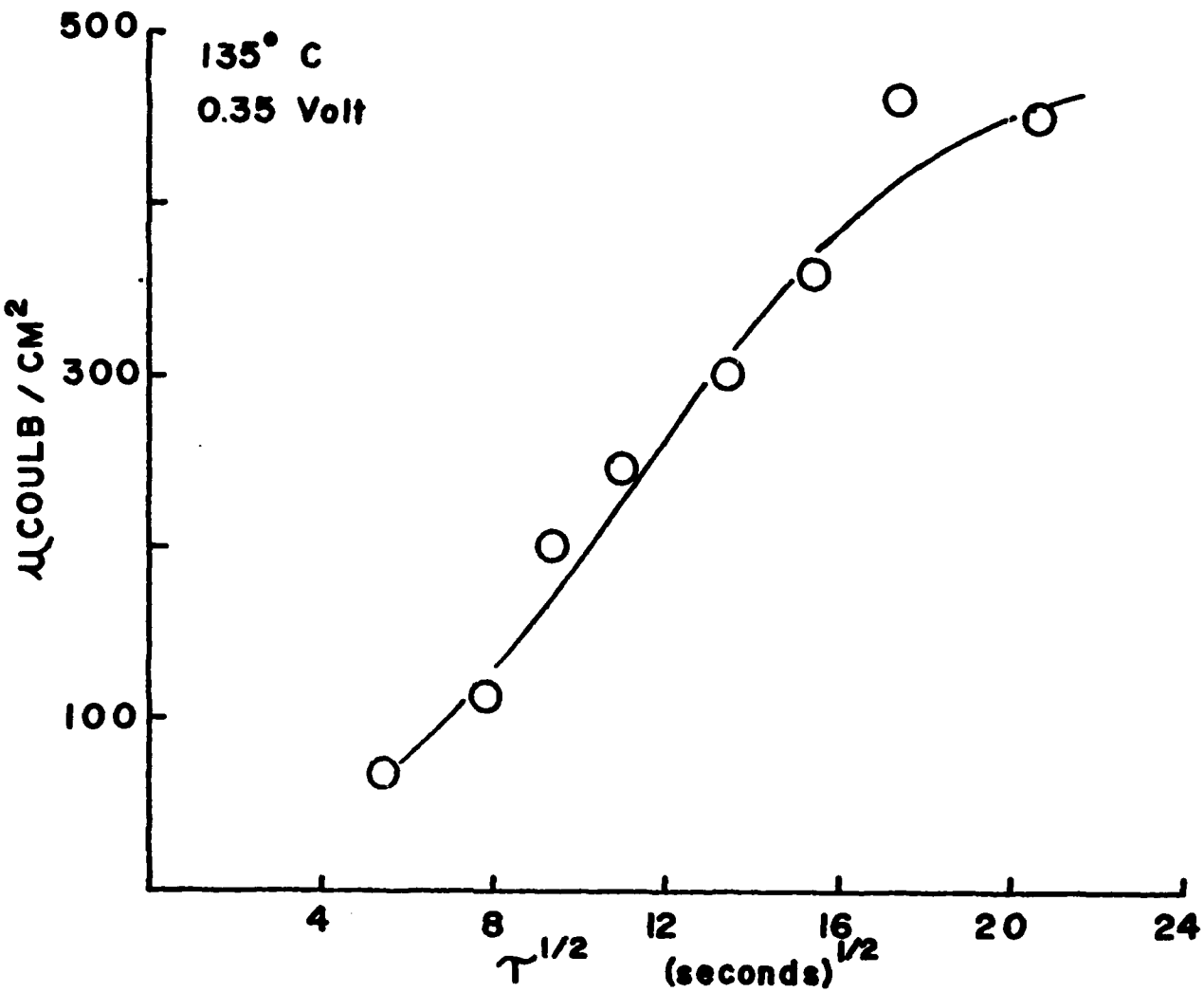

Figure 32. Charge as a function of $(\text{time})^{1/2}$ of adsorption at 0.35 volts and 135°C.

of the curve extends further in time than the previously reported results. It is felt that this is a function of the nature of the electrode surface produced by frequent flaming of the electrode rather than the experimental procedure.

At short times the linearity of the plot of charge/cm^2, Q, versus $(time)^{1/2}$, $\tau^{1/2}$, suggests that the adsorption is initially limited by the diffusion of the propane in solution to the electrode surface. For semi-infinite linear diffusion, Q would be given by the following equation derived by Laitinen and Kolthoff (38).

$$Q_{ads}^{C_3H_8} = 2\,nF\,\frac{D^{C_3H_8}{}^{1/2}}{\pi}\,C^{C_3H_8}\,\tau_{ads}^{1/2} \qquad (1)$$

Here $Q_{ads}^{C_3H_8}$ is given in coulombs/cm^2, n is the number of electrons released in the oxidation of the adsorbate, $D^{C_3H_8}$ is the diffusion coefficient and the $C^{C_3H_8}$ is the concentration (moles/cm^3) of propane. The initial slope from figure 32 is

$$\frac{dQ_{ads}^{C_3H_8}}{d\tau_{ads}^{1/2}} = 3.2 \times 10^{-4}\ \text{coulombs/sec}^{1/2}\text{cm}^2.$$

Since one geometric cm^2, under the conditions of the experiment was equivalent to 1.6 cm^2, this gives

$$\frac{dQ_{ads}^{C_3H_8}}{d\tau_{ads}^{1/2}} = 5.12 \times 10^{-4}\ \text{coulombs/sec}^{1/2}\text{cm}^2.$$

Brummer, et.al. (15), in their development of the 3 site adsorption model calculated a value of n of 17.

Taking the value for the solubility of propane as the concentration of propane, the value for $C^{C_3H_8}$ is 1.6×10^{-7} (36). The diffusion

coefficient at 135° C is then calculated to be 2.99×10^{-6} cm/sec and may be compared with the diffusion coefficient at 130°C of 3.5×10^{-6} cm/sec previously reported (14).

The steady-state adsorption of propane as a function of potential is given in Figure 33 for 120° C and in Figure 34 for 135° C. The general shape of the curve has been previously reported (37). Adsorption below 0.2 volt is low, and the results in this region are scattered. This is probably due to the type of intermediate species produced when propane is adsorbed at 0.2 volt and below. Adsorption of propane rises rapidly with potential to approximately 0.35 volt. In all runs with this cell and this technique the maximum adsorption occurred between 0.30 and 0.37 volts. Adsorption drops off with increased potential to become nearly zero at 0.7 volt.

The polarization curve for the reaction of propane on a platinum mesh electrode is shown in Figure 35. The open circuit potential occurred in all runs between 0.32 and 0.34 volts. It can be definitely stated that adsorption at 0.30 volt or less occurs where there is a net cathodic current. Adsorption at any potential above 0.40 volt occurs where the net current is anodic.

From earlier work with formic acid (39) it was determined that the measurement of hydrogen coverage, θ_H, gives an estimate of the extent of coverage of the electrode surface with organic species. The parameter $\theta_H^{\tau_1 C_3H_8}$ is defined as the ratio of the observed value of charge of hydrogen, Q_H, (under C_3H_8) under particular conditions, to the total maximum charge due to hydrogen, Q_H^{max}, at the same temperature. $\theta_H^{\tau_1 C_3H_8}$ is calculated from data obtained using a cathodic pulse as

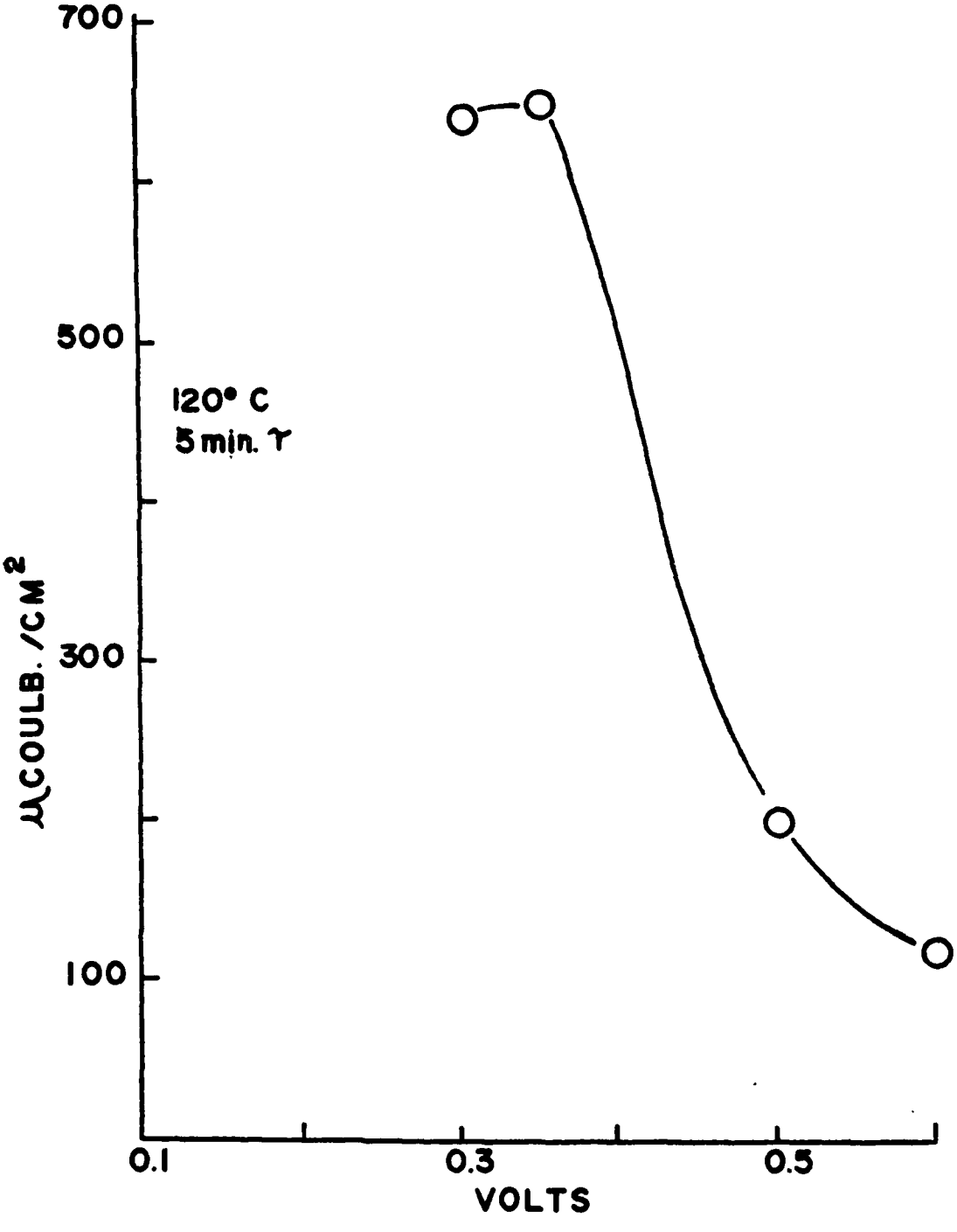

Figure 33. Charge as a function of the voltage of adsorption for 5 minutes adsorption at 120°C.

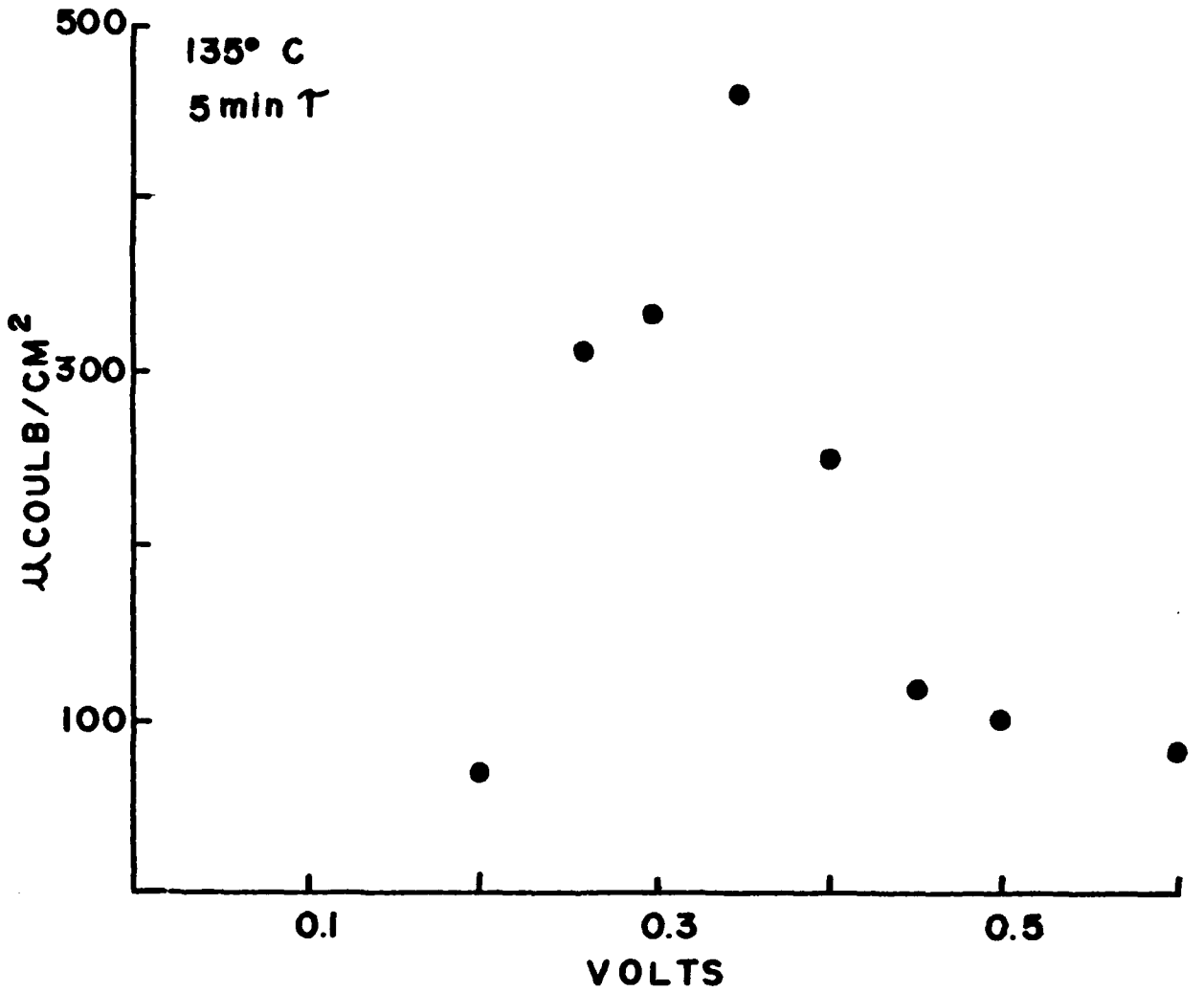

Figure 34. Charge as a function of the voltage of adsorption for 5 minutes adsorption at 135°C.

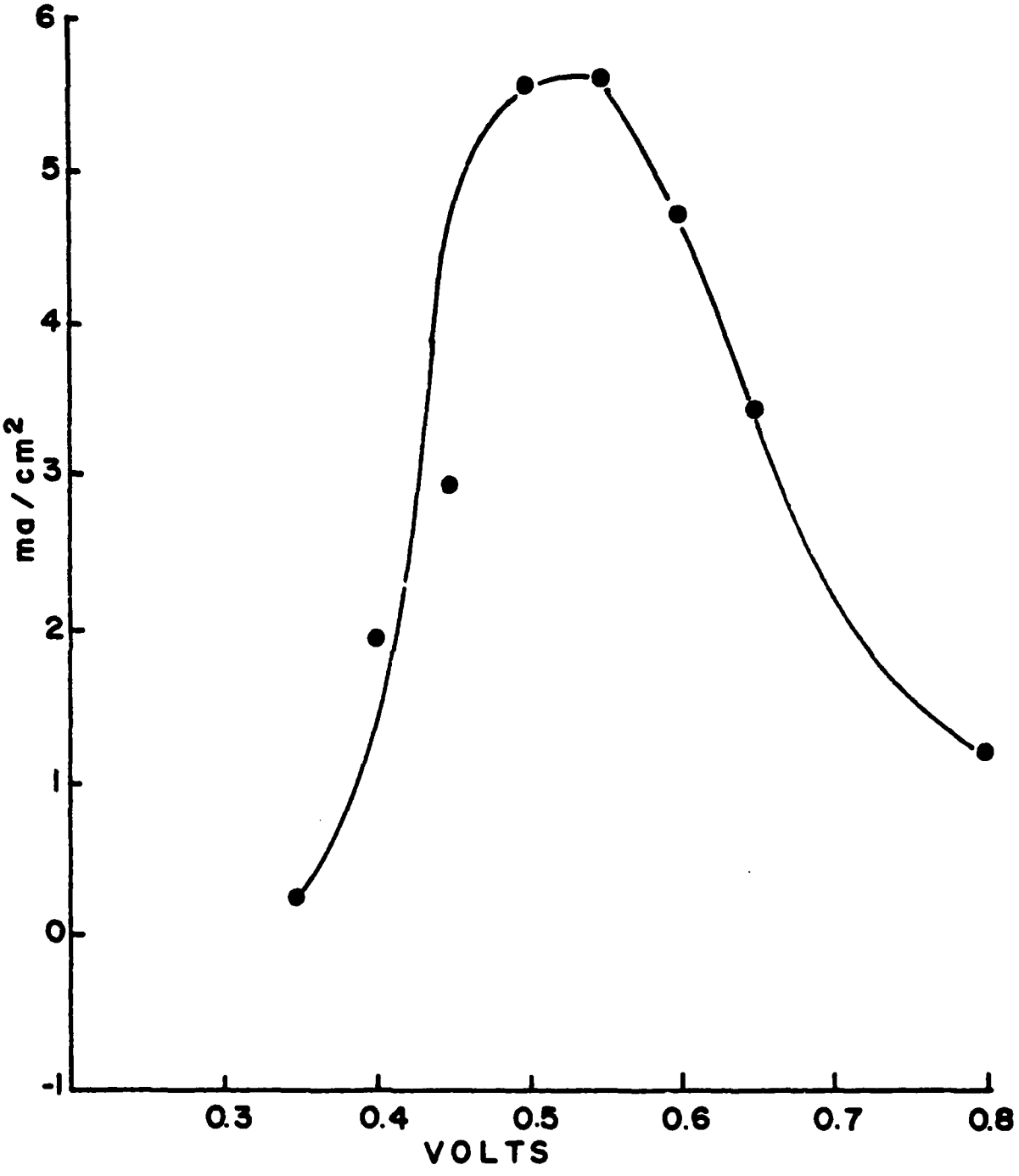

Figure 35. The polarization curve for the reaction of propane on a platinum mesh electrode.

shown in Figure 3c using propane as the gas. The quantity $(1-\theta_H^{\tau_1 C_3H_8})$ gives a measure of the fraction of the surface covered by adsorbed propane, $\theta_{C_3H_8}$.

The curves for $\theta_H^{\tau_1 C_3H_8}$ versus time, shown in Figure 36, are given for various voltages. The data were collected using galvanostatic pulses of approximately 50 ma/cm^2. The curves indicate that at a fixed potential the available surface for hydrogen coverage decreases with an increase of time. It is considered that the increased adsorption of hydrocarbon accounts for this response. At short times little hydrocarbon adsorption is observed. This is in agreement with data obtained from the anodic charging curves giving the total charge due to hydrocarbon oxidation.

If the initial period of propane adsorption is diffusion controlled, equation 1 above must apply. A plot of $\theta_H^{\tau_1 C_3H_8}$ versus the square root of the time, $\tau^{1/2}$, is shown in Figure 37. It has been previously calculated and reported that 0.060 $\theta_H/sec^{1/2}$ corresponds to a three-site adsorption for propane on platinum (15). For very short times, less than 2 seconds to approximately 30 seconds adsorption time, no measurable adsorption took place. In general, all data were taken at $>$ 10 seconds adsorption time. At the very short adsorption times recorded for 0.30 volt at 135° C a value of 0.07 $\theta_H/sec^{1/2}$ was found. This value does not hold beyond 30 second adsorption time. After 30 seconds, for all the adsorption voltages, the curves deviate from equation 1 describing diffusion controlled adsorption. This would tend to indicate that by 30 seconds the surface is becoming covered with an equilibrium or steady-state concentration of propane.

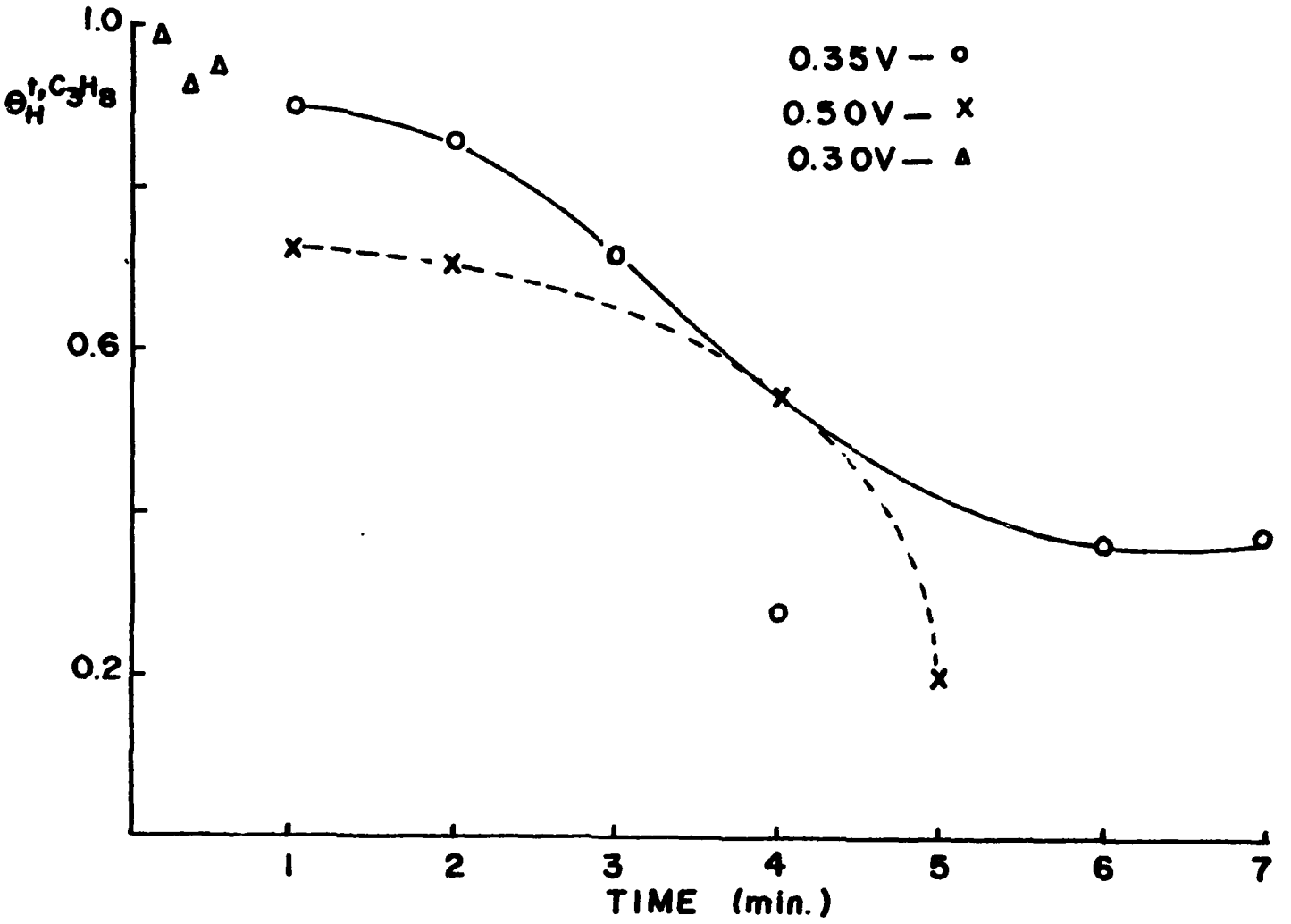

Figure 36. The fraction of hydrogen coverage as a function of time for 0.30, 0.35, and 0.50 volts.

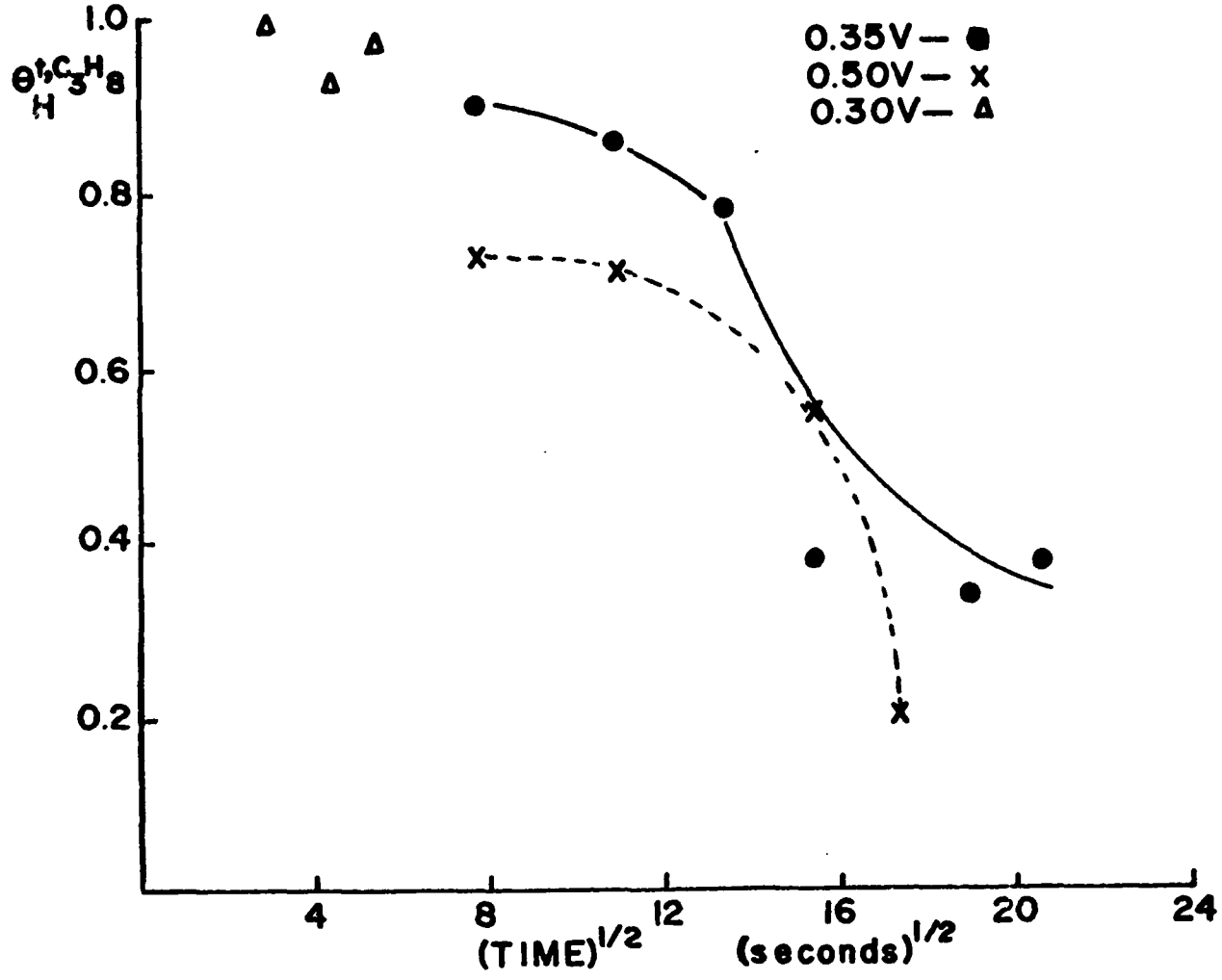

Figure 37. The fraction of hydrogen coverage as a function of (time)$^{1/2}$ for 0.30, 0.35, and 0.50 volts.

A galvanostatic anodic pulse without cathodic treatment under helium only, (a), followed by a galvanostatic pulse without cathodic pretreatment under propane, (b), followed by a galvanostatic anodic pulse with cathodic treatment, (c), results in a series of traces as shown in Figure 38. Initially galvanostatic anodic pulses under helium were run with and without the cathodic treatment step. This step was found to be unnecessary, as both traces coincide. The difference between (a) and (b) corresponds to the charge to oxidize the total adsorbed propane. The difference between (a) and (c) corresponds to the charge to oxidize the nonreducible quantity or the nondesorbable quantity of the adsorbed propane. The difference between (c) and (b) corresponds, therefore, to the charge necessary to reduce the cathodically desorbable portion of the adsorbed propane.

The total anodic charge, the charge after cathodic pulse (charge due to nondesorbable species), and the charge due to reducible species at 0.30 volt is shown in Figure 39. The times used were quite long in comparison to those used in previous investigations (15). By the one minute adsorption time the charge due to the desorbable species was almost constant. The adsorption potential, 0.30 volt, is in the region where the net current is cathodic (refer to Figure 35). The desorbable/nondesorbable ratio at the 5 minute adsorption time is 0.24. This value is slightly lower than that obtained by Brummer and Turner (37), 0.4 on a platinum wire.

The net current at 0.50 volt is anodic as shown in Figure 35. The total anodic charge, the charge due to nondesorbable, and charge due to desorbable species is seen in Figure 40. Again, the charge due to the desorbable species reaches a constant value and is lower

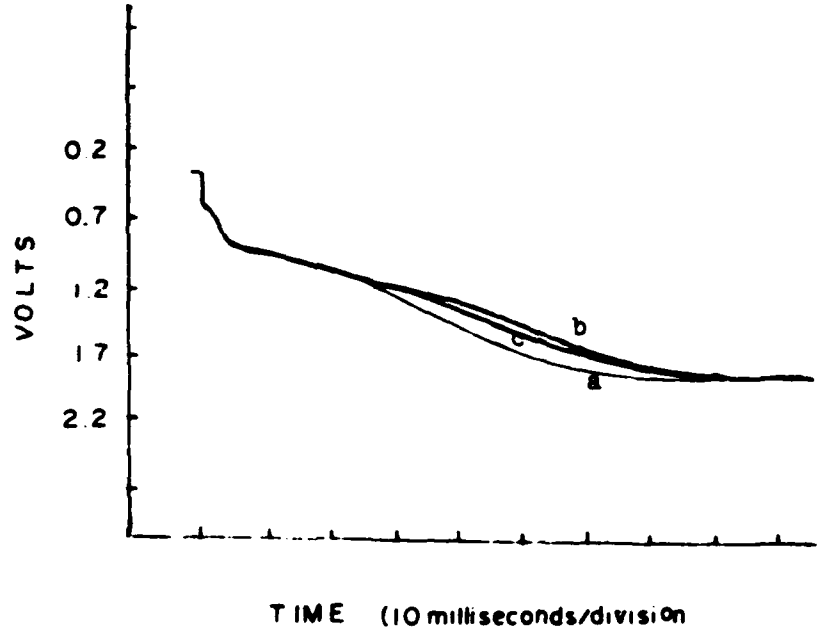

Figure 38. a. An anodic charging curve under He only.
b. An anodic charging curve under propane without cathodic pre-treatment.
c. An anodic charging curve under propane with cathodic pre-treatment.

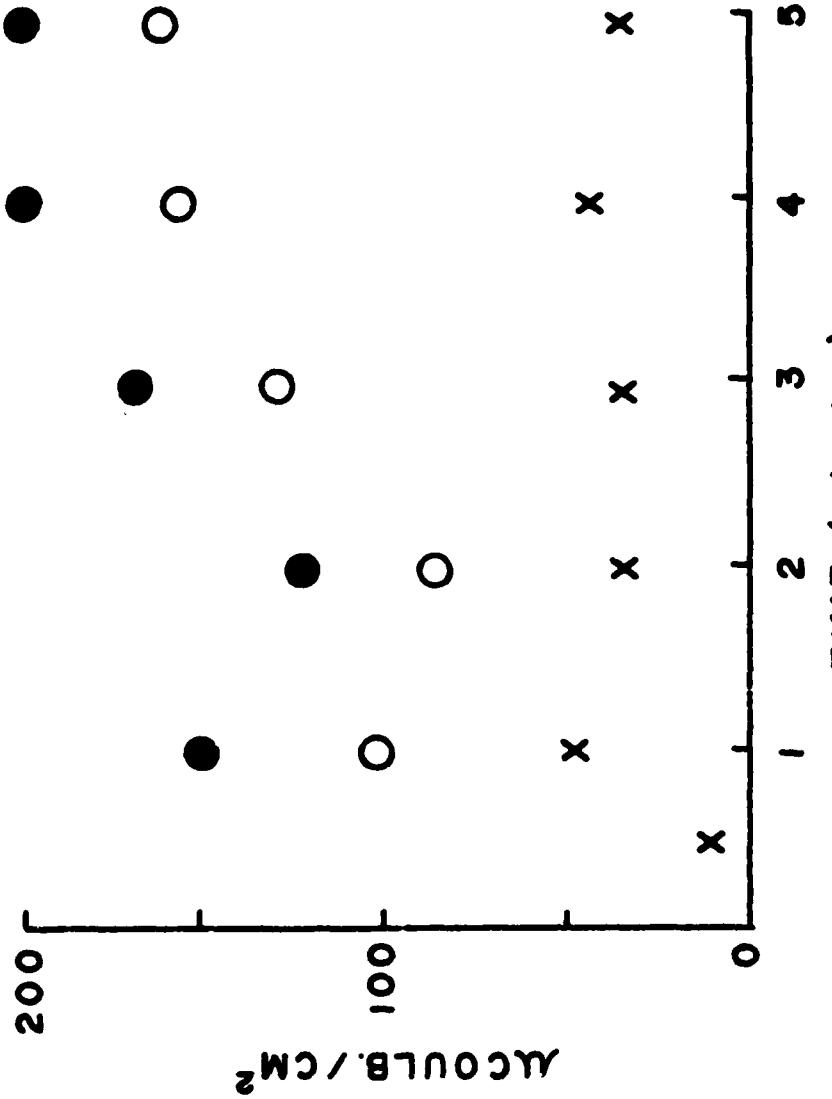

Figure 39. The charge as a function of time for total adsorbed species, non-desorbed, and desorbed species at 0.3 volt. ●, total adsorbed species, O, non-desorbed, X, desorbed.

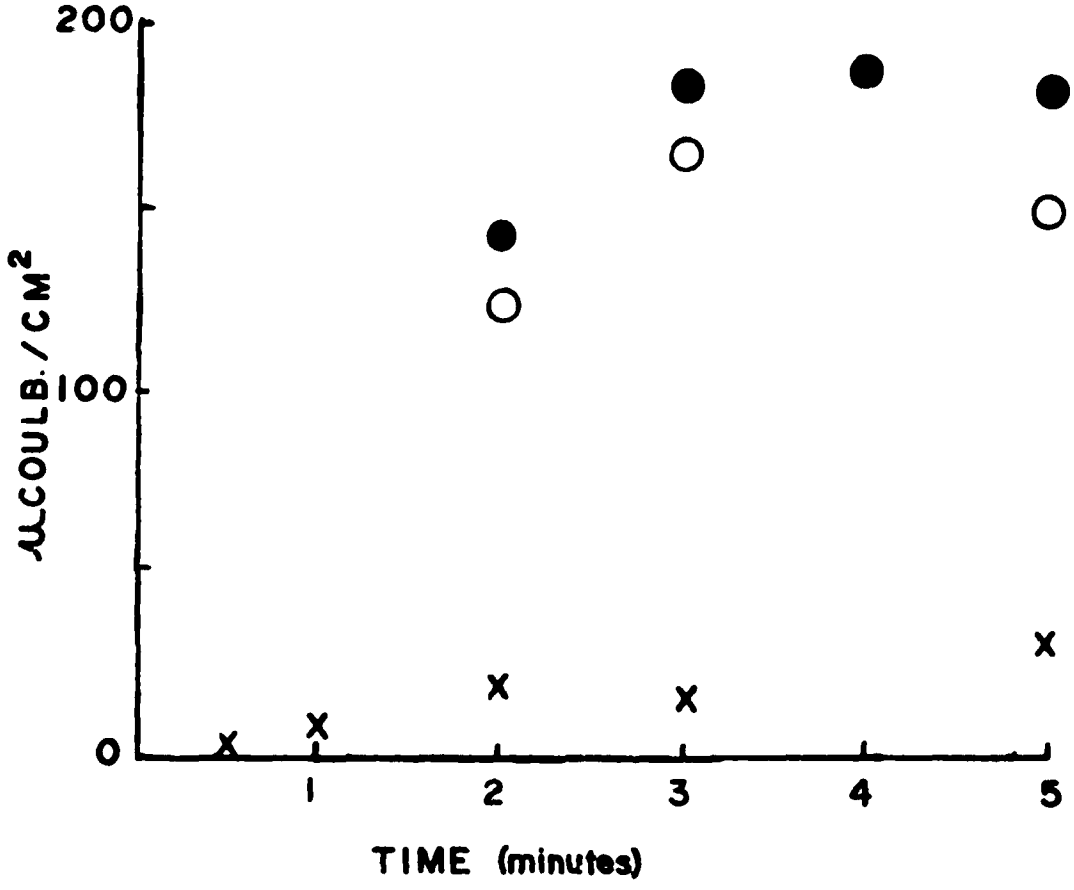

Figure 40. The charge as a function of time for total adsorbed species, non-desorbed species, and desorbed species at 0.5 volts. ● total adsorbed species, O, non-desorbed, X, desorbed.

in value than the charge due to nondesorbable species, the ratio of adsorbable/nondesorbable being 0.22 after 5 minutes adsorption of propane. Other values of the rates of desorbable, nondesorbable species for 0.20 volt, 0.40 volt, and 0.60 volt are 0.23, 0.20 and 0.24.

Three species have been proposed to occur, depending on the potential of adsorption. The material which can be removed by cathodic pulsing has been designated CHα; another species not removed by cathodic pulsing has been designated CHβ; and a third species called the O-type, which contains at least one C-O bond (37). Recent work using mass spectrometry indicates that the CHβ material at 0.2 and 0.3 volt contains little or no oxygen (40). A third species is definitely indicated from the shape of the oxidation curve for propane. No effort was made here to isolate or identify intermediates, hence no conclusions will be drawn as to their type or composition. The quantity of desorbable species found on the electrode varied with potential but the ratio of desorbable to nondesorbable species was approximately the same for all adsorption potentials for 0.2 to 0.6 volt, that is, a ratio of 0.20 to 0.24.

2.3.3 Additional Electrolytes Investigated

2.3.3.1 Results with dichloroacetic acid

As is usual with new electrolyte systems, first experiments dealt with polarization behavior. Figure 41 shows polarization results obtained at 90°C and 100°C using the procedure described above. Since "real" surface areas could not be obtained from these studies, a value of 50 cm^2 was chosen as an approximation based on phosphoric acid measurements. Thus approximate limiting current densities of 9 $\mu amp/cm^2$ at 100°C and 6 $\mu amp/cm^2$ at 90°C were found. These values correspond

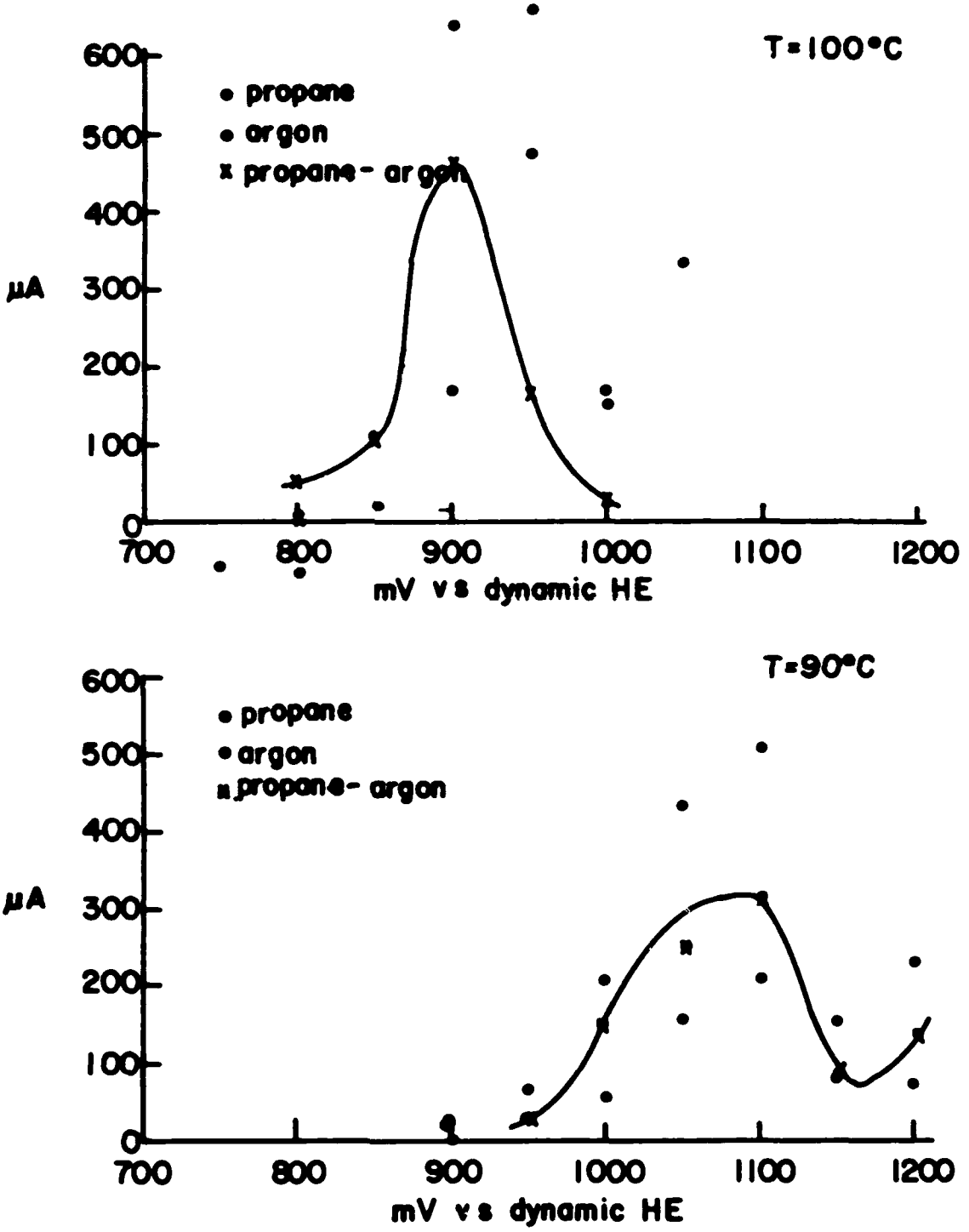

Figure 41. Polarisation curves for argon, propane, and propane minus argon in dichloroacetic acid.

to approximate efficiences for phosphoric acid electrolyte at 135°C. However, the voltage corresponding to the polarization maximum is shifted from a value of about 0.55 volt for the phosphoric acid to 0.90 volt (at 100°C) and 1.08 volts (at 90°C) in the $CHCl_2CO_2H \cdot H_2O$ system. Also, a minimum at about 100 mv above the polarization maximum was found in all experiments and, for voltages more anodic than the voltage at the minimum, polarization currents rose dramatically until the limits of the Wenking were reached at voltages approximately 350 mv above the polarization maximum. A "domain test" was made for this electrolyte system and results are shown in Figure 42. The high voltage cut-off appeared at lower voltages at higher temperatures. There were no apparent limiting cathodic reactions and the counter-working electrode circuit showed constant cell resistances to all polarizations. The rather extraordinarily high potential corresponding to the propane polarization maximum can be explained several ways: (a) reference system is sensitive to electrolyte contamination (or decomposition) and is unreliable; (b) propane has an extraordinarily high oxidation overpotential in this electrolyte; (c) the electrolyte had a very high oxygen concentration driving a potentially weak oxidation reaction towards much higher voltages; or (d) the apparent polarization maximum is an artifact of some side reaction related to the possible decomposition reaction responsible for the high voltage cut-off. The shift of the voltage cut-off to lower values at higher temperatures is consistent with thermodynamic expectations — increased thermal energy reduces amounts of electrochemical energy needed to promote the reaction. However, no definite answer to explain the source reaction for the high-voltage cut-off was found.

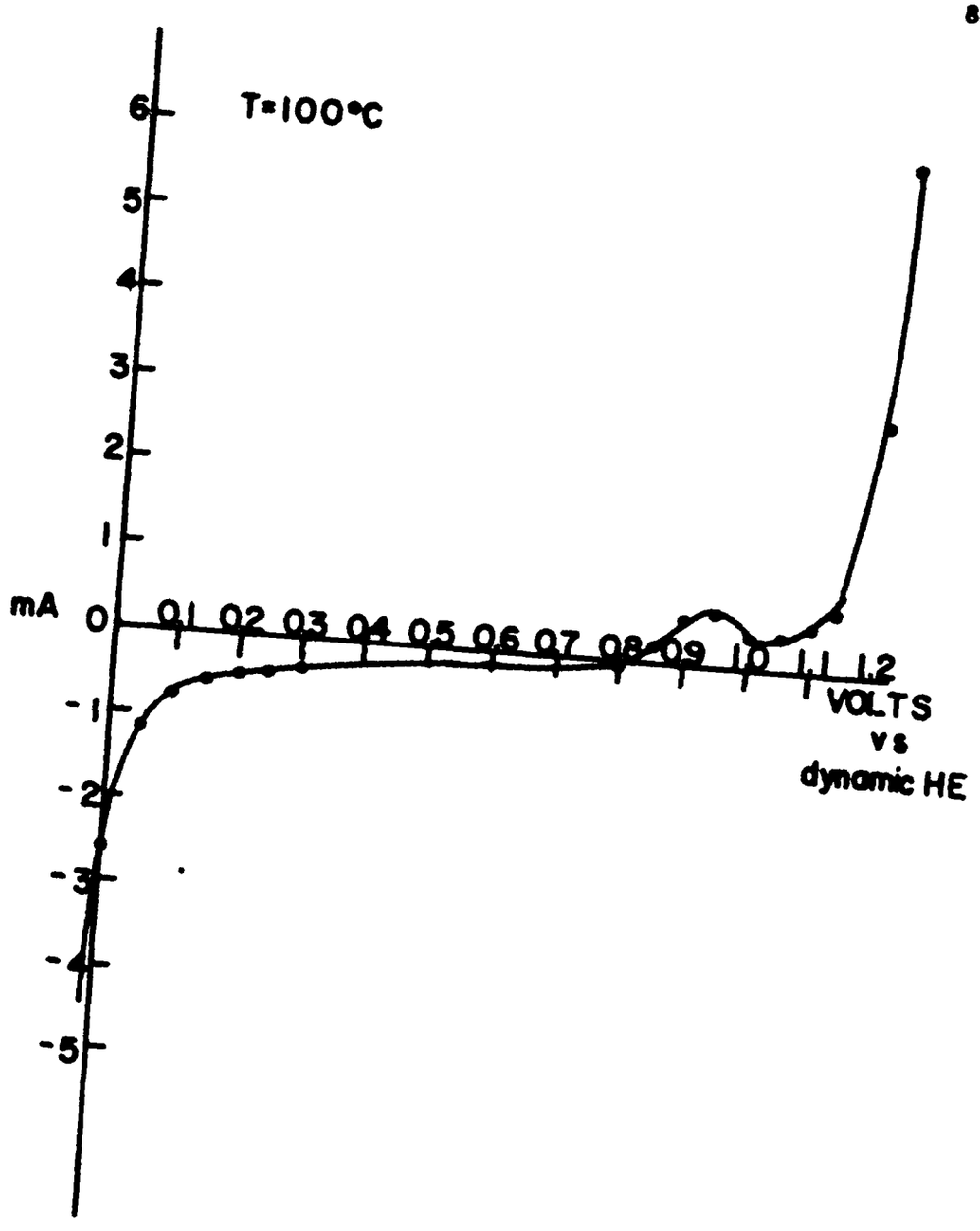

Figure 42. "Domain" region for $CHCl_2COOH$ electrolyte

2.3.3.2 Results with perfluorobutyric acid

A representative plot for the behavior of propane in perfluorobutyric acid on an electrode of 35 cm^2 is shown in Figure 43. An open circuit potential of 0.30 volt and a limiting current density of 42 $\mu amp/cm^2$ were obtained at 105°C.

An adsorption study for 5 minutes adsorption at 0.30 volt gave a value of 104 $\mu coulomb\ cm^{-2}$ charge. This may be compared with data obtained for propane adsorption in H_3PO_4 or in $CF_3SO_3H \cdot H_2O$.

2.3.4 Solubility Measurements

In the calibration of a new technique for the determination of the solubility of gases in liquids it is standard procedure to use a measurement of the solubility of oxygen in water. This measurement has been reported by a large number of investigators using a large number of techniques. These investigations have been reviewed and summarized by Morrison and Billett (41).

The solubility of oxygen in water was used to check the apparatus and procedure described in section 2.2.2 above. These results are compared with the accepted literature values in Figure 44 and good agreement is observed. From these data it appeared that the apparatus and technique were sufficiently accurate and adequate to proceed to make solubility determinations of oxygen, air, and propane in $CF_3SO_3H \cdot H_2O$.

The solubility of propane was determined at 90°, 104° and 126°C. With the existing apparatus it was not possible to work over 126°C because during the degassing procedure for the solvent some of the $CF_3SO_3H \cdot H_2O$ charge in the solvent bulb was carried over and condensed in the other portions of the apparatus. It was not possible to

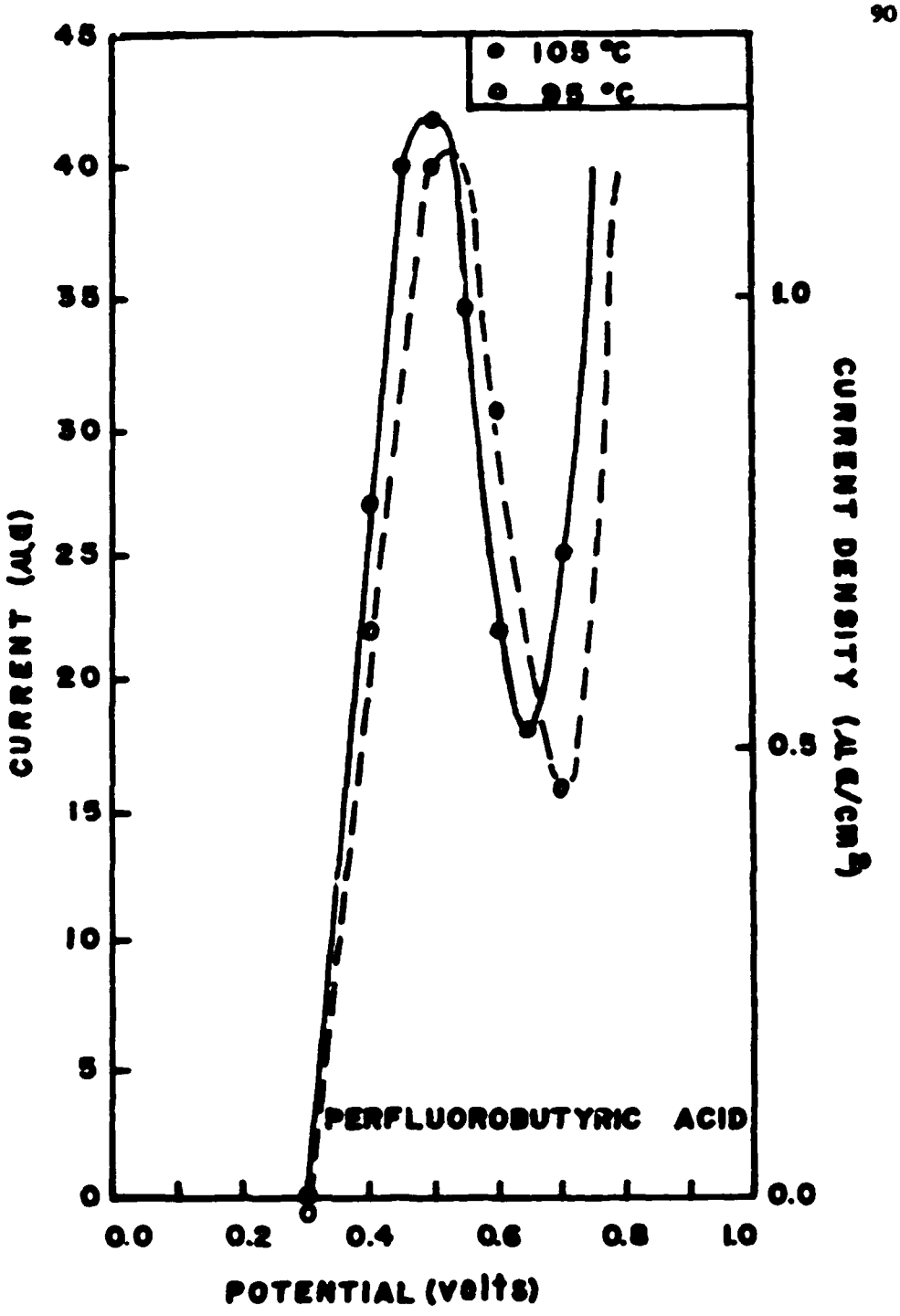

Figure 43. Current density-potential behavior of propane in perfluorobutyric acid

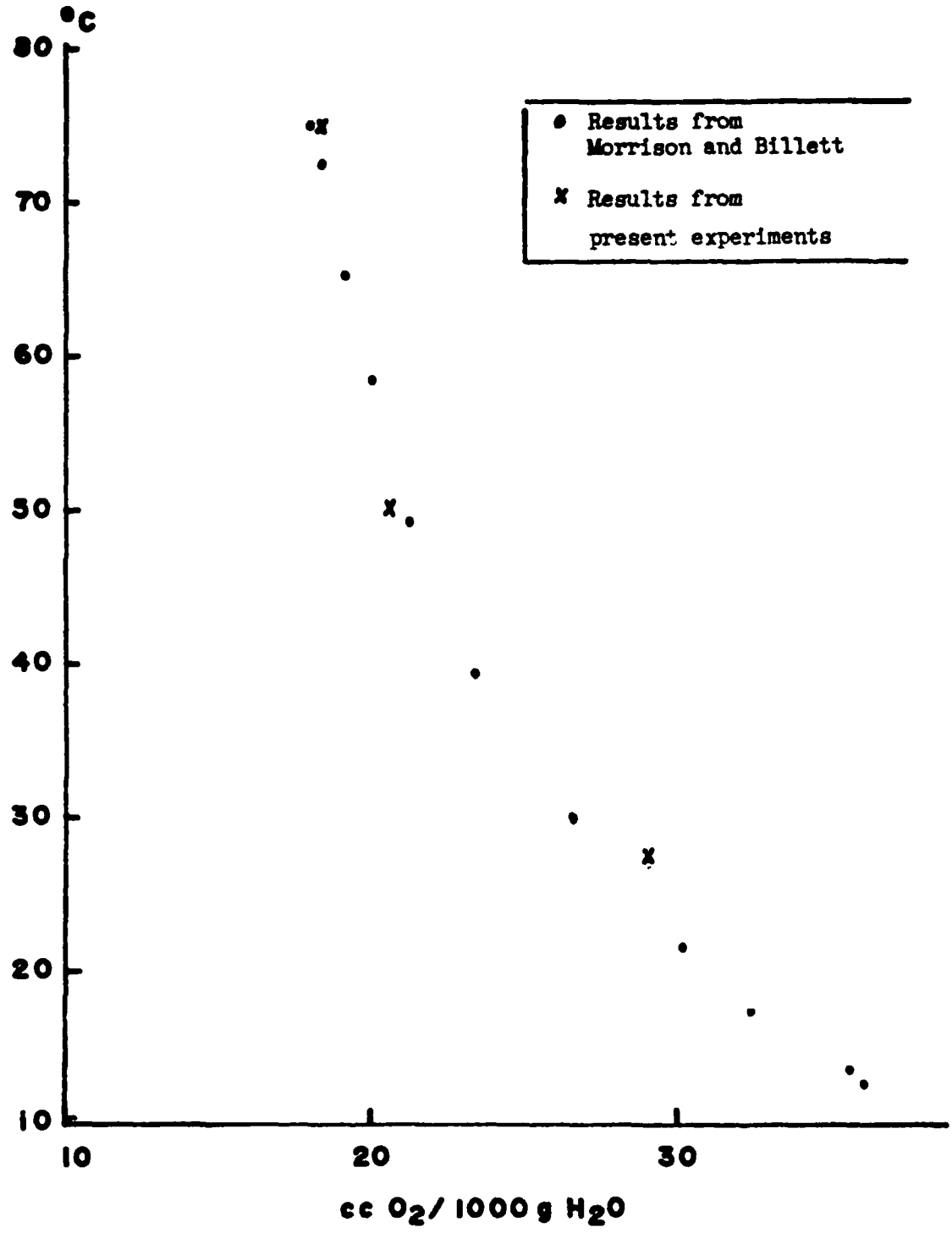

Figure 44. Solubility of Oxygen in Water

accurately determine this volume of solvent lost from the bulb but this volume was available to absorb the gas when the propane was introduced.

The solubility of propane in $CF_3SO_3H \cdot H_2O$ at three temperatures is as follows:

Temperature	Solubility (millimoles of propane/liter $CF_3SO_3H \cdot H_2O$)	Pressure of propane
90°C	0.127	770 mm
104°C	0.102	780 mm
126°C	0.35	770 mm

The 126°C value is considered less reliable than the other two for the reasons given above. The values in the above table may be compared with a literature value for the solubility of propane in concentrated H_3PO_4. MacDonald reports (36) a value of 0.153 millimole of propane per liter of 93% H_3PO_4 at 100°C and 754 mm of propane.

2.3.5 Silver Reference Electrode

In view of some of the problems in finding suitable reference electrodes, studies were undertaken to test the feasibility of a silver reference system. Initially, pure silver tabs, 2x5x0.01 cm, were anodized in dilute phosphoric acid to achieve a thin coating of, presumably, Ag_3PO_4. The potential of these tabs was tested against a normal hydrogen electrode. Figure 45a shows the temperature coefficient and reproducibility for the system. Figure 45b shows the reversibility test for the system. In addition, corrosion tests indicate a negligible corrosion rate over the temperature range of

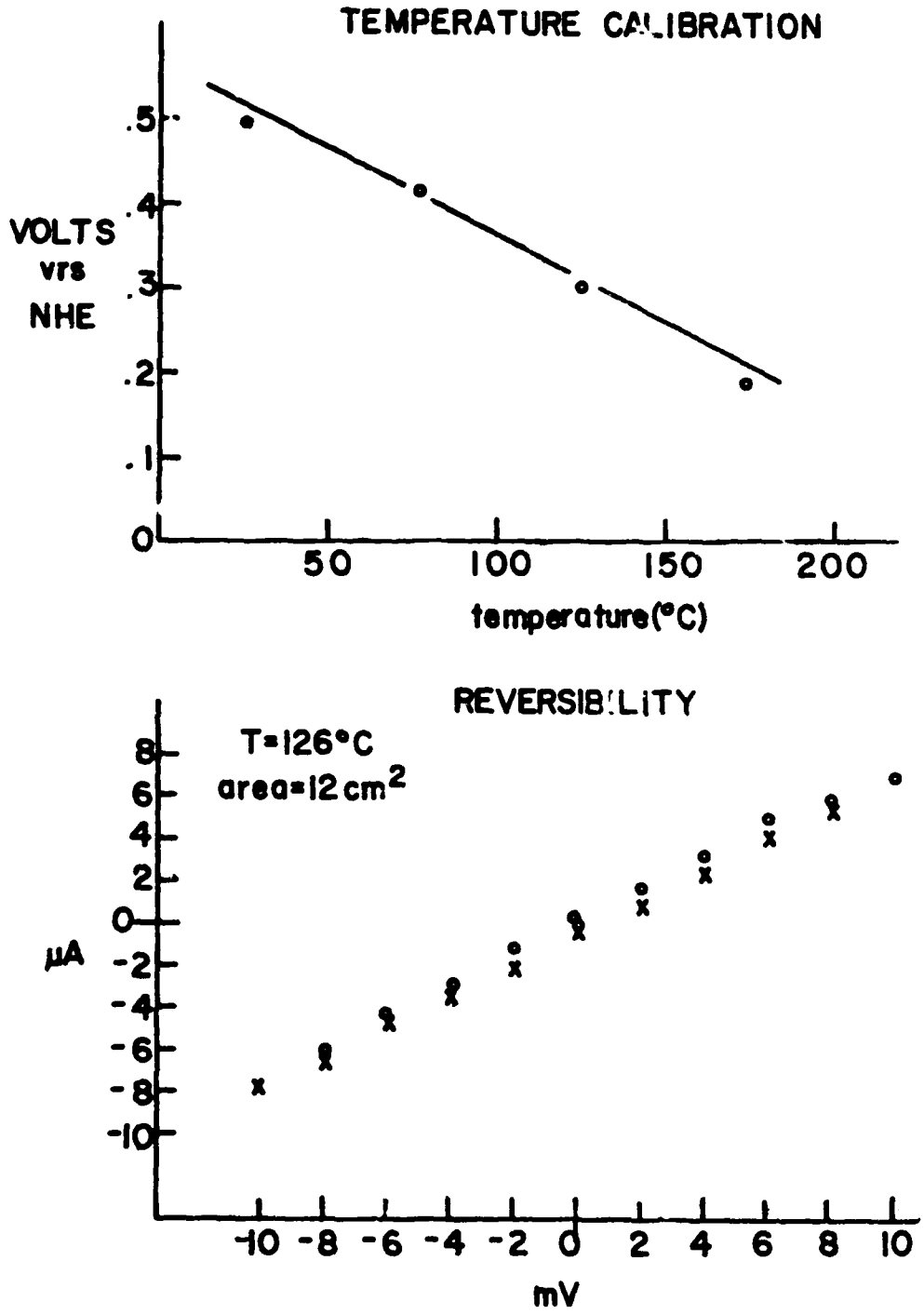

Figure 45. Silver reference electrode

22°C to 150°C. These tests indicate the feasibility of developing a reference system based on the silver electrode. In view of the main objective of the research to test new electrolyte systems, it was considered inappropriate to pursue the development of anion-specific reference systems, especially as some of the proposed electrolyte systems contained rather large or unusual anions rather difficult to relate to a reference system. Hence, the utilization of the dynamic hydrogen reference electrode for all studies reported above. However, it seems evident that for in-depth studies of the mechanism of fuel cells using phosphoric acid electrolytes (and also $CF_3SO_3H \cdot H_2O$ electrolyte), a silver reference system could prove to be a simple, convenient, and perhaps more stable alternative.

2.3.6 Porous Nickel Electrode

A porous nickel electrode was obtained from the Battery Products Division, Union Carbide Corporation, Parma, Ohio. It was anticipated that this electrode, when activated, could be used as a gas electrode with methanol. The porous nickel was activated by platinization. The electrode was stable at room temperature in $CF_3SO_3H \cdot H_2O$ for a test period of 3 weeks, but at 135°C the electrode broke down after 3 days in $CF_3SO_3H \cdot H_2O$. The electrode was completely disintegrated after a week at 135°C. As the temperature was decreased to 85°C, a longer time was required for the electrode to break up but even at the lower temperature it had disintegrated in two weeks. From these brief tests it was concluded that it would not be feasible to use this nickel electrode as a gas electrode in a methanol-air cell.

2.4 Conclusions

The effect of the electrolyte on fuel cell performance is again reinforced with the results of this study of $CF_3SO_3H \cdot H_2O$. In this case hydrogen oxidation and propane oxidation support higher current densities and the reduction of air begins from a higher open circuit potential. The net effect of these results is a theoretical cell of higher available potentials and currents. The reasons for the higher activity with this electrolyte are not well understood and deserve further study. If the properties of the "ideal" electrolyte could be well characterized, the choice of electrolytes for future investigation could be done more intelligently.

The electrode development for use in $CF_3SO_3H \cdot H_2O$ has been hampered by the flooding of conventional fuel cell electrodes. Additional electrode development for use in this electrolyte is essential to investigate actual fuel cell performance and perform life tests. Further, it may be desirable to alter the composition of the electrolyte to improve its characteristics by circumventing some of the existing problems in electrode development.

3.0 Task II A Study of the Corrosion Characteristics of Electrolytes for Intermediate-Temperature Hydrocarbon-Air Fuel Cells

3.1 Introductory

The objective of this phase of the project was to make corrosion measurements on selected alloys in 85% phosphoric acid and to develop procedures by which alloys might be evaluated for service in other alternate electrolytes such as $CF_3SO_3H \cdot H_2O$. The selection of metals or alloys for service in phosphoric acid is rather restricted. Reviews (42, 43) of corrosion studies conducted with phosphoric acid have indicated that only highly alloyed steels and alloys of Ta, Mo, or Cr are suitable for service in 85%-95% H_3PO_4 at temperatures in the range of 125-170°C. In previous studies it was demonstrated that tantalum possessed exceptional resistance to corrosion in concentrated phosphoric acid. However, as a material of construction tantalum is too expensive and the alternative is to use tantalum coated steel.

3.2. Experimental

The alloys and their approximate compositions are given in Table II. With the exception of the tantalum coated steel the alloys were of commercial origin. Stainless steel (AISI type 304) can be considered as a reference material.

Prior to testing, the alloy samples were pretreated according to the following procedure. They were cleaned in acetone to remove grease from the surface. After drying in air the samples were immersed in HCl (6 N) at 95°C for 1 - 2 minutes. Following this they were rinsed in distilled water and then dipped in a solution of HNO_3 and H_2SO_4 (1:1). They were again rinsed with distilled water and placed in a 5% NaCN solution for 5 minutes. Finally, the samples were rinsed with distilled water and then with acetone. They were stored in acetone until just prior to testing. At that time they were removed and allowed to dry in the air before being weighed.

For the testing in phosphoric acid the samples were immersed in a solution of 85% H_3PO_4 in a flask equipped with a reflux condenser. The test assembly was held in a constant temperature oil bath, a "Magni Whirl" Model MW-1145-1 unit manufactured by the Blue M Co. The phosphoric acid solution was allowed to equilibrate for one hour at the temperature (150°C or 175°C) before the sample was immersed.

The weighed samples were immersed in 160 ml of 85% H_3PO_4 at 150°C and 175°C for varying lengths of time. They were then removed from the H_3PO_4 and rinsed well with distilled water and then acetone. They were dried in the air for one hour and then weighed

Table II

Composition of Alloys Used in Corrosion Tests

Alloy	Composition
AISI Type 304	18.0 - 20.0 Cr; 8.00 - 11.0 Ni; 0.03 C (max); 2.0 Mn (max); 1.00 Si (max); 0.045 P (max); 0.03 S (max).
Incoloy 825	42 Ni; 21 Cr; 3.0 Mo; 33 Fe.
Hastelloy C	56 Ni; 15 Cr; 3.7 W; 16 Mo.
Carpenter 20 Cb-3	34.03 Ni; 19.91 Cr; 2.25 Mo; 3.30 Cu; 0.21 Co; 0.86 Cb; 0.039 C; 0.39 Mn; 0.41 Si; 0.016 P; 0.004 S; balance Fe.
Ta coated steel	Steel plated with Ta by the Tantalum "Metalating" Process by the General Metals Technologies Corp. Thickness, 0.006 - 0.008 in.

a second time to determine the weight loss during the time of immersion in the H_3PO_4.

For the testing in $CF_3SO_3H \cdot H_2O$, immediately following distillation, 20 ml aliquots of the hydrate were transferred to test tubes fitted with Teflon stoppers. After the alloy samples were weighed they were immersed in the $CF_3SO_3H \cdot H_2O$ which had been equilibrated in the constant temperature oil bath for about one hour. The corrosion tests were run in duplicate for a duration of 4 hours at 110°C and 161°C. Following the exposure, the samples were rinsed successively with distilled water and acetone, dried and reweighed.

3.3 Results and Discussion

The weight losses of the alloys upon immersion in phosphoric acid at 150°C and 175°C are given as averages in Table III. It is obvious that stainless steel type 304 corrodes excessively at these elevated temperatures. The low corrosion rate of Incoloy 825 and Hastelloy C confirms previous results (42) indicating that these materials are substantially resistant to corrosion. Tantalum-coated steel is essentially immune to corrosion in phosphoric acid at these elevated temperatures. This suggests the construction of a fuel cell with support parts being fabricated with low cost steel plated on those faces that would be exposed to phosphoric acid.

The corrosion rates of the alloys in $CF_3SO_3H \cdot H_2O$ are given as weight losses in Table IV. These weight losses are good measures of the corrosion of the alloys in the sense that the coupons did not develop corrosion product films, the weight of which would be included in the weight of the sample after exposure to the acid. Further, there was no evidence for the formation of high resistivity surface films. It is apparent that the corrosion rates for all four alloys are quite low at 161°C. The 4 hr rate of 0.3 mg cm^{-2} for stainless steel type 304 compares with a 4 hr rate of 40 mg cm^{-2} observed in phosphoric acid. A corrosion rate of 0.3 mg cm^{-2} may be converted to an engineering corrosion rate unit of 0.036 inches penetration per year, a rate that usually can be tolerated in construction materials for tanks, piping, and valves.

Table III Corrosion of Alloys in 85% Phosphoric Acid

Temperature	Alloy	Corrosion Rate Weight Loss ($mg/cm^2/hr$)
150° C	AISI Type 304	9.0
	Incoloy 825	0.061
	Hastelloy C	0.010
	Ta Coated Steel	+0.003
175° C	AISI Type 304	19.1
	Incoloy 825	0.12
	Hastelloy C	0.042
	Ta Coated Steel	0.018

Table IV

Corrosion of Alloys in Trifluoromethanesulfonic Acid Monohydrate

Alloy	Loss at weight (mg cm^{-2}) in 4 hours			
	At 110°C		At 161°C	
AISI type 304 (Stainless steel)	0.21 0.07	Avg. 0.14	0.28 0.33	Avg. 0.31
Incoloy 825	0.026 0.026	Avg. 0.03	0.22 0.33	Avg. 0.28
Hastelloy C	0.06 0.06	Avg. 0.06	0.37 0.36	Avg. 0.37
Carpenter 20-Cb3	0.14 0.09	Avg. 0.11	0.31 0.29	Avg. 0.31

3.4 Conclusions

The preliminary work has shown that it is possible to select alloys or materials of construction that would be highly resistant to corrosion in phosphoric acid at 175°C. It would also appear that it will not be necessary to use these highly alloyed Ni or Cr steels as construction materials in trifluoromethanesulfonic acid monohydrate. Stainless steel AISI type 304 or Ni-plated steel should provide adequate corrosion resistance to serve as a construction material. Rather it is possible that the problem might be shifted to an electrochemical question dealing with the concentration (in trace quantities) of Fe^{++}, Ni^{++}, etc., that can be tolerated in the electrolyte. In this preliminary study the metals reacted at their corrosion potential. The probability exists that a different rate, greater or lesser, would exist if the metal was held at a positive or negative potential, e.g., as a current collector.

4.0 References

1. A. A. Adams, R. T. Foley, and R. M. Goodman, Interim Technical Report No. 3 on Contract No. DAAK02-72-C-0084, June 1973.
2. T. Gramstad and R. N. Haszeldine, J. Chem. Soc., 1956, 173.
3. A. A. Adams and R. T. Foley, Interim Technical Report No. 2 on Contract No. DAAK02-72-C-0084, February 1973.
4. A. A. Adams and R. T. Foley, Interim Technical Report No. 5 on Contract No. DAAK02-72-C-0084, July 1974.
5. T. Gramstad and R. N. Haszeldine, J. Chem. Soc., 1957, 4069.
6. J. Bardon, I. Farazmand, M. Stacey, and J. C. Tatlow, J. Chem. Soc., 1957, 2574.
7. "3 M Brand Perfluoro Carboxylic Acids," Technical Bulletin issued by 3 M Co., October, 1970.
8. J. R. Hollahan and G. H. Cady, J. Phys. Chem., 63, 757 (1963).
9. Handbook of Chemistry and Physics, 45th Edition, Chemical Rubber Co., 1964, p. D77.
10. ibid., p. C91.
11. J. O. Smith, "Study of Fuel Cells Using Storable Rocket Propellant," NAS 3-2791 (1964).
12. U. P. Strauss and S. Bluestone, J. Am. Chem. Soc., 71, 5292 (1959).
13. J. Giner, J. Electrochem. Soc., 111, 376 (1964).
14. S. B. Brummer, Contract No. DA 44-009-AMC-410 T, November 1, 1964-March 31, 1965.
15. S. B. Brummer, J. I. Ford, and M. J. Turner, J. Phys. Chem. 69, 3424 (1965).
16. S. Gilman, Trans. Faraday Soc., 61, 2561 (1965).

17. F. J. Loprest, J. Phys. Chem., 61, 1128 (1957).

18. S. B. Brummer, Contract No. DA 44-009-AMC-410T, Oct. 30, 1964.

19. G. Brauer, "Handbook of Preparative Inorganic Chemistry," Vol. I, 2nd ed., pp 549-552, Academic Press (1963).

20. D. E. C. Corbridge, M. S. Pearson, and C. Walling, "Topics in Phosphorus Chemistry," Vol. 3, p 277, Interscience Pub. (1966).

21. K. J. Vetter, "Electrochemical Kinetics," Academic Press, London, 1967, p. 521.

22. E. J. Cairns, "Anodic Oxidation of Hydrocarbons," Advances in Electrochemistry and Electrochemical Engineering, Vol. 8, Wiley-Interscience, New York, 1971.

23. J. Giner, Electrochimica Acta, 8, 857 (1963).

24. A. A. Adams, R. T. Foley, and R. M. Goodman, Interim Technical Report No. 4 on Contract No. DAAK02-72-C-0084, February 1974.

25. E. J. Cairns, Abstract No. 140, Meeting of the Electrochemical Society, San Francisco (May 1965).

26. J. Giner, First Technical Report, Contract No. DAAE15-67-C-0048, August 1967.

27. V. S. Bagotzky and Yu. B. Vassilyev, Electrochimica Acta, 12, 1323 (1967).

28. C. E. Heath, Proceedings of the 17th Annual Power Sources Conference, pp 96 (1963).

29. J. P. Hoare, J. Electrochem. Soc., 113, 846 (1966).

30. A. Streitwieser, Jr., C. L. Wilkins, and El Kiehlmann, J. Am. Chem. Soc., 90, 1598 (1968).

31. J. O. Bockris and S. Srinivasen, "Fuel Cells: Their Electrochemistry," Chapter 8, McGraw-Hill, Inc., New York, N.Y. (1969).

32. S. Schuldiner and R. M. Roe., J. Electrochem. Soc., 110, 1142 (1963).

33. W. Visscher and M. A. V. Devanathan, J. Electroanal. Chem., 8, 127 (1964).

34. H. Wroblowa, M. L. B. Rao, A. Damfanovic, and J. O. Bockris, J. Electroanal. Chem., 15, 139 (1967).

35. R. J. Barger, Jr, and M. L. Savitz, J. Electrochem. Soc., 115, 686 (1968).

36. D. I. MacDonald and S. Gilman, General Electric Contract No. DA 44-009-ENG-4909, DA 44-009-ENG-479(T),ARPA Order No. 247, January 1, 1964-June 30, 1964.

37. S. B. Brummer and M. J. Turner, J. Phys. Chem. 71, 2825 (1967).

38. H. A. Laitinen and I. M. Kolthoff, J. Am. Chem. Soc., 61, 3344 (1939).

39. S. B. Brummer and A. C. Makrides, J. Phys. Chem., 68, 1448 (1964).

40. J. Comeau and S. Bruckenstein, Univ. Buffalo Contract No. DAAK 02-71-C-0306, June 1972.

41. T. J. Morrison and F. Billet, J. Chem. Soc., 1952, 3819

42. R. R. Sayono, E. T. Seo and H. P Silverman, Final Report on Contract No. DA 44-009-AMC-1452(T), January 1971.

43. Corrosion Engineering Bulletin, CEB-4, "Corrosion Resistance of Nickel-Containing Alloys in Phosphoric Acid," International Nickel Co., 1966.

Commander (12)
Defense Document Center
Cameron Station, Bldg. 5
Attn: TISIA
Alexandria, Va. 22314

Commanding General (1)
Headquarters, U.S. Army Materiel Command
Attn: AMCRD-GP,
Mr. John M. Horstkamp
5001 Eisenhower Ave.
Alexandria, Va. 22304

Commanding General (1)
Headquarters, U.S. Army Materiel Command
ATTN: AMCRD-TE, Mr. John Crellin
5001 Eisenhower Ave.
Alexandria, Va. 22304

Commanding General (1)
U.S. Army Tank Automotive Command
Technical Library
Warren, Michigan 48090

Director, Technical Information
Advanced Research Project Agency
1400 Wilson Blvd.
Arlington, Va. 22209

Commanding Officer (1)
U.S. Army Electronics Command
ATTN: AMSEL-KL-P, Mr. David Linden
Fort Monmouth, New Jersey 07703

Commanding Officer (1)
U.S. Army Transportation Research
and Engineering Command
ATTN: Research Directorate
Fort Eustis, Virginia 23604

Chief of Research and Development (1)
Office, Chief of Staff
Department of the Army
Washington, D.C. 20310

Chief (1)
U.S. Army Security Agency
Arlington Hall Station
Arlington, Virginia 22212

Commanding Officer
Harry Diamond Laboratory
AMXDO-RCB, ATTN: Dr. Morrison
Washington, D.C. 20438

Office of the Assistant Secretary (1
of Defense (R and D)
Department of the Army
ATTN: Technical Library
Washington, D.C. 20310

Office of Assistant Director (1)
Defense Research and Engineering
ATTN: Col. G.D. McPherson
Pentagon
Washington, D.C. 20310

Power Information Center (1)
University City Science Institute
3401 Market Street
Room 2210
Philadelphia, Pa. 19104

Institute of Defense Analysis (1)
400 Army-Navy Drive
ATTN: Mr. Robert Hamilton
Arlington, Va. 22202

Director (1)
National Aeronautics and Space
Administration
ATTN: Code RPP, Mr. E.M. Cohn
Washington, D.C. 20546

Director (1)
George Marshall Space Flight Center
ATTN: M-ASTR-E
Huntsville, Alabama 38809

Electric Power Research Institute
3412 Hillview Avenue
Palo Alto, CA 94304

State University of New York at Bu
Attn: Stanley Bruckenstein, Ph.D.
220 Acheson Hall
Buffalo, NY 14214

Hugh J. Barger, Jr.
Box 2232
Davidson, North Carolina 28036

Commanding Officer (1)
Aerospace Power Division
ATTN: AFAPL/PO (Mr. George W. Sherman)
Wright-Patterson Air Force Base
Dayton, Ohio 45443

Director (1)
Lewis Research Center
National Aeronautics and Space Administration
ATTN: Mr. H.J. Schwartz (M.S. 309-1)
21000 Brook Park Road
Cleveland, Ohio 44135

Commanding Officer
Rome Air Development Center
ATTN: TUGG Mr. F.J. Mollura
Griffiss AFB, N.Y. 13440

Commanding Officer (1)
U.S. Air Force Security Service
ATTN: DCS/Communications - Electronics (ESO)
San Antonio, Texas 78241

Chief (1)
Naval Ships Engineering Center
ATTN: Code 6157D
Mr. C.F. Viglotti
Washington, D.C. 20360

Director, Power Branch (1)
Office of Naval Research
ATTN: Code 473, Dr. Ralph Roberts
800 N. Quincy Street
Arlington, Va. 22217

Chief (1)
Naval Ship Systems Command
Department of the Navy
ATTN: Mr. B.B. Rosenbaum
Code 03422
Washington, D.C. 20360

Technical Documents Center (2)
USAMERDC
Fort Belvoir, Virginia 22060

Electrochemica Corporation (1)
2485 Charleston Rd.
ATTN: Mr. V. Sparks, Technical Library
Mountain View, California 94040

Office of Naval Research (1)
Department of the Navy
ATTN: Code 425
800 N. Quincy Street
Arlington, Va. 22217

Commanding Officer (1)
Naval Ordnance Test Station
China Lake, California 93555

Commanding Officer (1)
U.S. Naval Electronics Laboratory
San Diego, California 92152

Director (1)
U.S. Naval Research Laboratory
ATTN: Code 2027
Washington, D.C. 20390

Commanding Officer (1)
Naval Ships R and D Center, Annapoli
Division
ATTN: Mr. John H. Harrison
Annapolis, Maryland 21402

Argonne National Laboratory
9700 South Cass Avenue
ATTN: Dr. A. Tevebaugh
Argonne, Illinois 60439

Dr. Paul C. Milner (1)
Bell Telephone Laboratories
Murray Hill, New Jersey 07974

Mr. Sidney Gross (1)
Mail Stop 88-06
The Boeing Company
P.O. Box 3999
Seattle, Washington 98124

TRW Systems (1)
R1/2094
One Space Park
ATTN: Dr. Herbert P. Silverman
Redondo Beach, California 90278

U.C.L.A. (1)
Dept. of Chemical Engineering
ATTN: Prof. D. Bennion
Los Angeles, California 90007

Engelhard Industries, Inc. (1)
Military Service Dep artment
113 Astor Street
ATTN: Mr. V.A. Forlenza
Newark, New Jersey 07114

Esso Research and Engineering Company (1)
Box 121
ATTN: Dr. G. Ciprios
Linden, New Jersey 07036

General Electric Company (1)
950 Western Avenue
ATTN: Mr. L. Nuttall
West Lynn, Massachusetts 01905

Institute of Gas Technology (1)
State and 34th Sts.
Technology Center
ATTN: Mr. L.G. Marianowski
Chicago, Illinois 60616

Massachusetts Institute of (1)
Technology
ATTN: Professor H.P. Meissner
Cambridge, Massachusetts 02138

P.L. Howard Associates, Inc. (1)
Millington, Maryland 21651

Pratt and Whitney Aircraft Division (1)
United Aircraft Corporation
ATTN: Mr. W.H. Podolny
400 E. Main Street
East Hartford, Connecticut 06108

Dr. D.C. Olson (1)
Shell Development Company
P.O. Box 262
Wood River, Illinois 62095

Dr. R.A. Wynveen
President
Life Systems, Inc.
23715 Mercantile Road
Cleveland, Ohio 44122

Union Carbide Corporation (1)
Parma Research Center
P.O. Box 6166
ATTN: Dr. R. Brodd
Parma, Ohio 44101

University of Florida (1)
Dept. of Chemical Engineering
P.O. Box 3027
ATTN: Professor R.D. Walker
Gainesville, Florida 32601

Globe-Union Inc. (1)
ATTN: Corporate Research
5757 North Green Bay Avenue
Milwaukee, Wisconsin 53201

Energy Research Corporation (1)
ATTN: Dr. B.S. Baker
15 Durant Avenue
Bethel, Connecticut 06801

Mr. Norman Rosenberg
U.S. Dept. of Transportation
Transportation Systems Center
55 Broadway
Cambridge, Massachusetts 02142

Dr. S.B. Brummer
Director of Physical Research
EIC, Inc.
55 Chapel St.
Newton, Massachusetts 02158

The Standard Oil Company (1)
Research Center
4440 Warrensville Center Rd.
ATTN: Dr. Robert A. Rightmire
Cleveland, Ohio 44128

Professor R.T. Foley (1)
Department of Chemistry
The American University
Washington, D.C. 20016